Supplementary Information

Azadipyrromethene Cyclometallation on Neutral Ru^{II} Complexes:

Sensitizers with Extended NIR Absorption for Solar Energy Conversion Applications

André Bessette[1,2], Mihaela Cibian[1], Dr Janaina G. Ferreira[1], Brian N. DiMarco[3], Francis Bélanger[2], Dr Denis Désilets[2], Gerald J. Meyer[3] and Prof. Garry S. Hanan[1].*

[1] Département de Chimie, Université de Montréal, Pavillon J.-A. Bombardier, 5155 Decelles Avenue, Montréal, Québec, H3T-2B1, Canada

[2] PCAS Canada Inc., 725 Trotter street, Saint-Jean-sur-Richelieu, Québec, J3B 8J8, Canada.

[3] Departments of Chemistry and Materials Science & Engineering, The University of North Carolina at Chapel Hill, Chapel Hill, North Carolina, 27599-3290, USA.

Table of Contents

Materials and Instrumentation

ADPM **1** was obtained from PCAS Canada Inc. and used as received. Literature procedures were used for the synthesis of complexes Ru(N^N)(MeOH)Cl_3 and Ru(tpy-Ph-Br)Cl_3.[1] Reagents and solvents were obtained commercially and used without further purification. Reactions were carried out under ambient atmosphere. Solvents were removed under reduced pressure using a rotary evaporator unless otherwise stated.

Nuclear magnetic resonance (NMR) spectra were recorded in $CDCl_3$ at room temperature (r.t.). 700 MHz ^{1}H and 175 MHz ^{13}C NMR of sensitizer **2** were obtained on a Bruker Avance 700. 500 MHz ^{1}H and 125 MHz ^{13}C NMR of sensitizers **3** and **4** were recorded on a Bruker Avance 500 spectrometer. 400 MHz ^{1}H of sensitizers **5** and **6** were recorded on a Bruker AV400 spectrometer, while the ^{13}C of the later was recorded on the Bruker Avance 700. Chemical shifts are reported in part per million (ppm) relative to residual solvent protons (7.27 ppm for chloroform-d and 2.50 ppm for DMSO-d_6) and the carbon resonance of the solvent (77.00 ppm for chloroform-d and 39.51 ppm for DMSO-d_6).

High-Resolution Electro Spray Ionization Mass Spectrometry (HR-ESIMS) was performed on a Liquid Chromatography / Mass Spectrometry with a Time of Flight detector (LC/MS TOF) from Agilent for sensitizer **2**. Compounds 3-6 were performed on a Bruker micrOTOF II.

Absorption spectra were measured in CH_2Cl_2 (DCM) at concentrations obeying Beer-Lambert's law at r.t. on a Cary 6000i UV-vis-NIR Spectrophotometer. The absence of fluorescence for the series of sensitizers investigated herein was assessed on a Cary Eclipse Fluorescence Spectrophotometer. The IR spectra were recorded on solid samples (powders) of the compounds, using a Perkin Elmer Spectrum Two FT-IR spectrometer equipped with an Universal Attenuated Total Reflectance Accessory (UATR).

Full details on crystal structure determination and refinement data for compounds **2**, **4** and **5** are reported in corresponding section of the ESI and on the Cambridge Crystallographic Data Centre (CCDC 1419506-1419508, respectively).

Electrochemical measurements were carried out in argon-purged CH_2Cl_2 at room temperature with a BAS CV50W multipurpose potentiostat. The working electrode used was a glassy carbon electrode for every compound. The counter electrode was a Pt wire, and the pseudo-reference electrode was a silver wire. The reference was set using an internal 1 mM ferrocene/ferrocenium sample at 0.46 V vs SCE in CH_2Cl_2. and 0.45 V vs SCE in DMF.[2] The concentration of the compounds was about 1 mM. Tetrabutylammonium hexafluorophosphate (TBAP) was used as supporting electrolyte and its concentration was 0.10 M. Cyclic voltammograms (CV) were obtained at scan rates of 50, 100, 200, and 500 mV/s. For reversible processes, half-wave potentials (vs. SCE) from CV were used. To establish the potential of irreversible processes, differential pulse voltammetry (DPV) experiments were performed with a step rate of 4 mV, a pulse height of 50 mV, and a frequency of 5 Hz. Criteria for reversibility were the separation of 60 mV between cathodic and anodic peaks, the close to unity ratio of the intensities of the cathodic and anodic currents, and the constancy of the peak potential on changing scan rate. In addition to the first electrochemical cycle with full sweep window reported in Figures S.15 – S.29, all processes were investigated independently to avoid complications from subsequent irreversible processes and further supported by DPV results before the final assignment was made.

Experimental uncertainties are as follows: absorption maxima, ±2 nm; molar absorption coefficient, 10%; IR stretch, ± 1 cm^{-1}; redox potentials, ± 10 mV.

Computational Methods

Computational modelization of sensitizers **2** – **6** was performed with the Gaussian 09 software (G09).[3] Geometry optimizations, frequency calculations and molecular orbital (MO) calculations were performed by DFT method under vacuum using the B3LYP[4] hybrid functional and 6-31G* as the basis set for all atoms except ruthenium, for which LanL2DZ was used. Crystallographic coordinates were used as starting points for geometry optimizations when available. When no crystallographic data were available for a given compound, modification of a similar derivative was used. Tight convergence criteria and no symmetry constraints were imposed during the optimization process. Only positive frequencies were found for the optimized structures. The 80 firsts absorption bands were calculated by TD-DFT (B3LYP / 6-31G* and LanL2DZ for Ru) from optimized structures with the PCM[5] of dichloromethane for sensitizers **2** – **6** and also of methanol for **6**. MOs were visualized (isovalue = 0.02) with GaussView 3 software.[6] GaussSum 6.5 was employed to extract from TD-DFT results the absorption energies and oscillator strengths, while molecular orbital energies were obtained from DFT.[7] Chemissian 4.23 program was used to represent MO's energy levels (Figure S.30) and determine the electronic distribution (in %) of the various parts of the sensitizers from DFT results and calculate the natural transition orbitals (NTO) (isovalue = 0.02) associated with absorption bands in the visible (> 400 nm) and NIR ranges obtained from TD-DFT results.[8]

Synthetic Methods

General procedure for sensitizers **2 – 4**

A suspension of ADPM **1** (1 equiv.), the corresponding Ru(N^N)(MeOH)Cl_3·MeOH (1 equiv.), and triethylamine (TEA) (6 equiv.) in a 9:1 *n*-butanol (13.5 mL) / MeOH (1.5 mL) solvent mixture was reacted in a microwave reactor at 150°C for 2 hours under magnetic stirring. The reaction mixture was evaporated to dryness, dissolved in CH_2Cl_2 and impregnated on silica. The crude product was purified by silica gel chromatography, isolated by evaporation and *in vacuo* drying to afford a black powder.

Sensitizer **2** *[Ru^{II}(ADPM)(2,2'-bpy)CO]*

ADPM **1** (100 mg; 0.175 mmol), Ru(2,2'-bpy)(MeOH)Cl_3·MeOH (75.0 mg; 0.175 mmol) and TEA (0.142 mL; 1.05 mmol). Black needles suitable for X-ray structural crystallized from slow evaporation of a concentrated solution in chlorobenzene. Yield = 87.5 mg (59 %). ^{1}H NMR ($CDCl_3$, 700 MHz) δ/ppm: 3.51 (s, 3 H), 3.76 (s, 3 H), 3.86 (s, 3 H), 3.91 (s, 3 H), 5.51 (d, J = 2.69 Hz, 1 H), 6.28 (s, 1 H), 6.31 (dd, J = 8.29, 2.46 Hz, 1 H), 6.48 (d, J = 8.29 Hz, 2 H), 6.86 - 6.94 (m, 4 H), 6.97 - 7.02 (m, 3 H), 7.06 (s, 1 H), 7.19 - 7.23 (m, 1 H), 7.41 (d, J = 8.29 Hz, 1 H), 7.53 (td, J = 7.73, 1.34 Hz, 1 H), 7.70 - 7.76 (m, 2 H), 7.87 (d, J = 8.73 Hz, 2 H), 7.89 (d, J = 8.06 Hz, 1 H), 8.09 (d, J = 5.82 Hz, 1 H), 8.16 (d, J = 8.73 Hz, 2 H), 8.82 (d, J = 5.15 Hz, 1 H). ^{13}C NMR ($CDCl_3$, 175 MHz) δ/ppm: 54.5, 55.2, 55.3, 55.4, 106.5 (2C), 111.5, 112.7 (2C), 113.3 (2C), 113.6 (2C), 117.4, 120.6, 120.8, 121.6, 125.2, 125.4, 125.6, 127.7, 128.2, 129.5, 130.0 (2C), 130.6 (2C), 130.7, 132.0, 136.3, 136.4, 142.6, 142.9, 144.3, 144.8, 149.3, 153.3, 153.9, 154.2, 158.5, 158.7, 158.9, 159.1, 163.9, 168.0, 179.1, 200.9. IR (powder): ν (CO) 1908 (s) cm^{-1}. Mass Spec (*m/z*); MS calcd for $C_{47}H_{37}N_5O_5Ru$: [M^+] 853.18327, found: 853.18673.

Sensitizer **3** *[Ru^{II}(ADPM)(4,4'-di-$^{t-}$Bu-2,2'-bpy)CO]*

ADPM **1** (79.1 mg; 0.139 mmol), Ru(4,4'-di-$^{t-}$Bu-2,2'-bpy)(MeOH)Cl_3·MeOH (75.0 mg; 0.139 mmol) and TEA (0.113 mL; 0.833 mmol). Yield = 34.6 mg (26 %). ^{1}H NMR ($CDCl_3$, 500 MHz) δ/ppm: 1.31 (s, 9 H), 1.42 (s, 9 H), 3.49 (s, 3 H), 3.78 (s, 3 H), 3.86 (s, 3 H), 3.91 (s, 3 H), 5.57 (d, J = 2.57 Hz, 1 H), 6.24 - 6.33 (m, 2 H), 6.51 (d, J = 8.80 Hz, 2 H), 6.88 - 7.02 (m, 7 H), 7.06 (s, 1 H), 7.20 (dd, J = 5.96, 1.93 Hz, 1 H), 7.40 (d, J = 8.25 Hz, 1 H), 7.68 (s, 1 H), 7.81 (s, 1 H), 7.85 - 7.95 (m, 3 H), 8.16 (d, J = 8.80 Hz, 2 H), 8.67 (d, J = 5.87 Hz, 1 H). ^{13}C NMR ($CDCl_3$, 125 MHz) δ/ppm: 30.4 (6C), 34.8, 35.1, 54.4, 55.1, 55.3, 55.4, 106.8 (2C), 111.5, 112.7 (2C), 113.3 (2C), 113.6 (2C), 117.1, 117.4, 118.0, 120.5, 122.4, 123.2, 125.3, 127.8, 128.3, 129.6, 130.0 (2C), 130.6 (2C), 131.0, 136.5, 142.7, 142.9, 144.0, 145.0, 148.7, 153.4, 153.5, 154.2, 156.9, 158.5, 158.7, 158.8, 159.1, 160.6, 163.8, 168.2, 180.0, 200.9. IR (powder): ν (CO) 1909 (s) cm^{-1}. Mass Spec (*m/z*); MS calcd for $C_{55}H_{53}N_5O_5Ru$: [M$^+$] 965.3100, found: 965.3083.

Sensitizer **4** *[Ru^{II}(ADPM)(1,10-phen)CO]*

ADPM **1** (94.6 mg; 0.166 mmol), Ru(1,10-phen)(MeOH)Cl_3·MeOH (75.0 mg; 0.166 mmol) and TEA (0.135 mL; 0.996 mmol). Yield = 50.1 mg (34 %). ^{1}H NMR ($CDCl_3$, 500 MHz) δ/ppm: 3.41 (s, 3 H), 3.76 (s, 3 H), 3.86 (s, 3 H), 3.87 (s, 3 H), 5.46 (d, J = 2.57 Hz, 1 H), 6.17 (s, 1 H), 6.23-6.29 (m, 3 H), 6.59 (d, J = 7.70 Hz, 2 H), 6.89 - 6.93 (m, 2 H), 6.93 - 6.98 (m, 2 H), 7.08 (s, 1 H), 7.31 (dd, J = 8.16, 5.23 Hz, 1 H), 7.40 (d, J = 8.44 Hz, 1 H), 7.44 (dd, J = 8.07, 5.14 Hz, 1 H), 7.77 (d, J = 1.83 Hz, 2 H), 7.83 - 7.88 (m, 2 H), 7.99 (dd, J = 8.25, 1.28 Hz, 1 H), 8.06 (dd, J = 8.07, 1.47 Hz, 1 H), 8.12 - 8.17 (m, 2 H), 8.32 (dd, J = 5.14, 1.47 Hz, 1 H), 9.11 (dd, J = 5.32, 1.10 Hz, 1 H). ^{13}C NMR ($CDCl_3$, 125 MHz) δ/ppm: 54.4, 55.1, 55.28, 55.33, 106.3 (2C), 111.6,

112.4 (2C), 113.3 (2C), 113.6 (2C), 117.5, 121.0, 124.4, 124.5, 125.5, 126.5, 126.9, 127.7, 128.2, 129.0, 129.2, 129.7, 130.1 (2C), 130.6 (2C), 130.7, 131.0, 135.2, 136.4, 142.9, 143.1, 144.2, 144.4, 145.0, 146.2, 149.1, 153.0, 158.3, 158.7, 158.8, 159.2, 164.0, 168.1, 178.9, 201.4. IR (powder): ν (CO) 1908 (s) cm^{-1}. Mass Spec (*m/z*); MS calcd for $C_{49}H_{37}N_5O_5Ru$: [M^+] 877.1846, found: 877.1876.

Sensitizer **5** *[Ru^{II}(ADPM)(Br-Ph-tpy)]*

ADPM **1** (0.956 g; 1.68 mmol), Ru(Br-Ph-tpy)Cl_3 (1.00 g; 1.68 mmol) and KO^{t}Bu (0.198 g; 1.68 mmol) were suspended in 75 mL of *n*-butanol. TEA (1.36 mL; 10.1 mmol) was added and the reaction mixture was refluxed for 72 hours under inert atmosphere and protected from light. The reaction mixture was evaporated to dryness, dissolved in CH_2Cl_2, washed with water (x3) and the organic layer was dried over anhydrous Na_2SO_4 and evaporated. Recrystallization in hot CH_2Cl_2 / heptane, filtration, heptane washes and *in vacuo* drying afforded the product as a black solid that was quickly took to the next step due to instability in solution. A X-ray quality crystal was isolated from the brown residue obtained after slow diffusion of heptane in a concentrated solution in CH_2Cl_2. Yield = 1.19 g (76 %). ^{1}H NMR ($CDCl_3$, 400 MHz) δ/ppm: 3.45 (s, 3 H), 3.81 (s, 3 H), 3.88 (s, 3 H), 4.31 (s, 3 H), 6.15 (s, 4 H), 6.77 (d, J = 8.30 Hz, 2 H), 7.13-7.22 (m, 2 H), 7.55-7.67 (m, 5 H), 7.70 (d, J = 8.30 Hz, 3 H), 7.77-7.88 (m, 5 H), 7.89-7.99 (m, 2 H), 8.07 (d, J = 8.48 Hz, 2 H), 8.61 (s, 2 H), 8.96 (br.s., 2 H), 9.24 (br. s., 1 H), 9.34 (br. s., 1 H). Mass Spec (*m/z*); MS calcd for $C_{57}H_{43}N_6O_4RuBr$: [M^+] 1056.1577, found: 1056.1537.

Sensitizer **6** *[Ru^{II}(ADPM)(tpy-Ph_2-COOH)]*

Sensitizer **5** (100 mg; 0.095 mmol) and 4-carboxyphenylboronic acid (23.5 mg; 0.142 mmol) were dissolved in 5 mL of THF. A 2M aqueous solution of K_2CO_3 (0.12 mL; 0.240 mmol) was added and the reaction mixture was degassed. $Pd(PPh_3)_4$ (11 mg; 0.009 mmol) was added and the reaction mixture was refluxed for 12 hours. The reaction mixture was allowed to cool down, filtered and the precipitate obtained was washed with cool THF followed by heptane. The isolated dark solid was further suspended in water, stirred, filtered and washed with isopropanol and methyl *t*-butyl ether (MTBE). Vacuum drying afforded the product as a black solid. Yield = 63.5 mg (61 %). ^{1}H NMR (DMSO-d_6, 400 MHz) (Poorly soluble) δ/ppm: 3.37 (br.s., 3 H), 3.43 (s, 3 H), 3.79 (s, 3 H), 4.03 (s, 3 H), 5.88 (d, J = 7.95 Hz, 2 H), 6.26 (d, J = 7.42 Hz, 2 H), 6.89 (d, J = 8.48 Hz, 3 H), 7.28 (d, J = 4.24 Hz, 3 H), 7.68 (s, 2H), 7.77-7.92 (m, 9 H), 7.95-8.11 (m, 8 H), 8.37 (d, J = 8.48 Hz, 2 H), 8.61 (d, J = 7.59 Hz, 2 H), 9.08 (s, 2 H). ^{13}C NMR (DMSO-d_6, 175 MHz) δ/ppm: 53.6, 54.5, 55.1, 55.2, 104.8 (2C), 112.3 (2C), 113.2 (2C), 113.4 (2C), 118.3, 122.3, 124.8, 125.9, 126.0 (2C), 126.1, 126.8, 127.1 (2C), 127.3 (2C), 127.5, 127.8, 127.9 (2C), 128.0, 128.7, 128.79, 128.84, 129.0, 129.1, 129.75, 129.78, 129.81, 129.83, 129.88 (2C), 129.93 (2C), 131.2, 131.45, 131.50, 132.6, 134.4, 137.3, 139.1, 142.4 (2C), 154.74, 154.75, 157.4, 157.8 (2C), 157.9 (2C), 158.1 (2C), 158.8, 167.7 (2C), 172.1. Mass Spec (*m/z*); MS calcd for $C_{64}H_{48}N_6O_6Ru$: [M^+] 1098.2691, found: 1098.2658.

NMR Characterization

Figure S.1 – ^{1}H of ADPM sensitizer **2** ($CDCl_3$; 700 MHz)

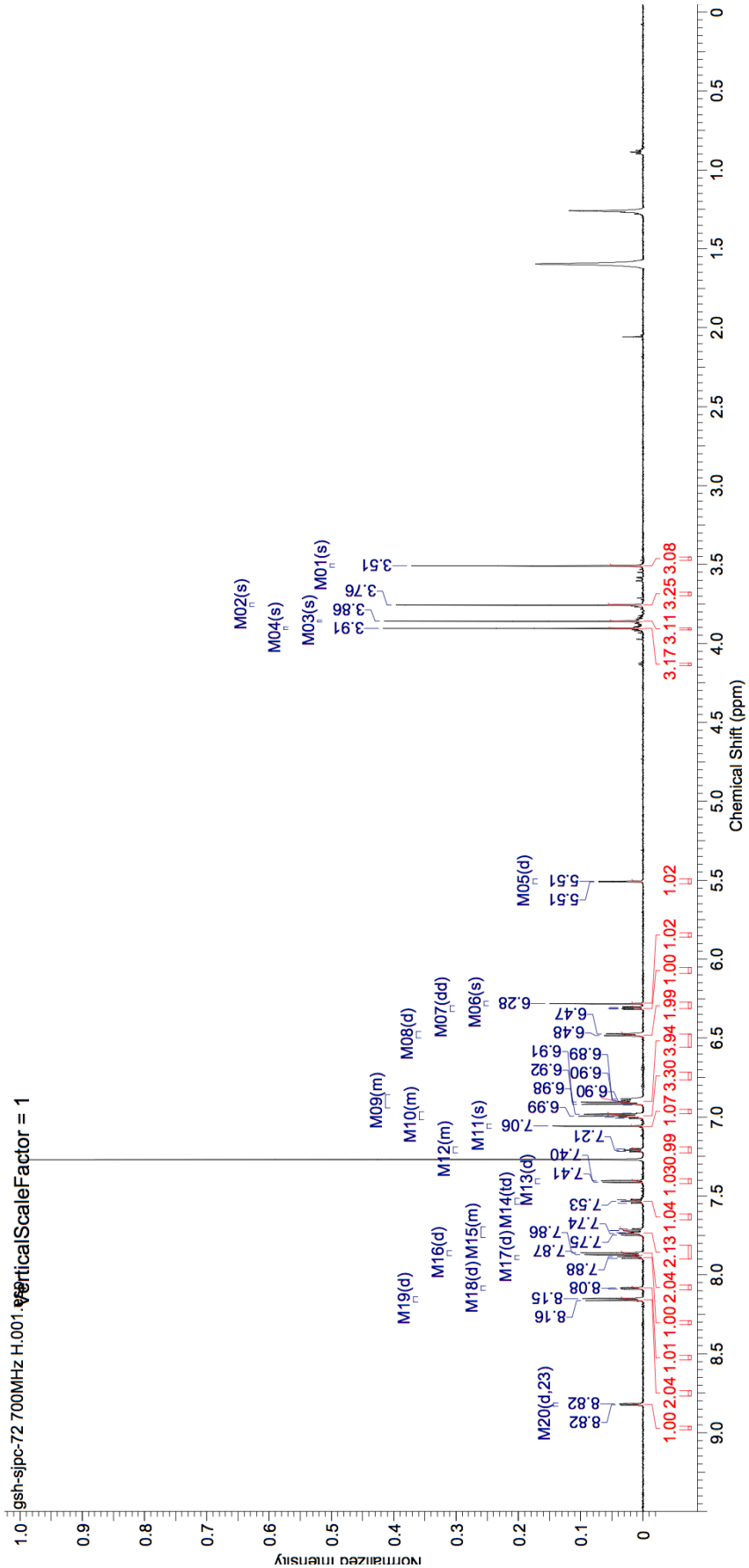

Figure S.2 – ^{13}C of ADPM sensitizer **2** ($CDCl_3$; 175 MHz)

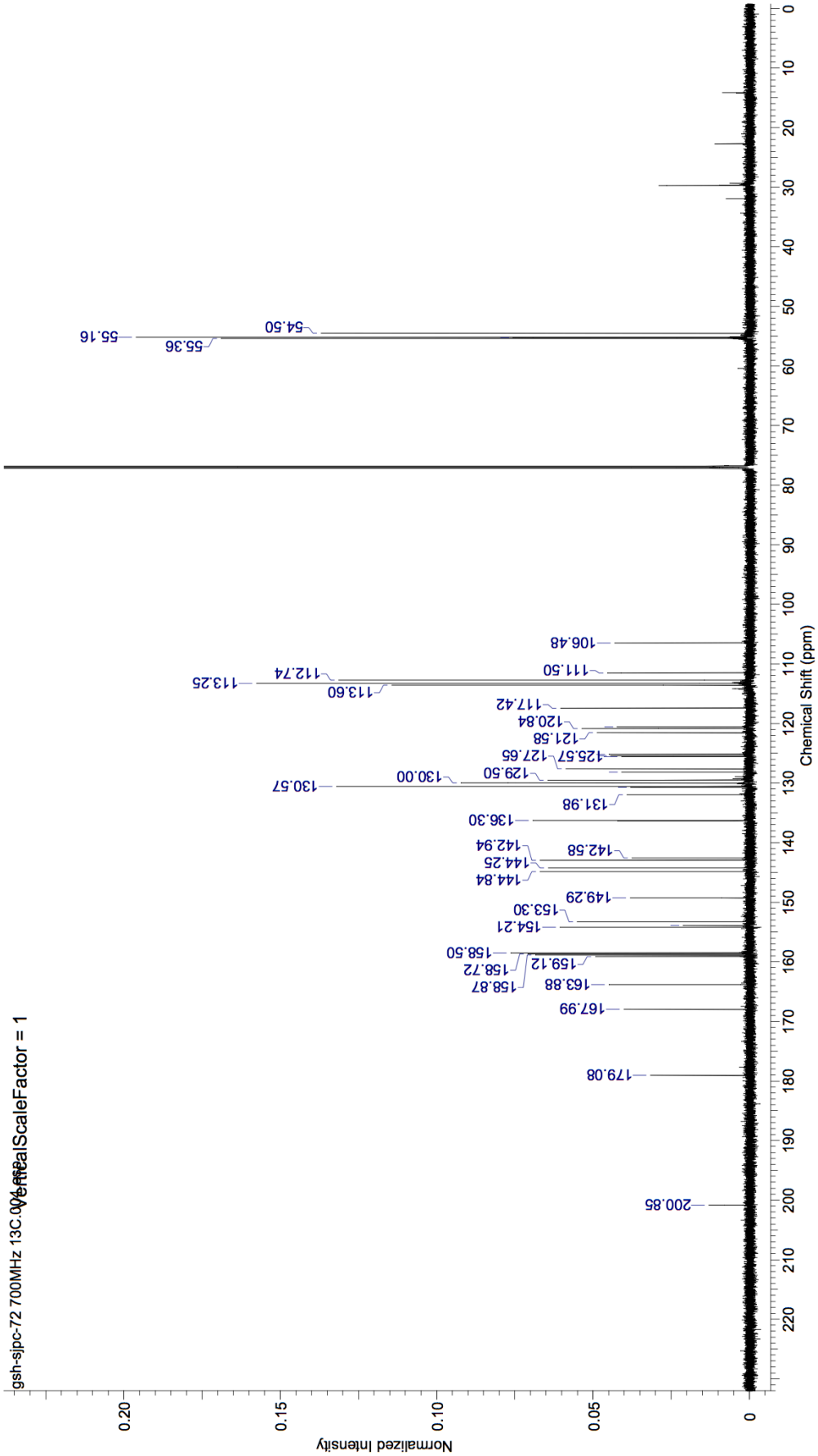

Figure S.3 – ^{1}H of ADPM sensitizer **3** ($CDCl_3$; 500 MHz)

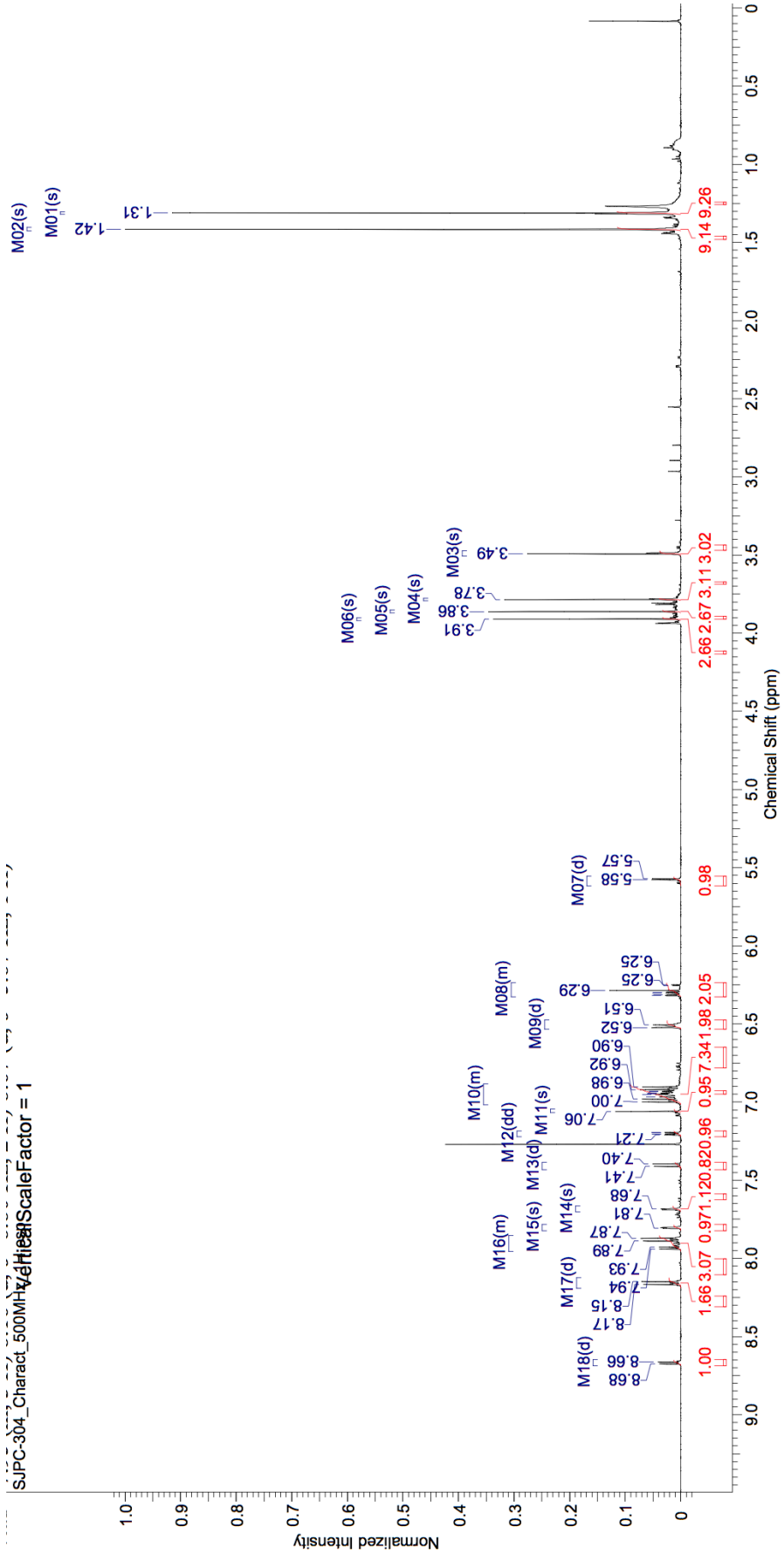

Figure S.4 – ^{13}C of ADPM sensitizer **3** ($CDCl_3$; 125 MHz)

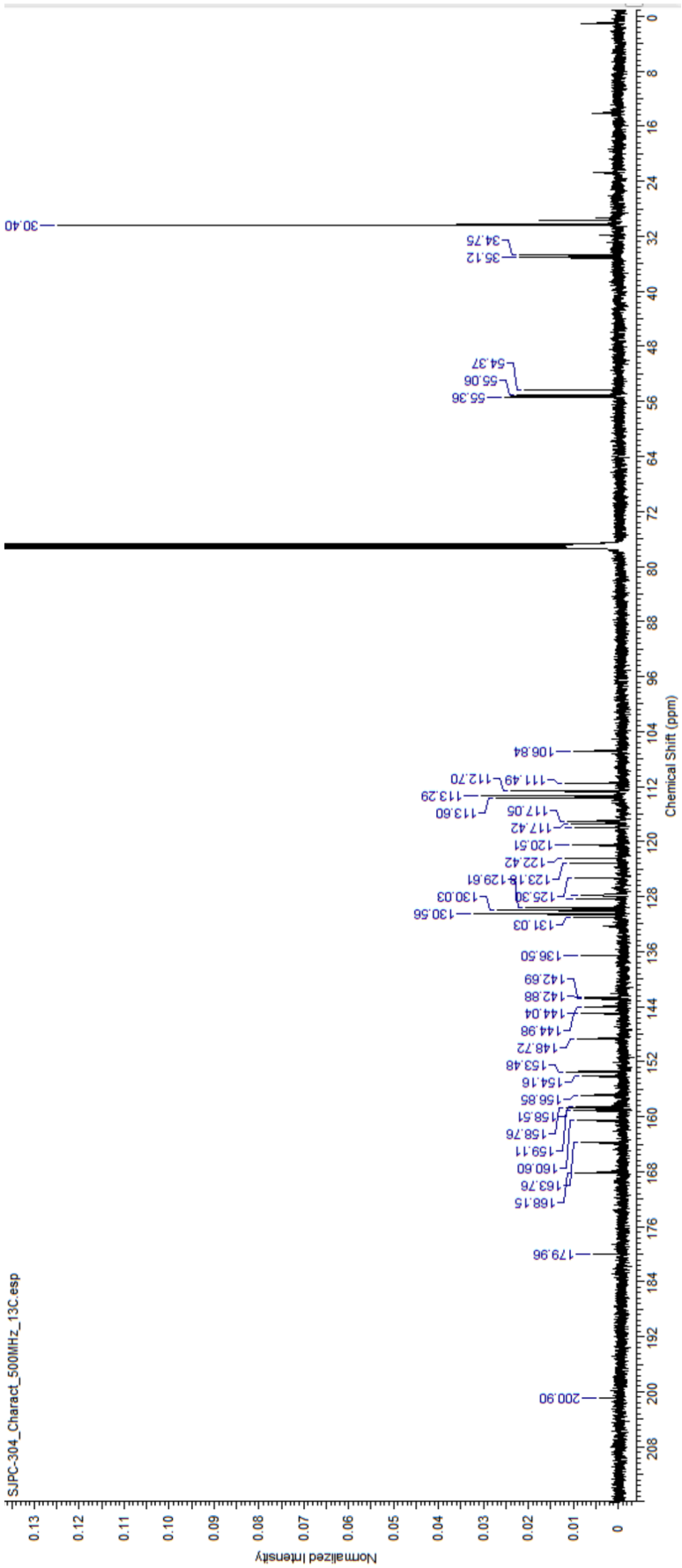

Figure S.5 – ^{1}H of ADPM sensitizer **4** ($CDCl_3$; 500 MHz)

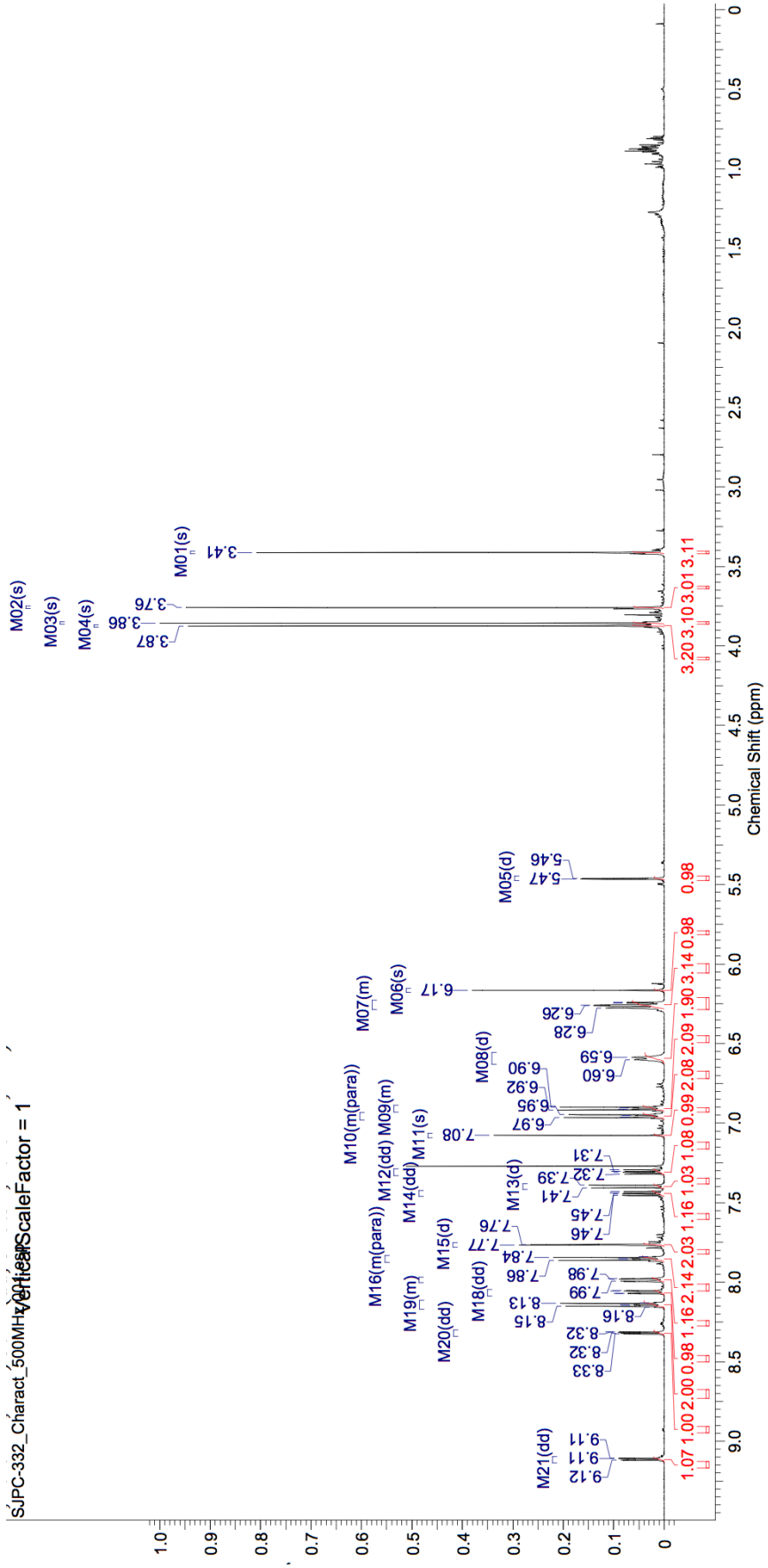

Figure S.6 – ^{13}C of ADPM sensitizer **4** ($CDCl_3$; 125 MHz)

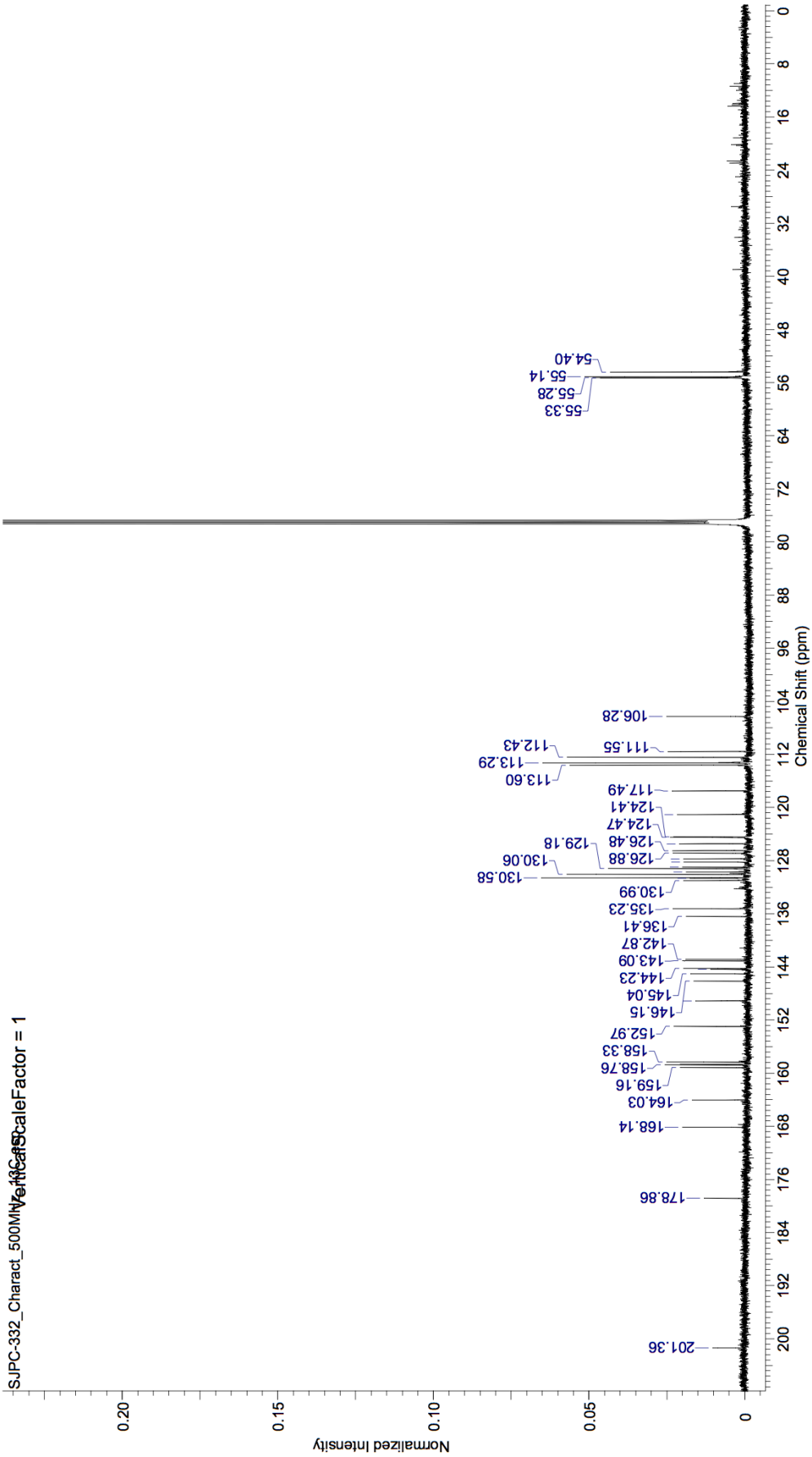

Figure S.7 – ^{1}H of ADPM sensitizer **5** ($CDCl_3$; 400 MHz)

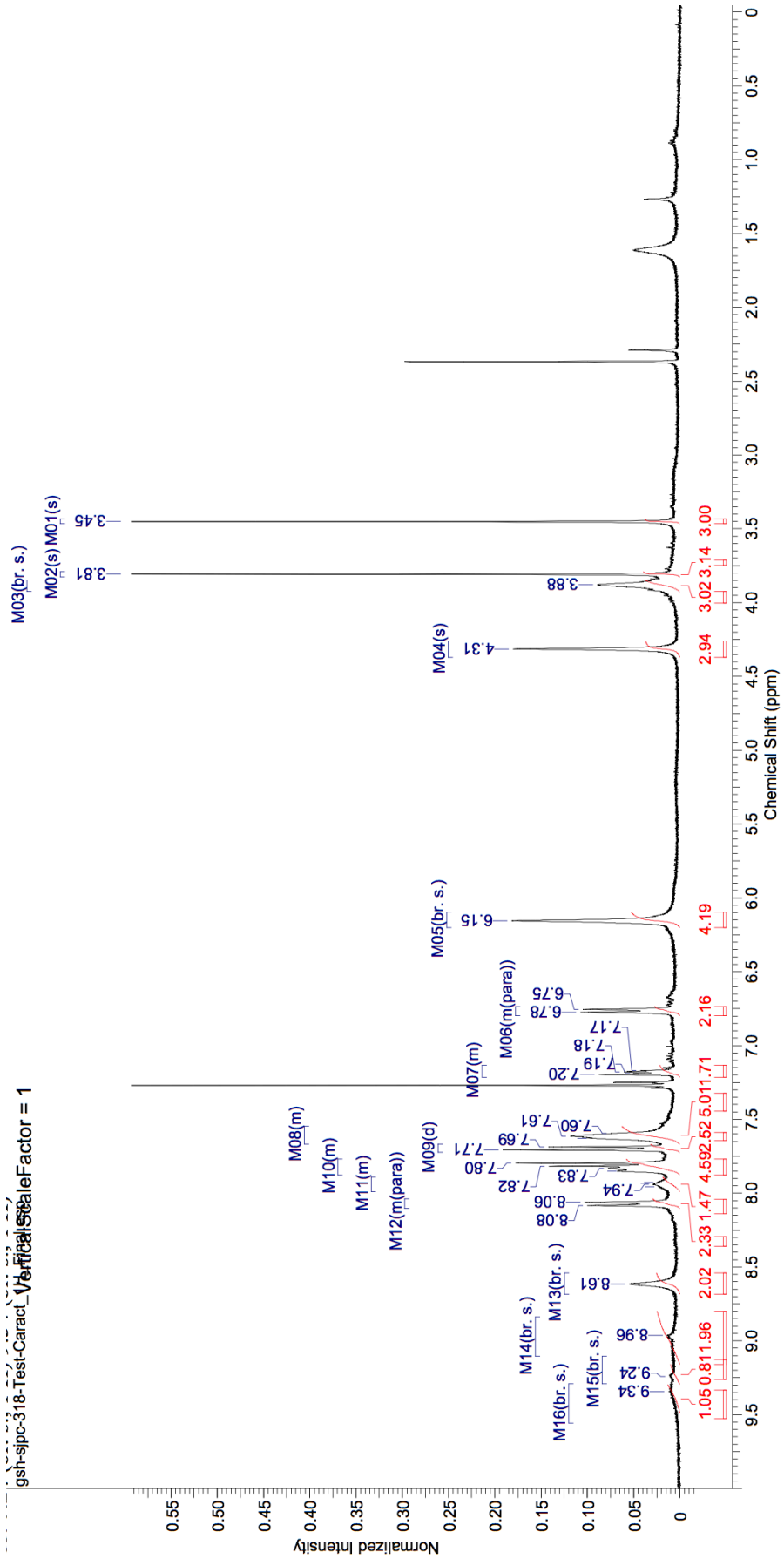

Figure S.8 – ^{1}H of ADPM sensitizer **6** (DMSO-d_6; 400 MHz)

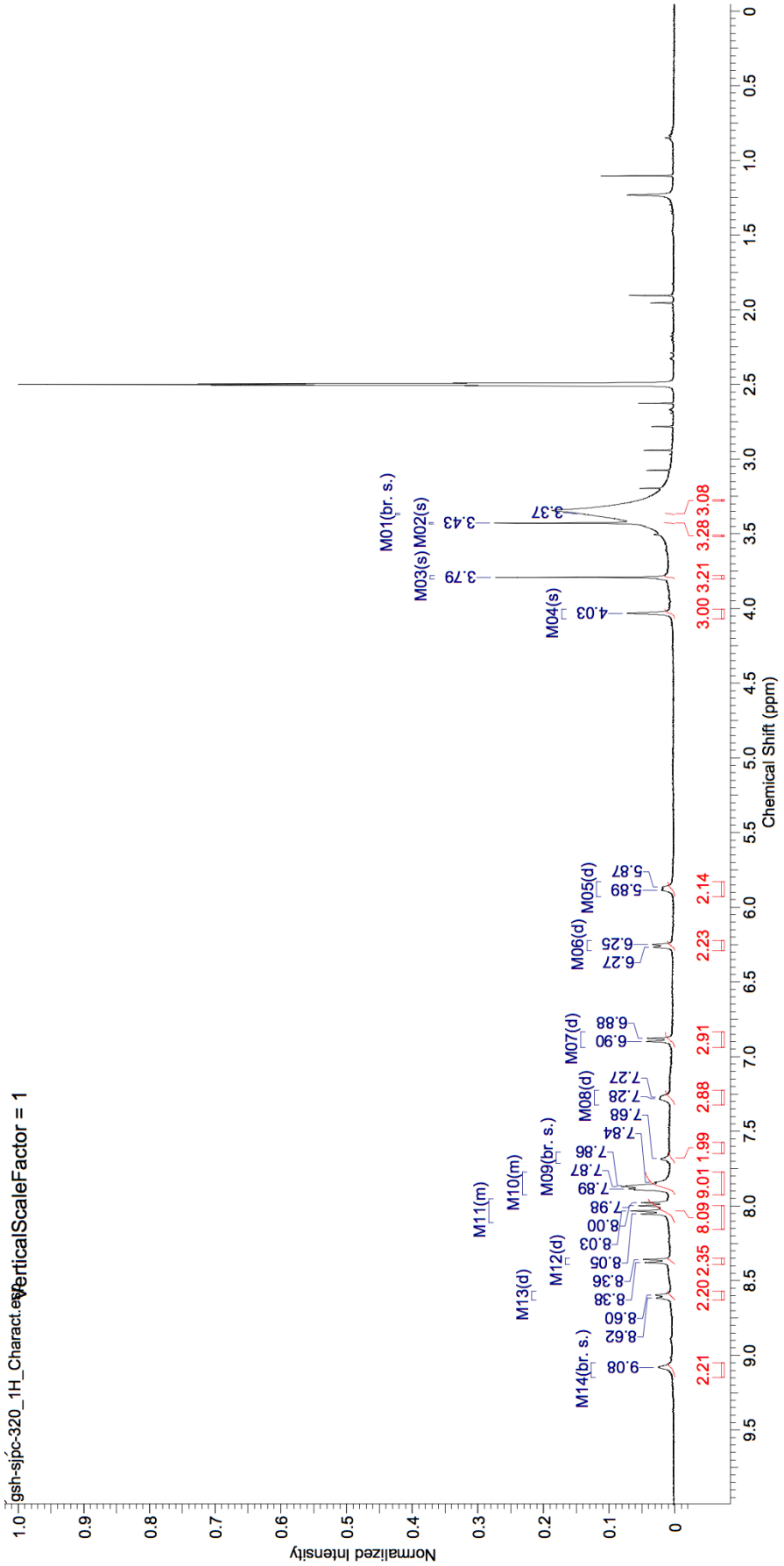

Figure S.9 – ^{13}C of ADPM sensitizer **6** (DMSO-d_6; 175 MHz)

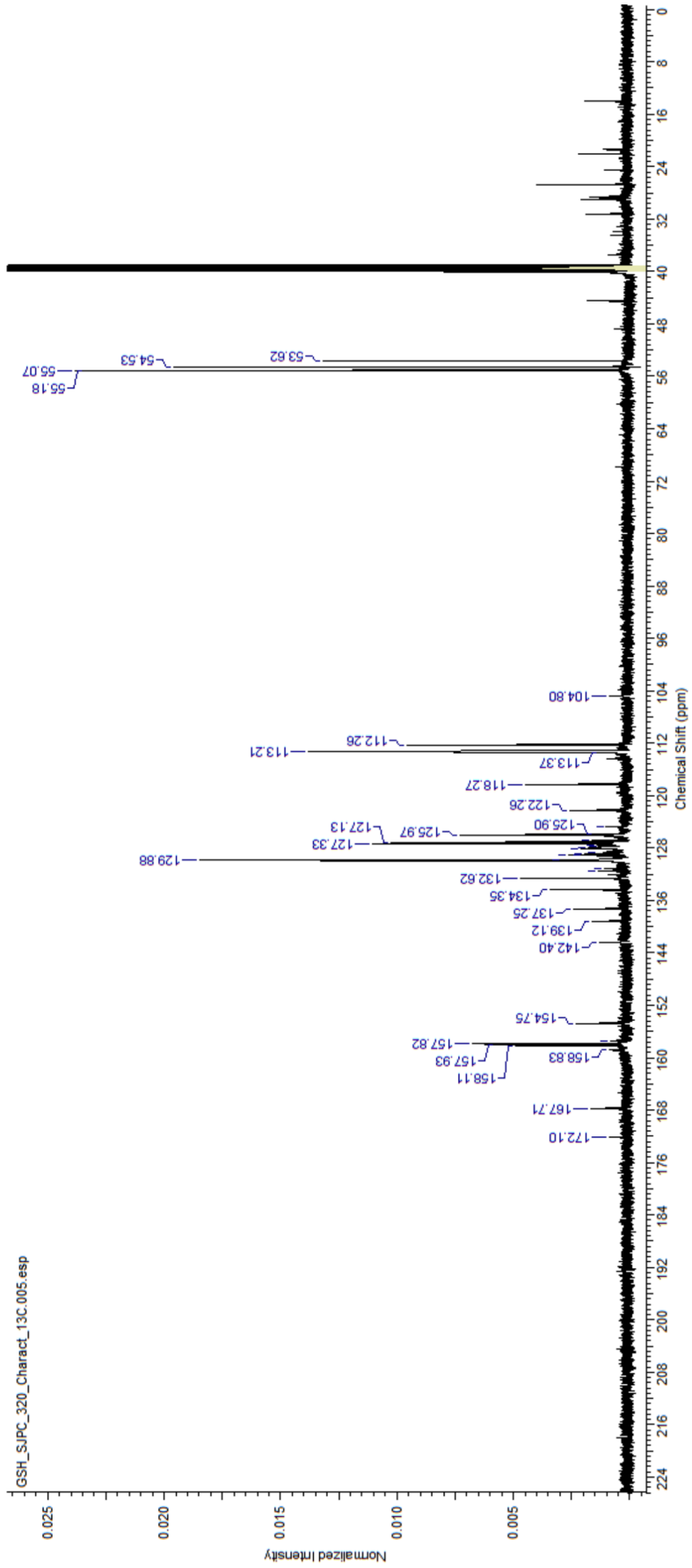

High-Resolution Mass Spectrometry (HRMS) Characterization

Figure S.10 – HRMS of ADPM sensitizer **2**

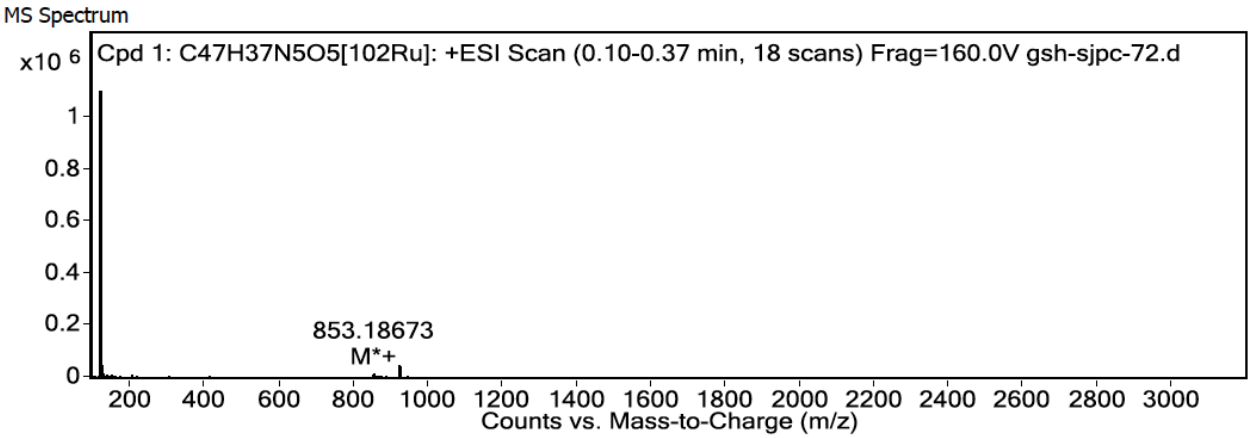

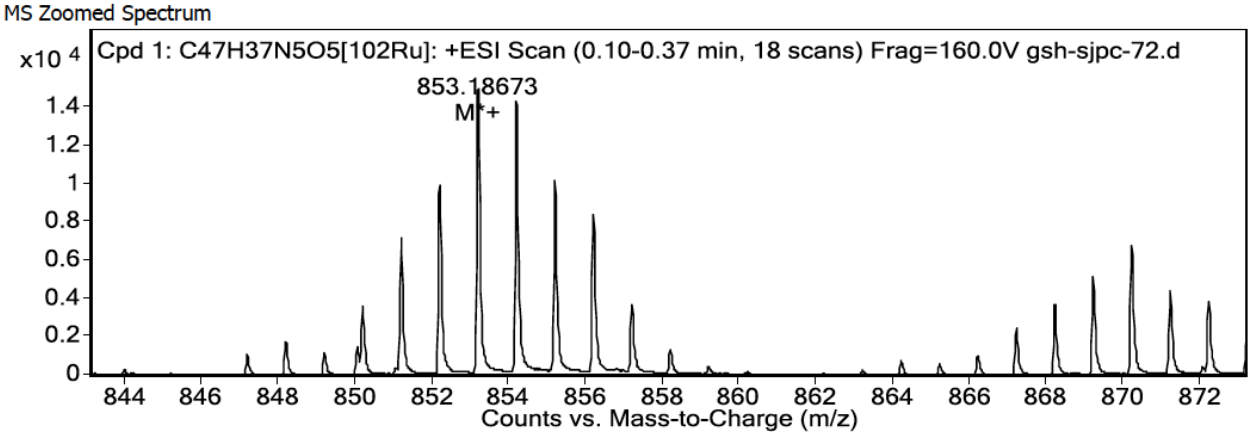

MS Spectrum Peak List

Ion	Ion Formula	Abund	*Expe. m/z*	*Calc. m/z*	Diff(ppm)
		1100181	118.12249		
M*+	C47 H37 N5 O5 [102Ru]	15270	853.18673	853.18327	4.05

Figure S.11 – HRMS of ADPM sensitizer **3**

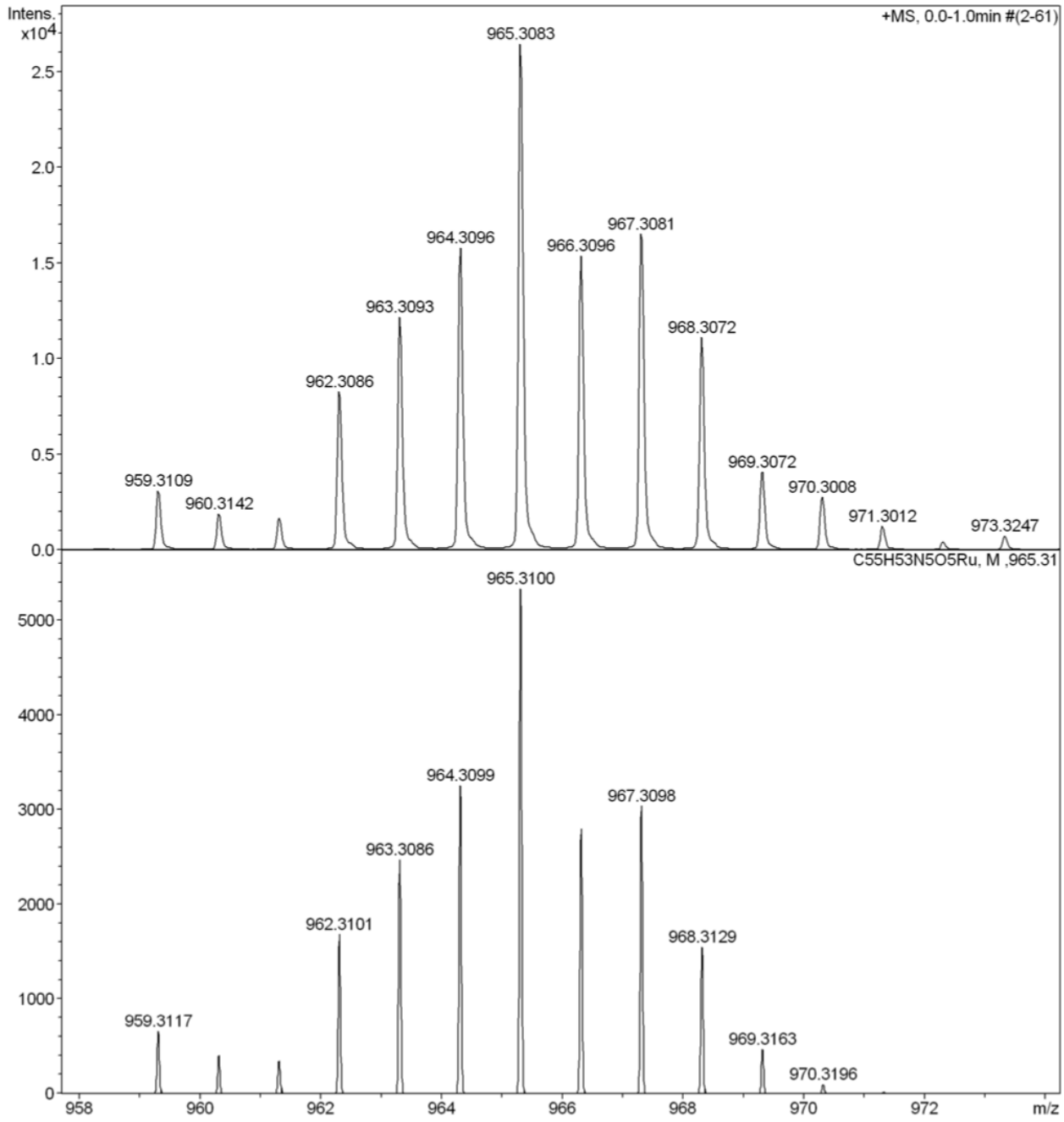

Figure S.12 – HRMS of ADPM sensitizer **4**

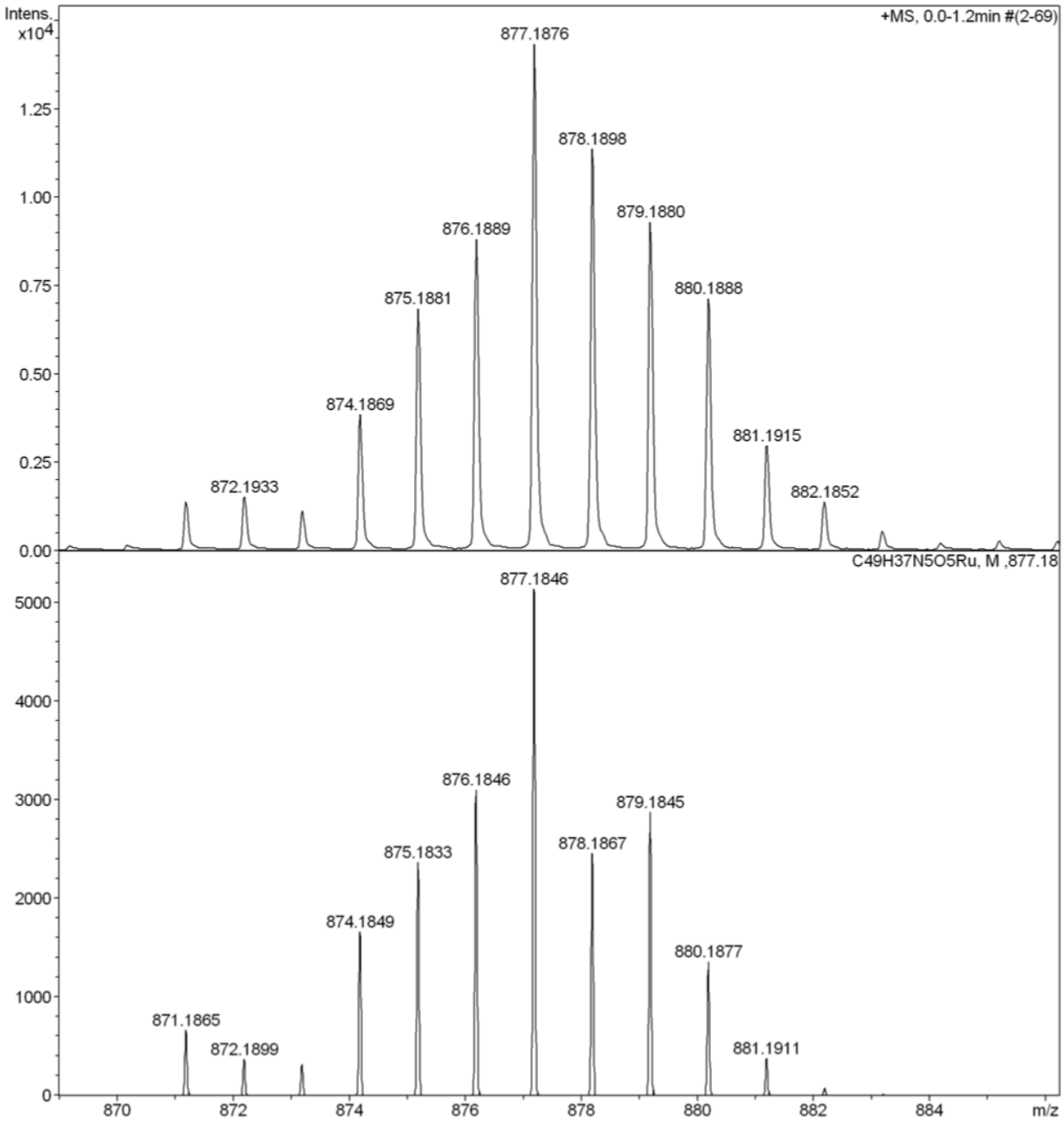

Figure S.13 – HRMS of ADPM sensitizer **5**

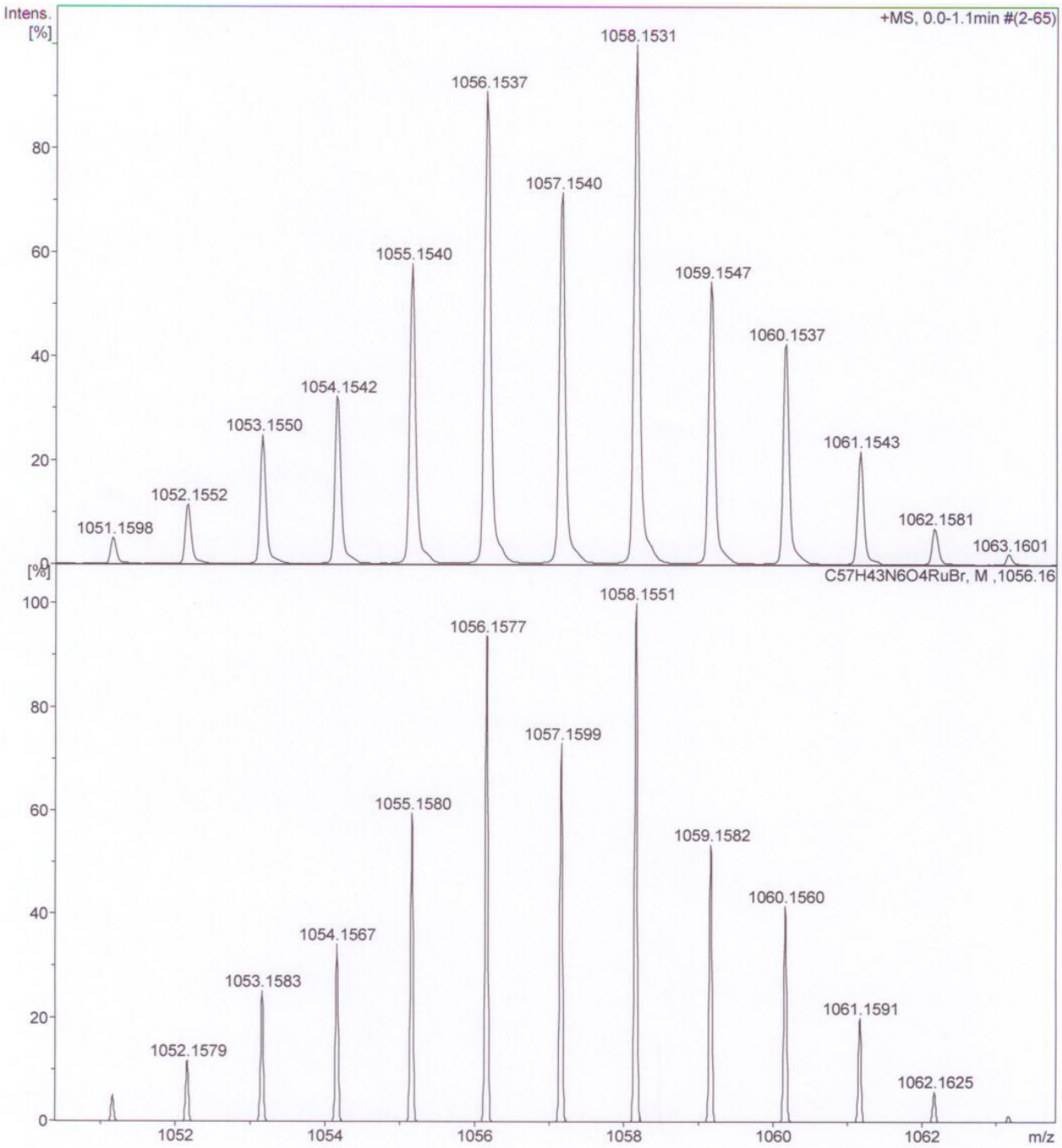

Figure S.14 – HRMS of ADPM sensitizer **6**

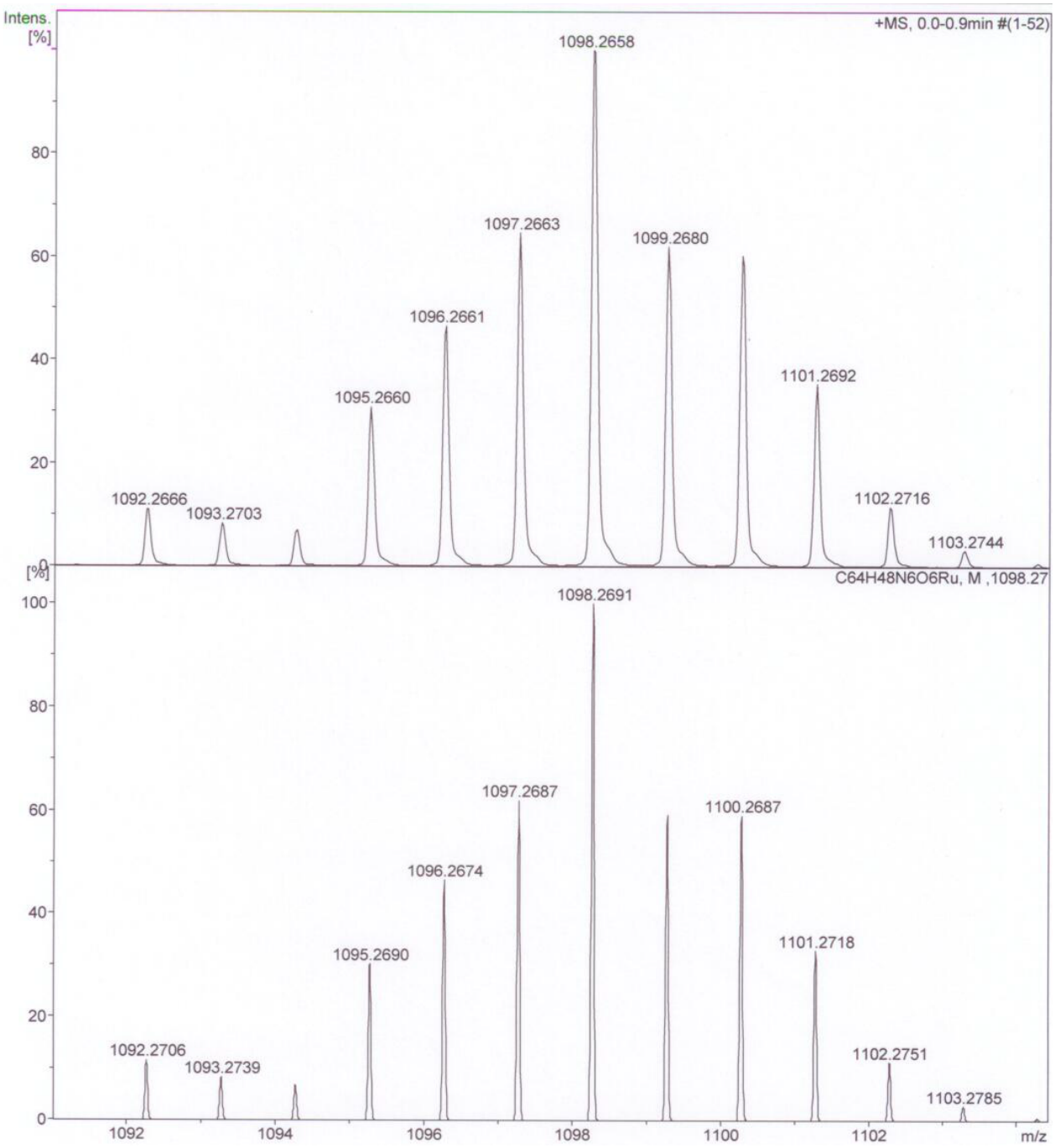

Electrochemistry

Figure S.15 – CV of ADPM sensitizer **2** before (top) and after addition of ferrocene internal reference (bottom). (Fc = 0.46 V vs SCE in DCM) (1st scan; 50 mV/s at R.T.)

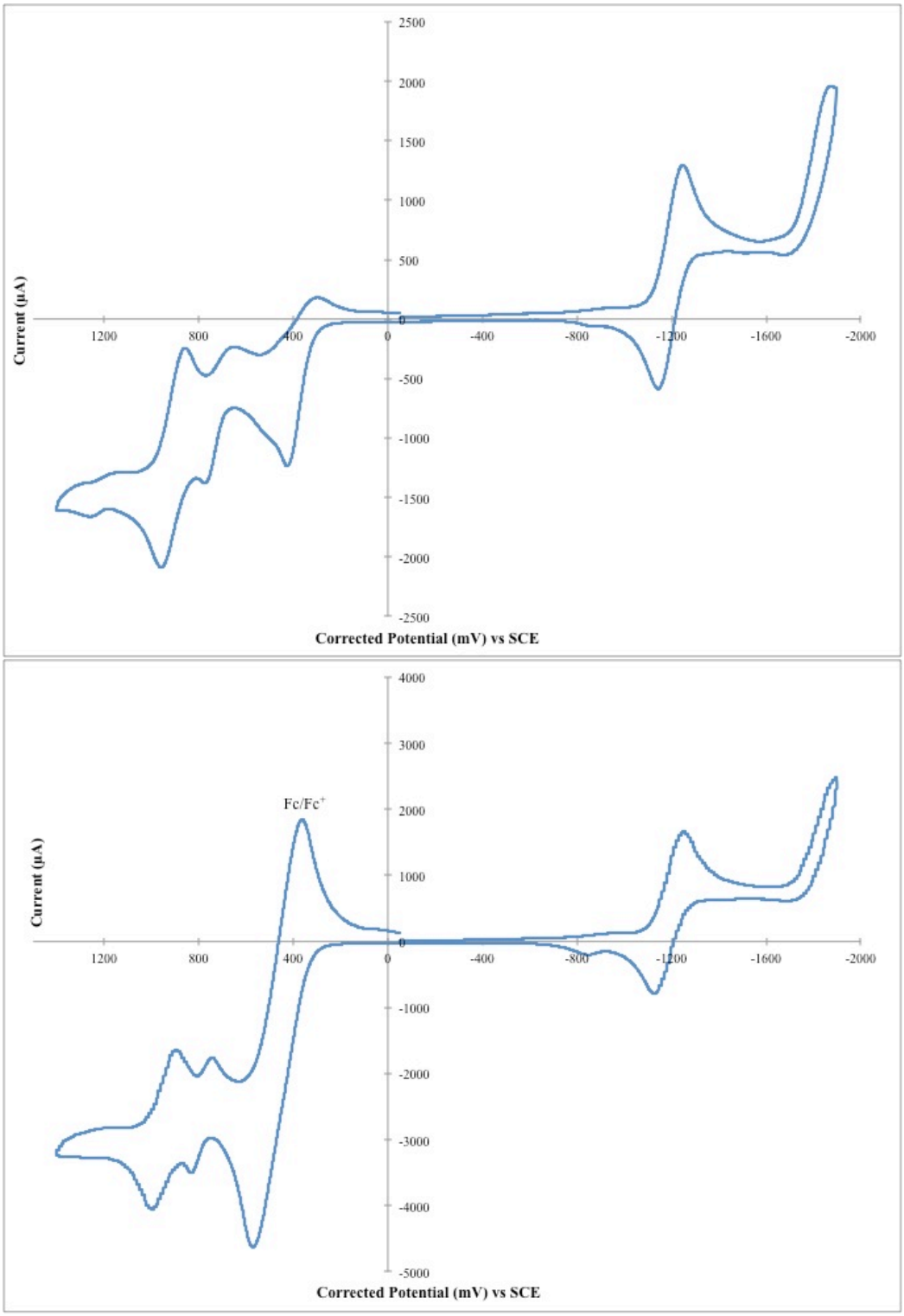

Figure S.16 – DPV of oxidation potentials for ADPM sensitizer **2** before (top) and after addition of ferrocene internal reference (bottom). (0.46 V vs SCE in DCM) (1st scan; 50 mV/s at R.T.)

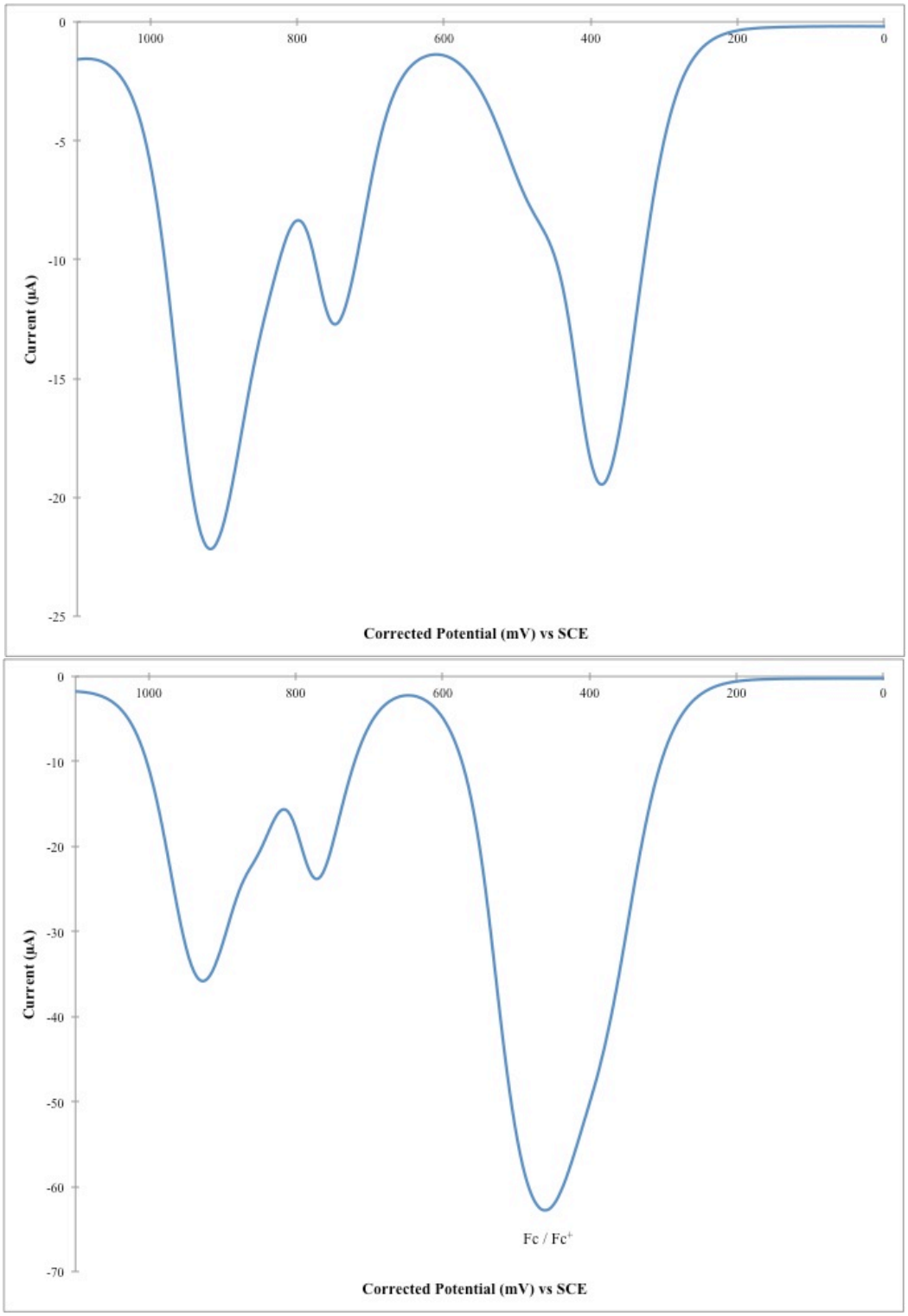

Figure S.17 – DPV of reduction potentials for ADPM sensitizer **2** before (top) and after addition of ferrocene internal reference (bottom). (0.46 V vs SCE in DCM) (1st scan; 50 mV/s at R.T.)

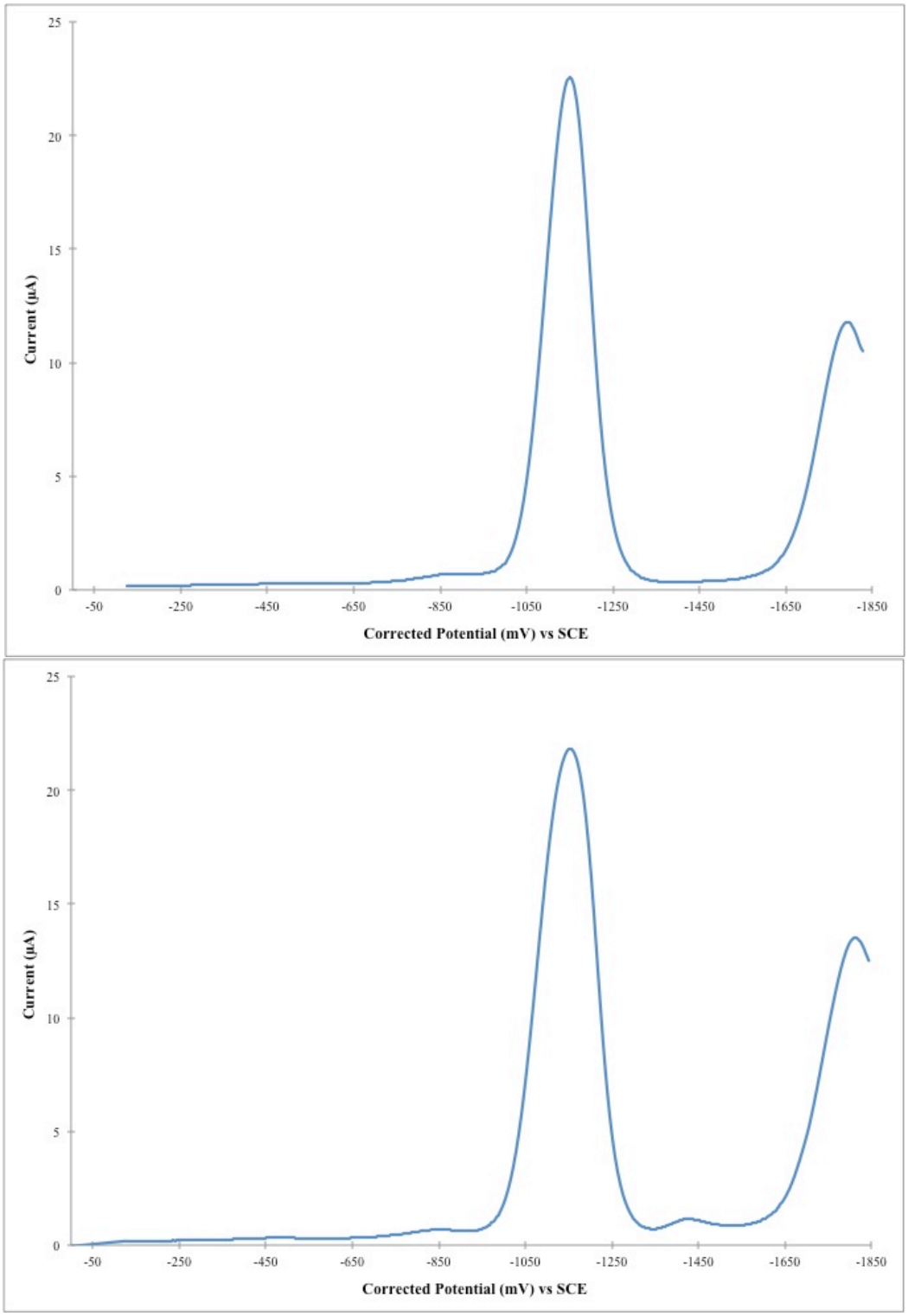

Figure S.18 – CV of ADPM sensitizer **3** before (top) and after addition of ferrocene internal reference (bottom). (0.46 V vs SCE in DCM) (1st scan; 50 mV/s at R.T.)

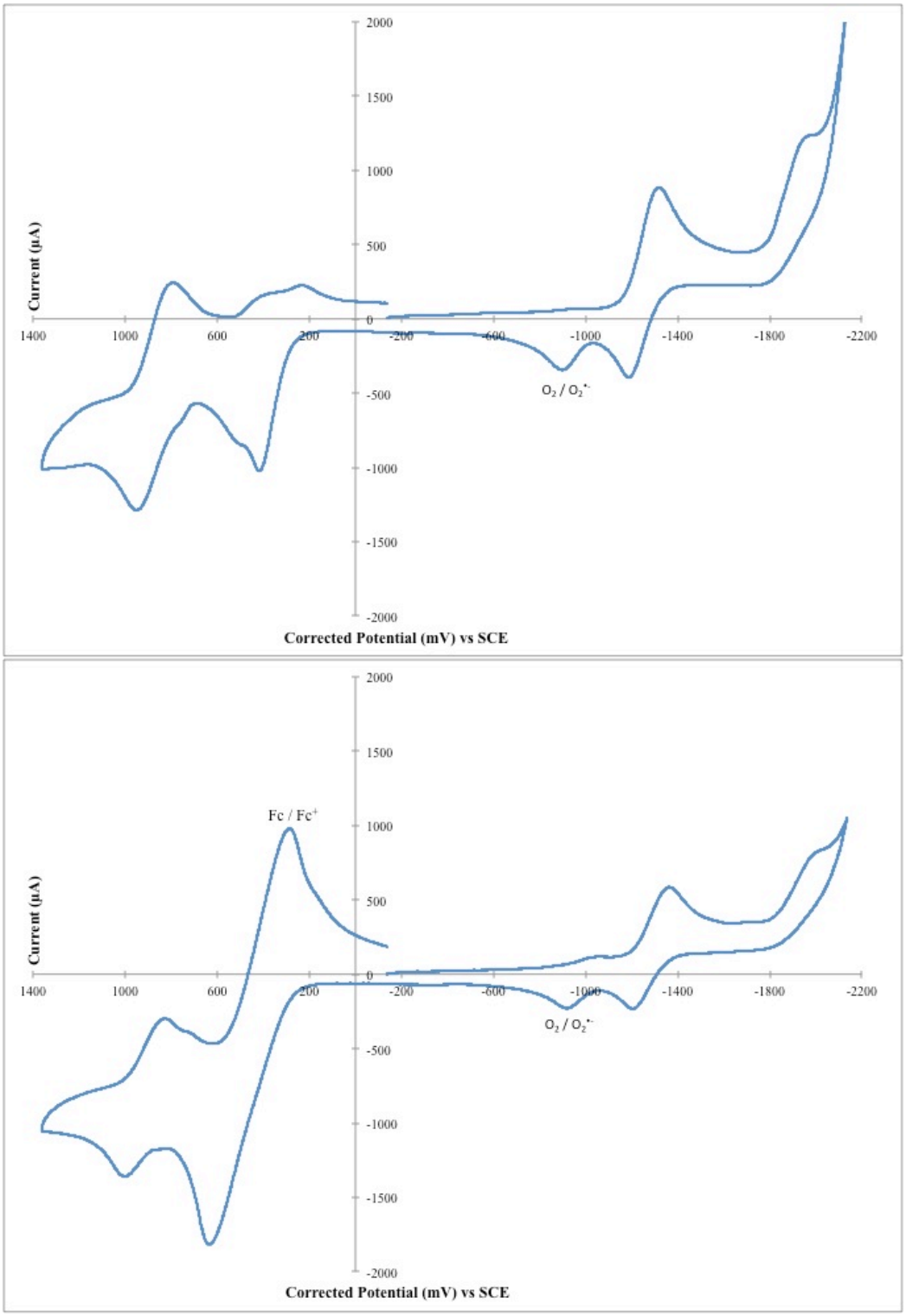

Figure S.19 – DPV of oxidation potentials for ADPM sensitizer **3** before (top) and after addition of ferrocene internal reference (bottom). (0.46 V vs SCE in DCM) (1st scan; 50 mV/s at R.T.)

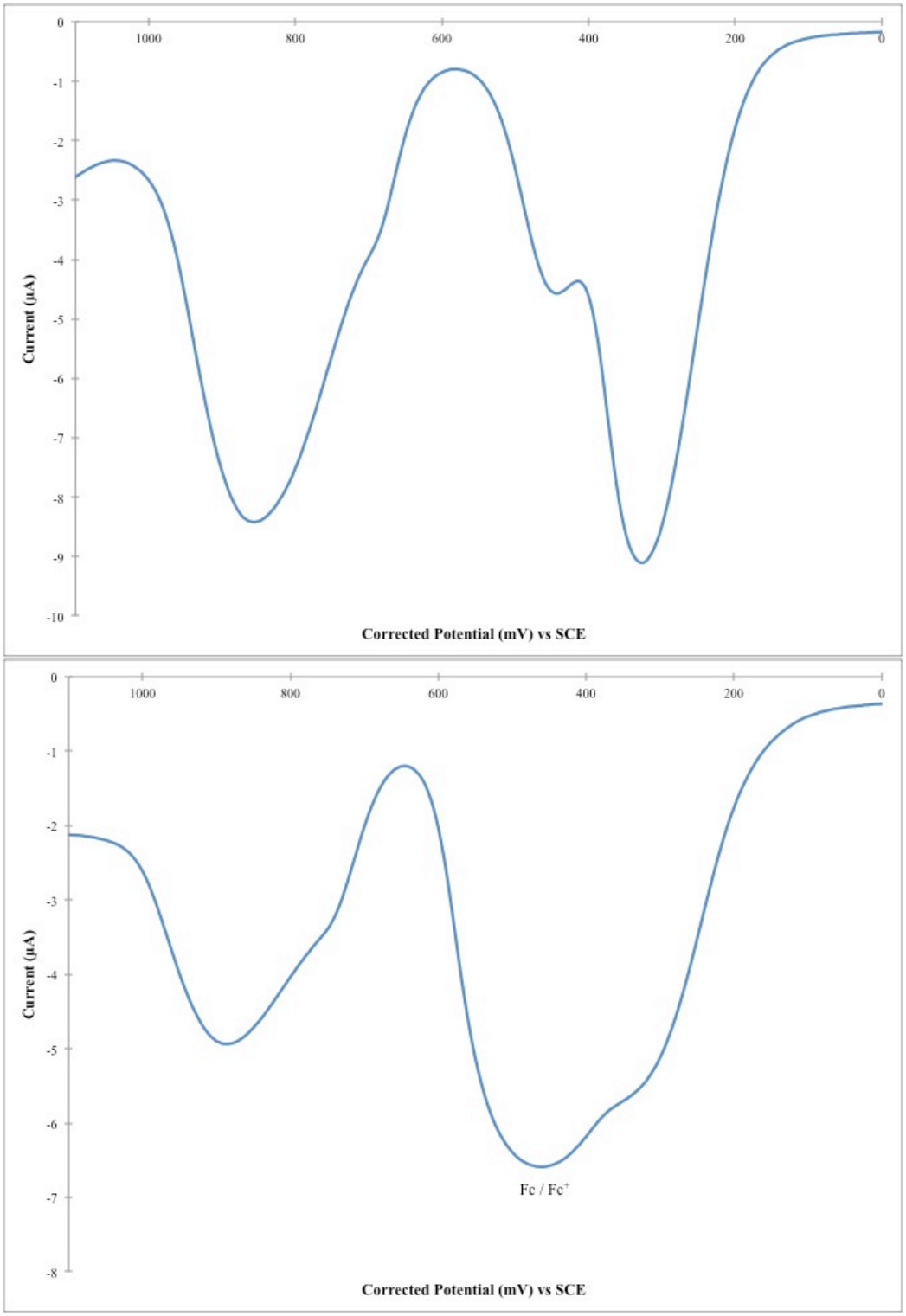

Figure S.20 – DPV of reduction potentials for ADPM sensitizer **3** before (top) and after addition of ferrocene internal reference (bottom). (0.46 V vs SCE in DCM) (1st scan; 50 mV/s at R.T.)

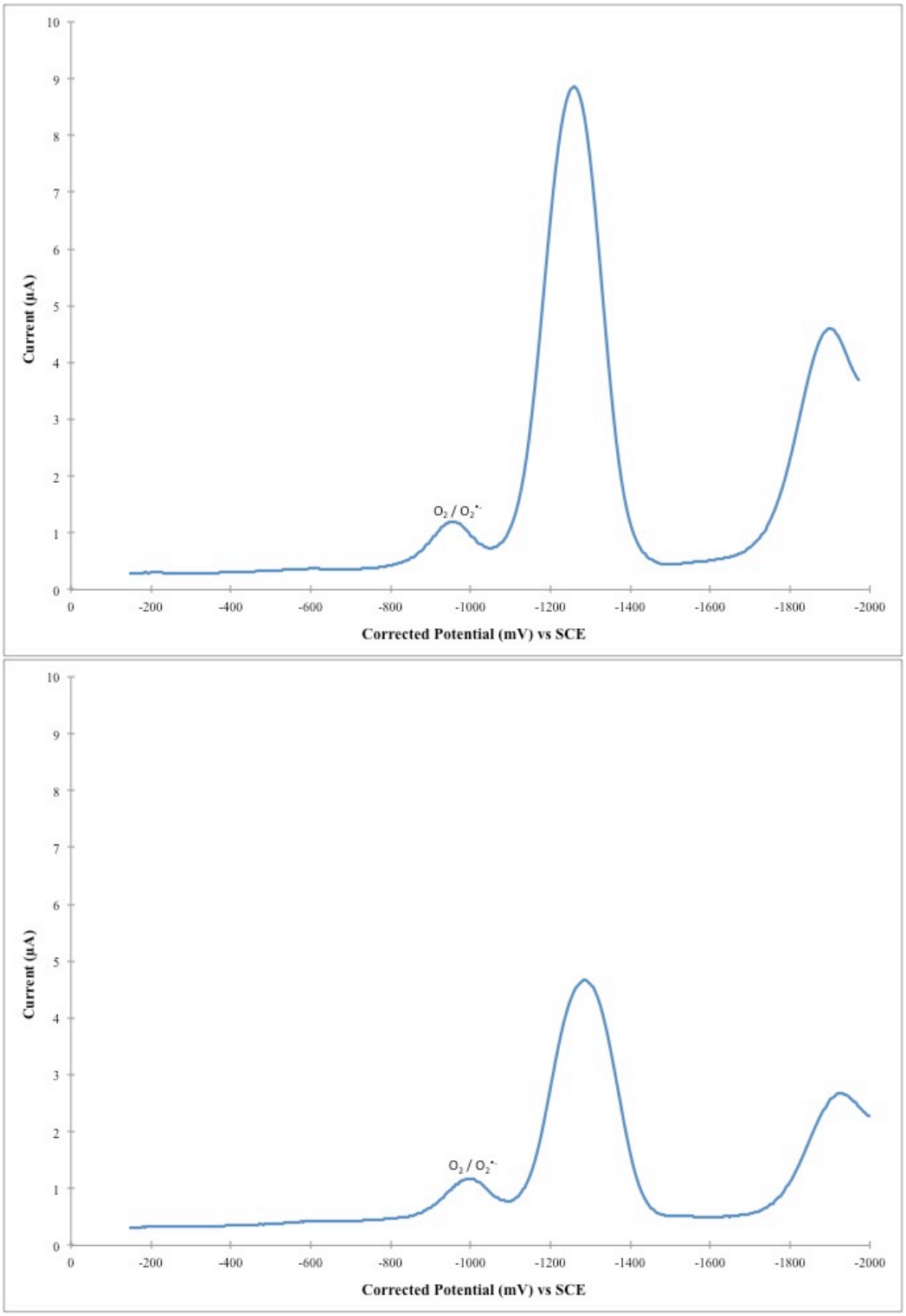

Figure S.21 – CV of ADPM sensitizer **4** before (top) and after addition of ferrocene internal reference (bottom). (0.46 V vs SCE in DCM) (1st scan; 50 mV/s at R.T.)

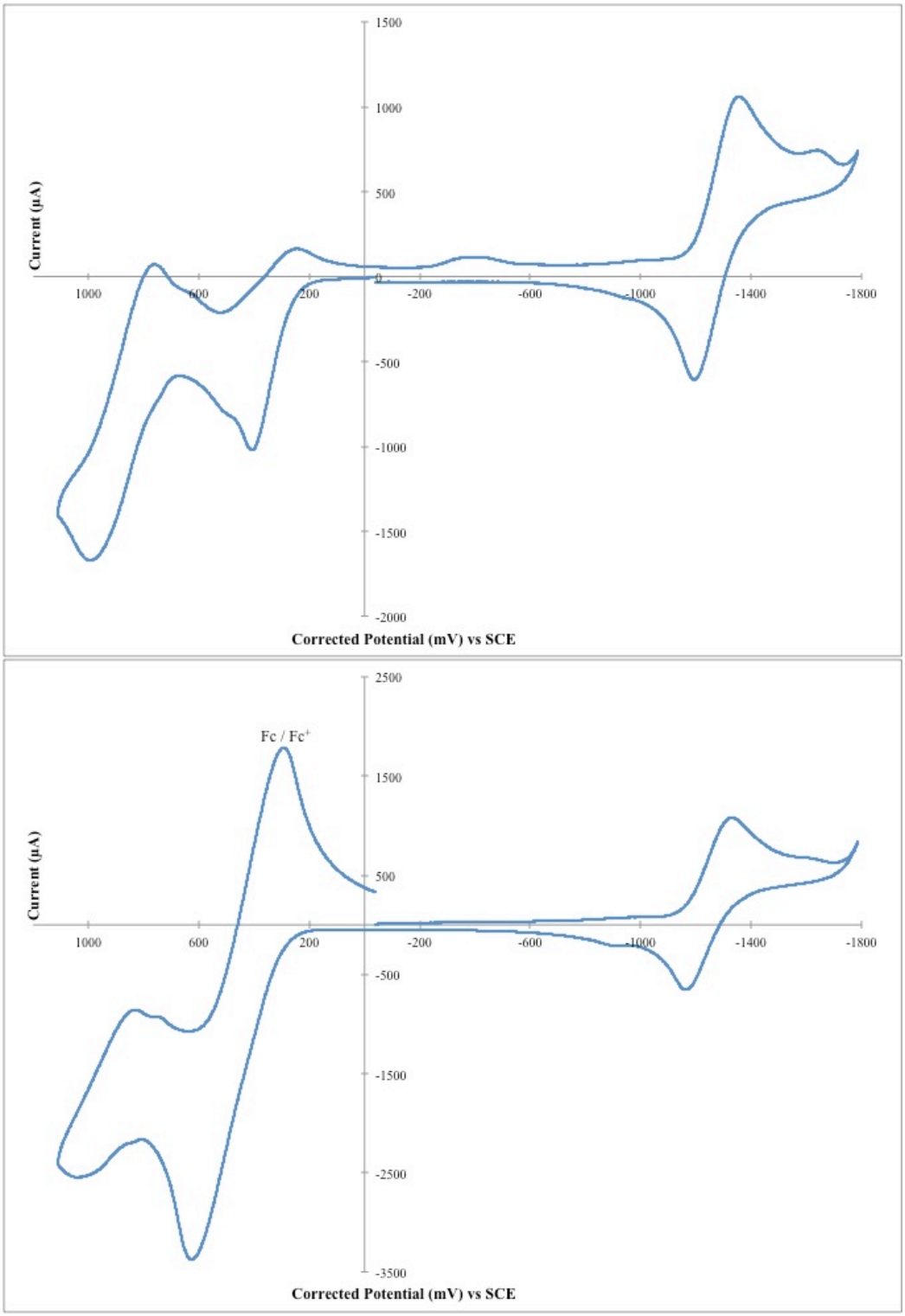

Figure S.22 – DPV of oxidation potentials for ADPM sensitizer **4** before (top) and after addition of ferrocene internal reference (bottom). (0.46 V vs SCE in DCM) (1st scan; 50 mV/s at R.T.)

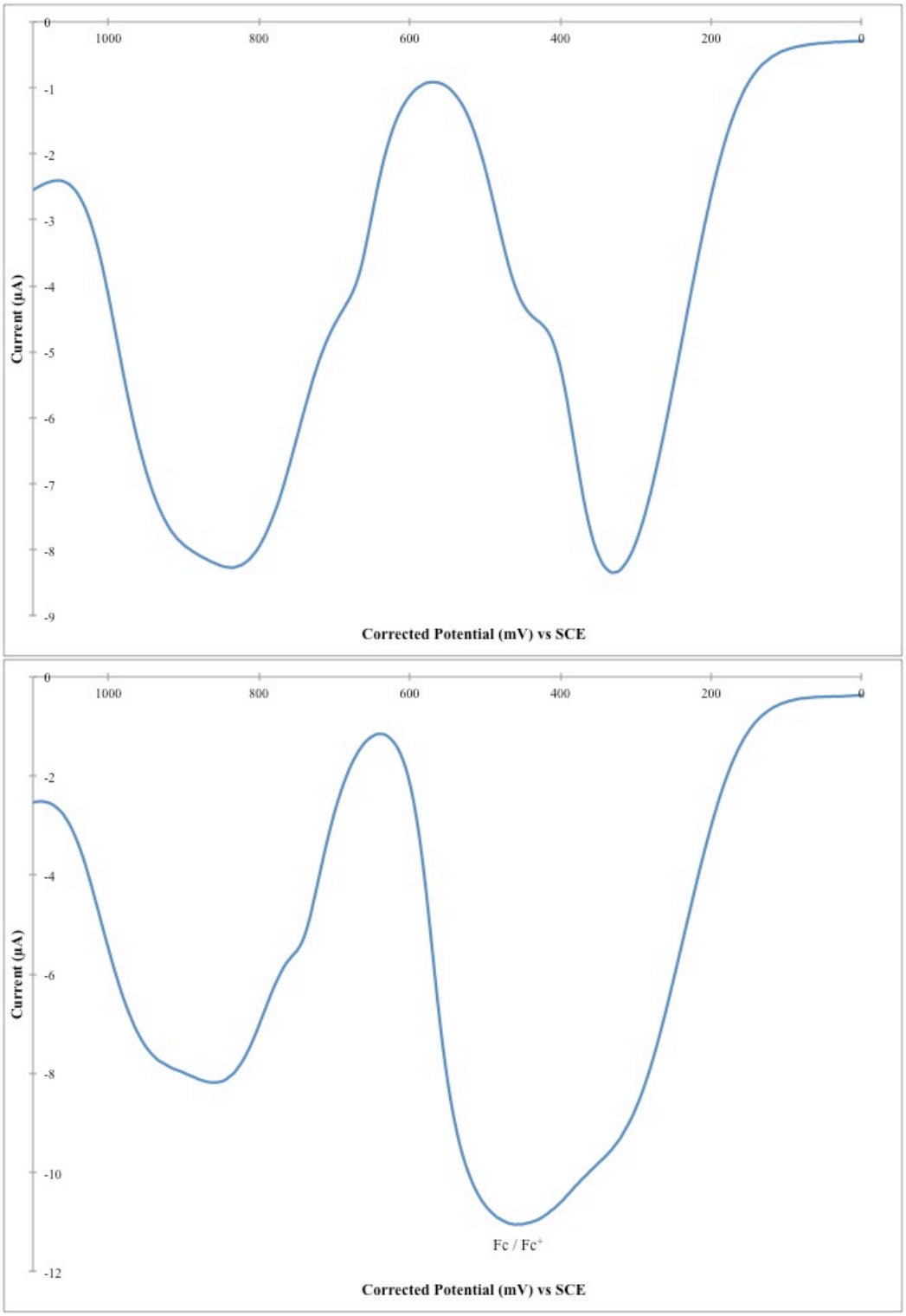

Figure S.23 – DPV of reduction potentials for ADPM sensitizer **4** before (top) and after addition of ferrocene internal reference (bottom). (0.46 V vs SCE in DCM) (1st scan; 50 mV/s at R.T.)

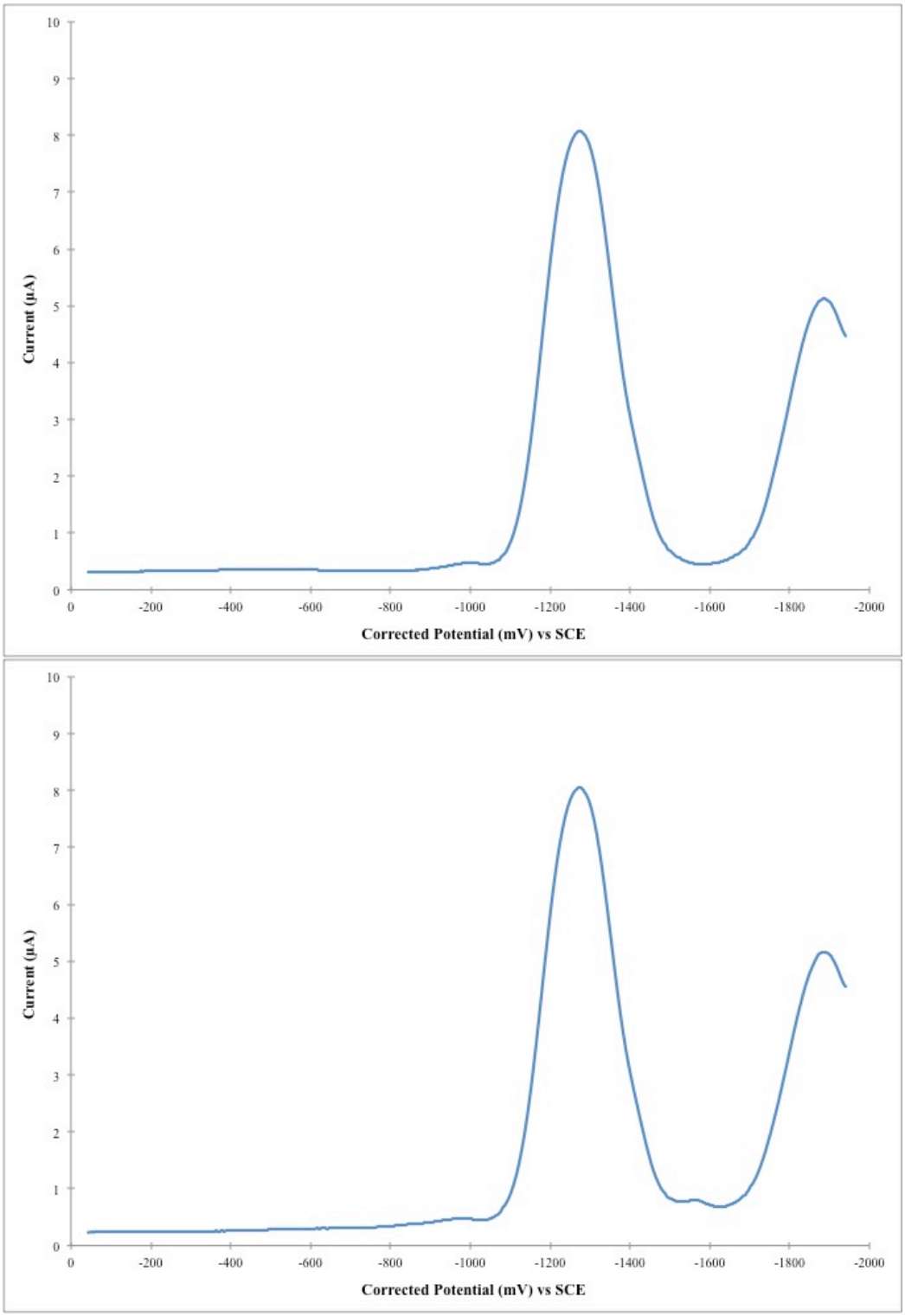

Figure S.24 – CV of ADPM sensitizer **5** before (top) and after addition of ferrocene internal reference (bottom). (0.46 V vs SCE in DCM) (1st scan; 50 mV/s at R.T.)

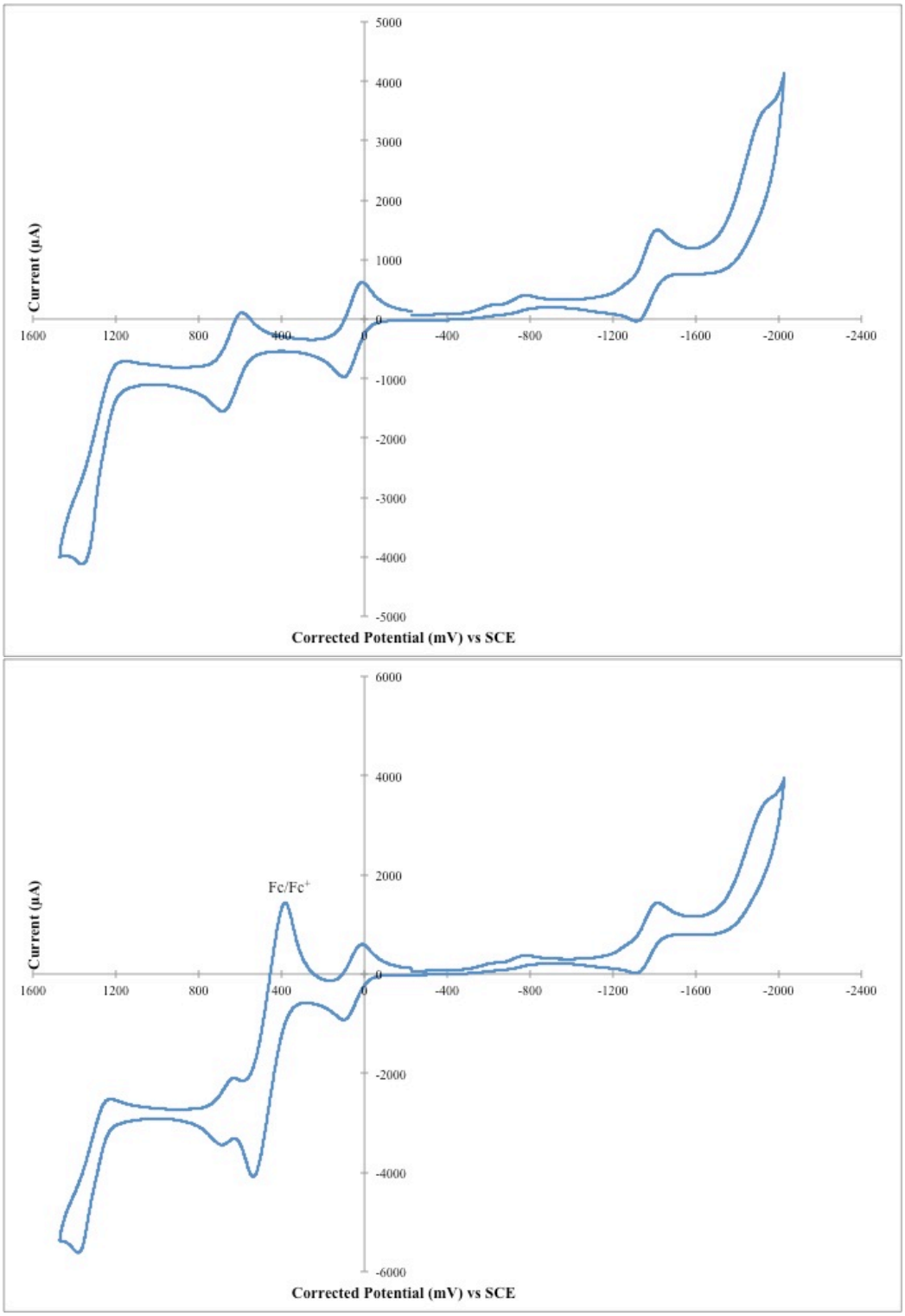

Figure S.25 – DPV of oxidation potentials for ADPM sensitizer **5** before (top) and after addition of ferrocene internal reference (bottom). (0.46 V vs SCE in DCM) (1st scan; 50 mV/s at R.T.)

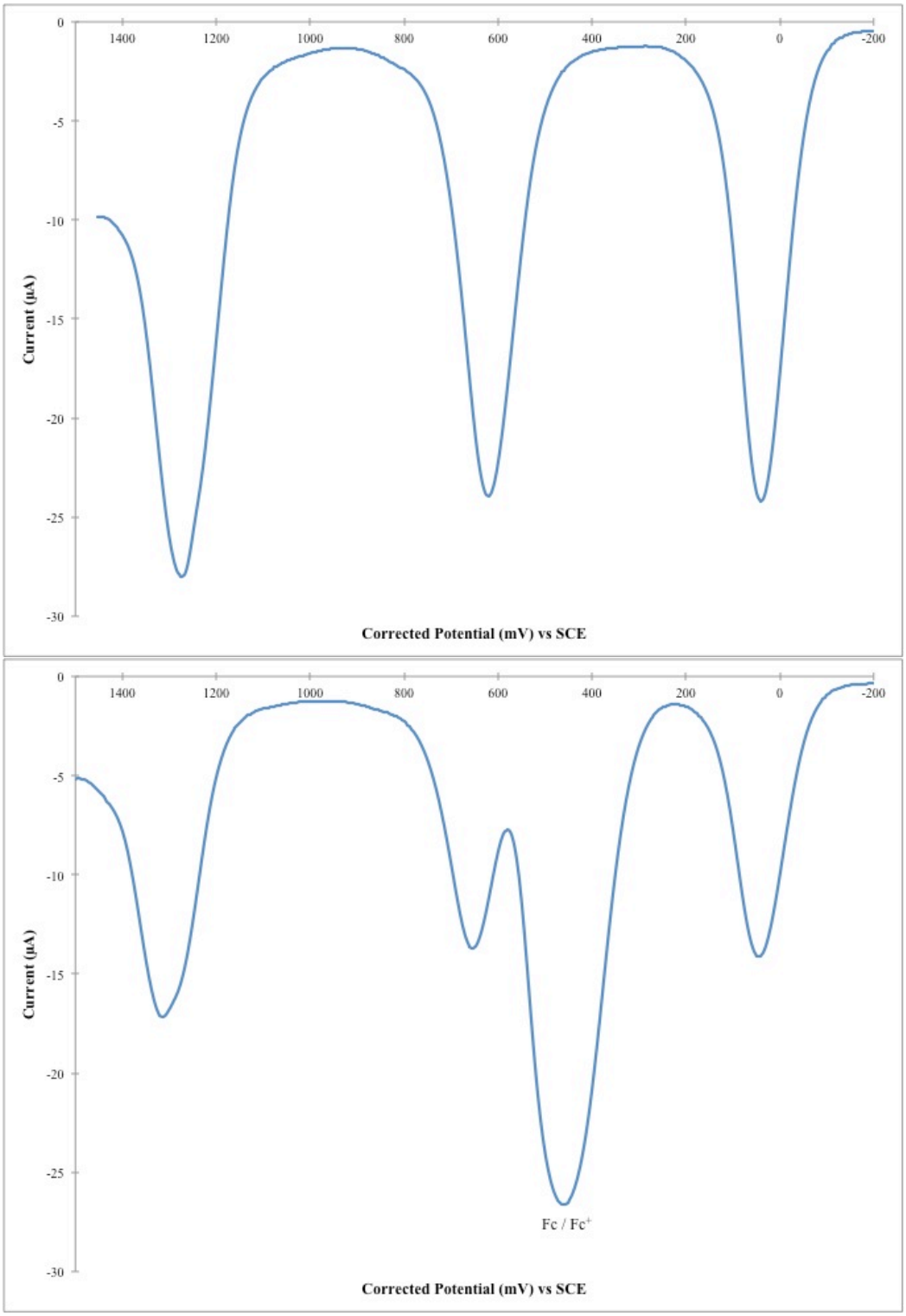

Figure S.26 – DPV of reduction potentials for ADPM sensitizer **5** before (top) and after addition of ferrocene internal reference (bottom). (0.46 V vs SCE in DCM) (1st scan; 50 mV/s at R.T.)

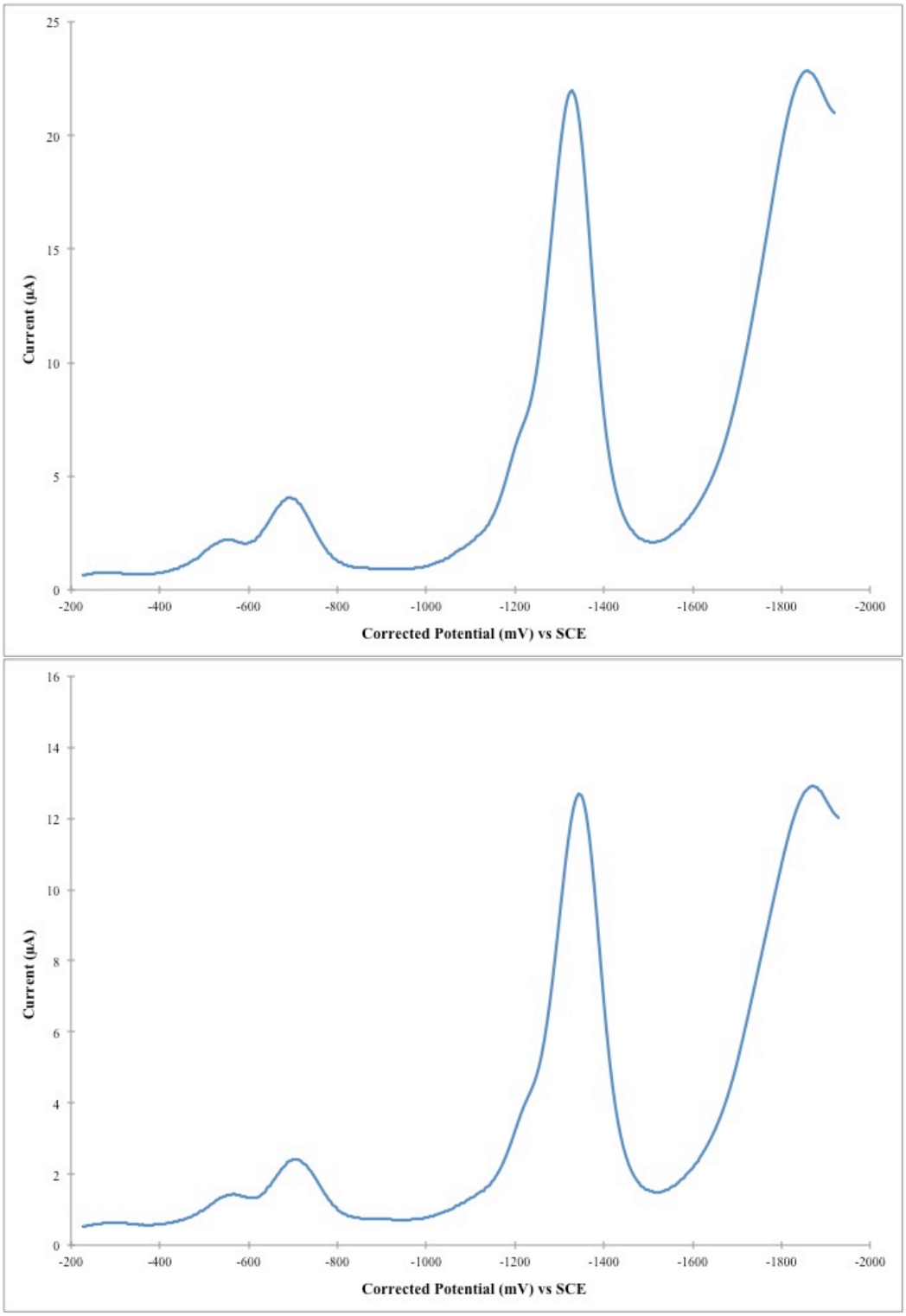

Figure S.27 – CV of ADPM sensitizer **6** before (top) and after addition of ferrocene internal reference (bottom). (Fc = 0.45 V vs SCE in DMF) (1st scan; 50 mV/s at R.T.)

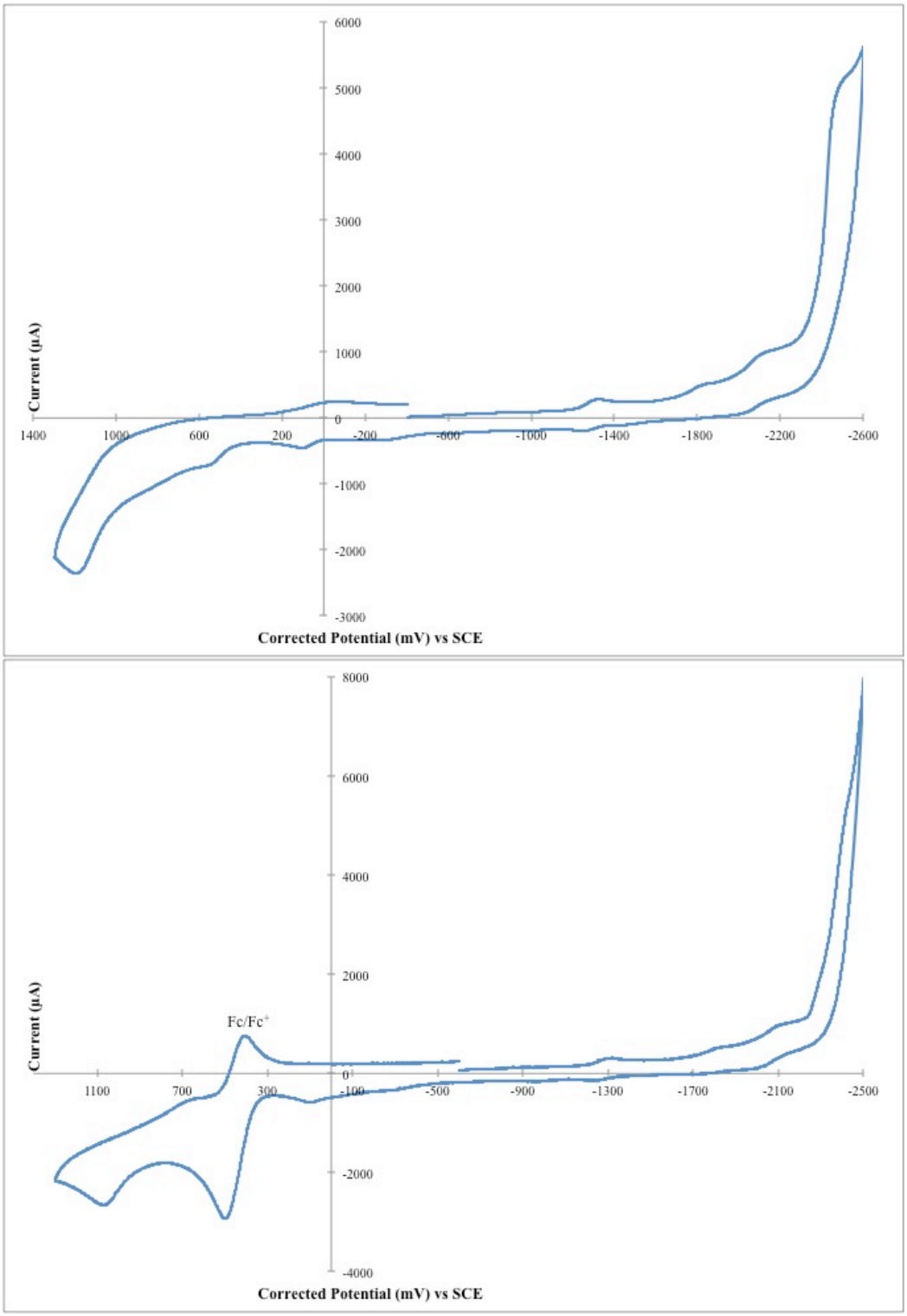

Figure S.28 – DPV of oxidation potentials for ADPM sensitizer **6** before (top) and after addition of ferrocene internal reference (bottom). (0.45 V vs SCE in DMF) (1st scan; 50 mV/s at R.T.)

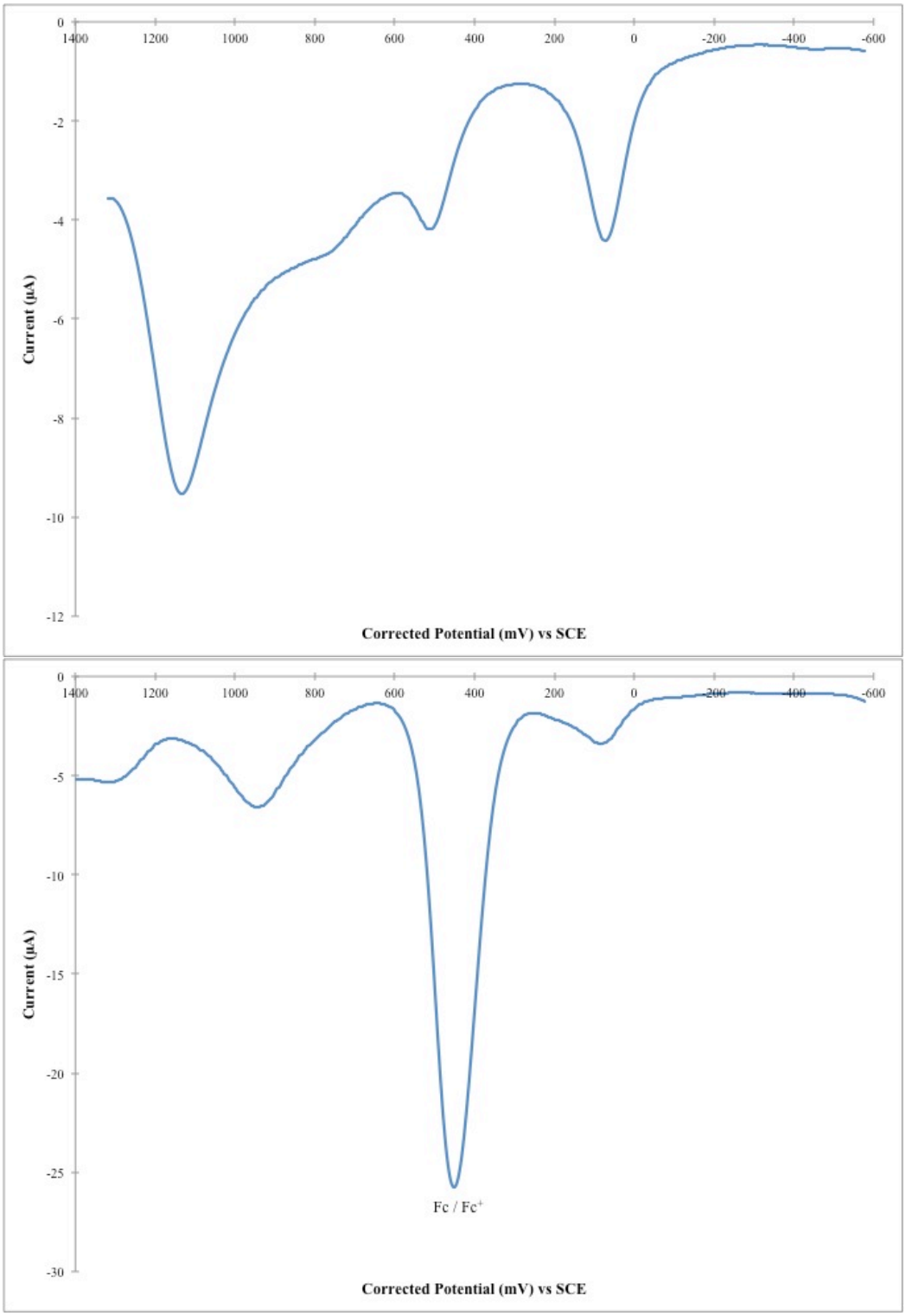

Figure S.29 – DPV of reduction potentials for ADPM sensitizer **6** before (top) and after addition of ferrocene internal reference (bottom). (0.45 V vs SCE in DMF) (1st scan; 50 mV/s at R.T.)

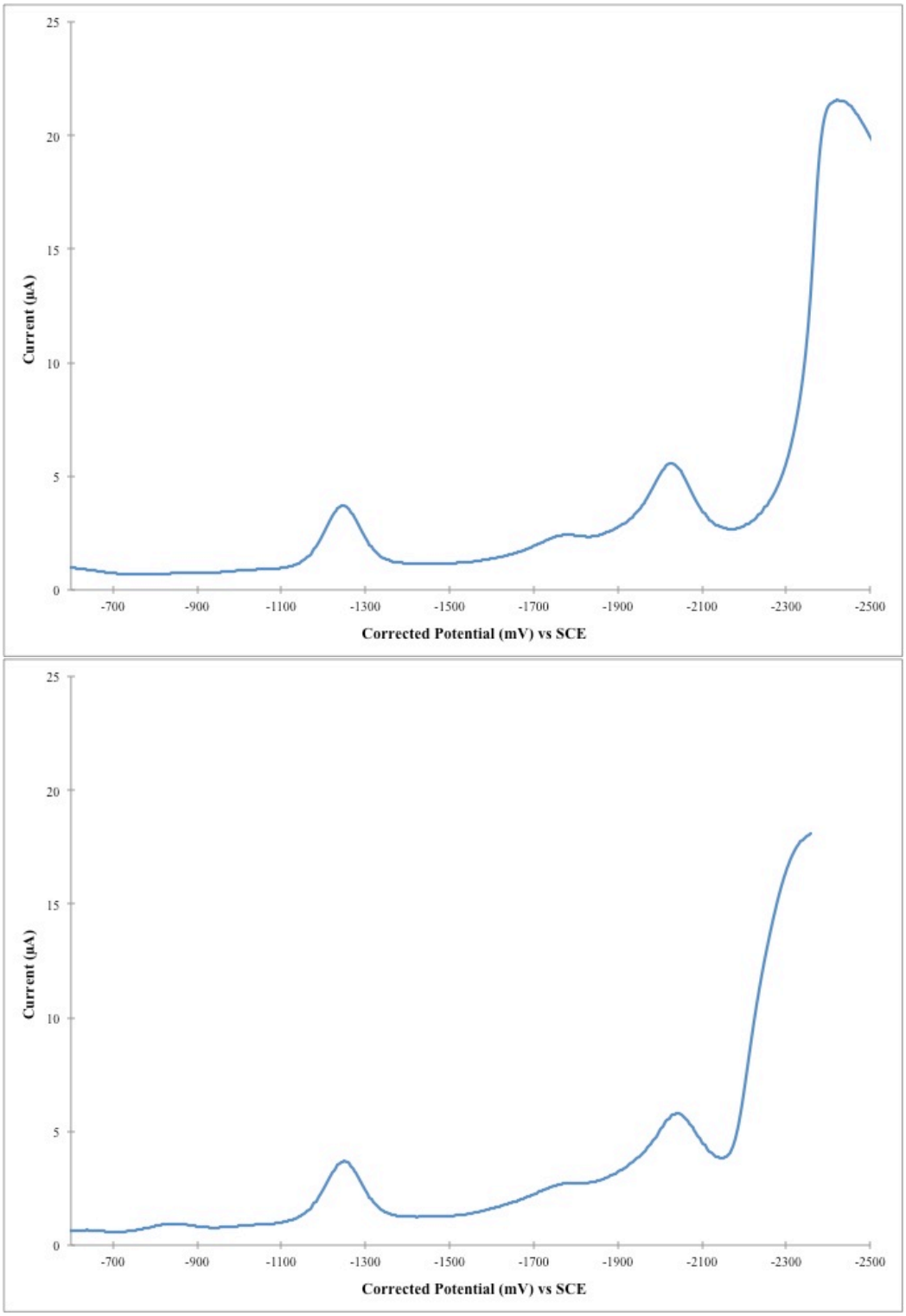

Table S.1 - HOMO/LUMO levels (in eV) determined by electrochemistry and theoretical calculation in CH_2Cl_2 along with corresponding ΔE for ADPM derivatives **1** – **6** and **8**.

	HOMO	LUMO	ΔE [a]	E_{Ox}*	HOMO Theo [b]	LUMO Theo [b]	ΔE Theo [b]	Dipole Moment [b]
1 [d]	-5.66	-4.03	1.63	---	---	---	---	---
2	-5.30	-3.76	1.54	-3.93	-4.20	-2.17	2.03	8.41
3	-5.28	-3.66	1.62	-3.89	-4.13	-1.97	2.15	9.95
4	-5.27	-3.70	1.57	-3.86	-4.19	-2.14	2.05	8.76
5	-5.00	-3.58	1.42	-3.90	-4.09	-1.94	2.15	4.88
6	-5.03 c)	-3.70 c)	1.33 c)	-3.97	-4.07	-1.99	2.08	4.94
8 [d]	-5.90	-4.36	1.54	---	---	---	---	---

[a] Energetic difference between the HOMO and the LUMO obtained by electrochemistry. [b] Theoretical calculations (B3LYP / 6-31g*; Ru : LANL2DZ) / Dipole moment in Debye. [c] In DMF solution. [d] Values from literature.[9]

Computational Modelization

Figure S.30 – Color legend for computational modelization analysis of ADPM photosentizers

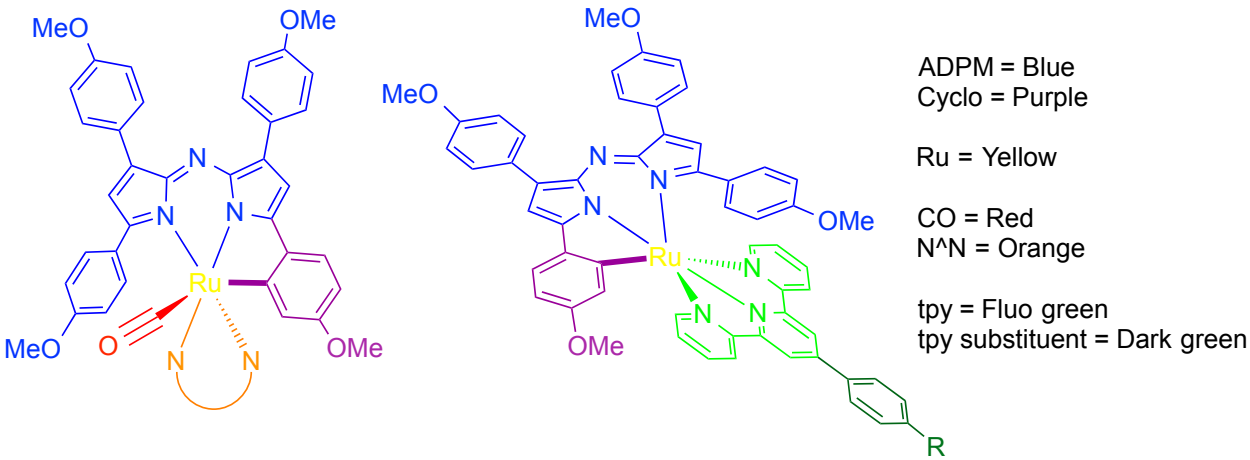

Figure S.31 – Representation of frontier molecular orbital's energy levels (in eV) of ADPM photosensitizers **2** – **6** and electronic distribution as obtained by DFT calculations (refer to Figure S.30 for color legend)

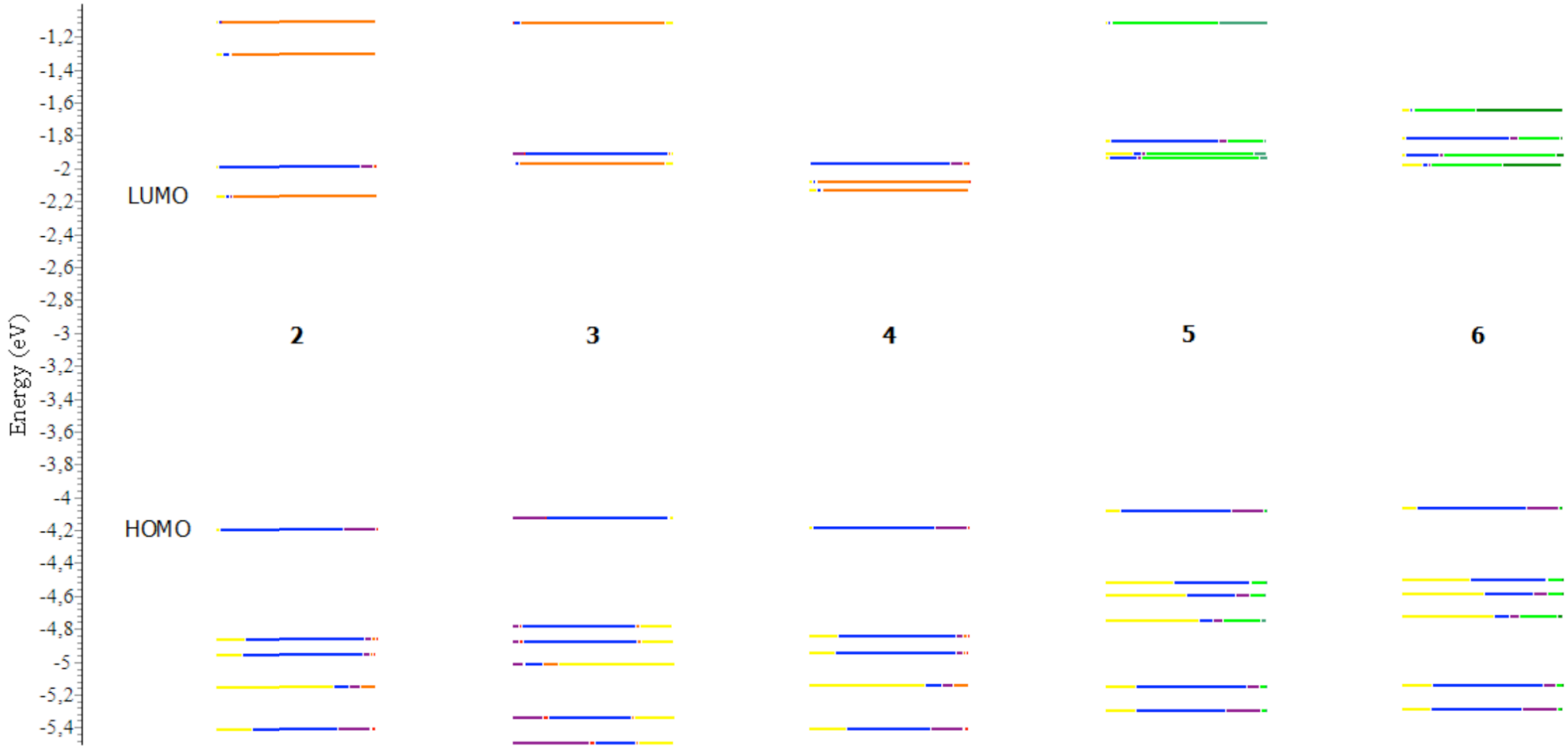

Table S.2 - Electronic distribution (%) of frontier molecular orbitals for ADPM photosensitizers

2 – **6** as obtained by DFT (B3LYP/6-31G*; Ru = LANL2DZ)

	MO	ADPM	Cyclo	Ru	N^N	CO	tpy	tpy subst
2	L + 1	88	8	1	2	0	---	---
	LUMO	3	2	6	89	0	---	---
	HOMO	76	20	3	1	0	---	---
	H -1	73	4	18	2	2	---	---
3	L + 1	88	8	1	2	0	---	---
	LUMO	2	1	5	91	0	---	---
	HOMO	76	20	3	1	0	---	---
	H -1	70	5	20	3	2	---	---
4	L + 1	3	2	8	87	1	---	---
	LUMO	1	0	0	99	0	---	---
	HOMO	76	20	3	1	0	---	---
	H -1	73	4	18	2	2	---	---
5	L + 1	5	3	18	---	---	67	8
	LUMO	17	2	2	---	---	73	5
	HOMO	68	20	10	---	---	2	0
	H -1	47	1	42	---	---	9	0
6	L + 1	21	3	2	---	---	68	6
	LUMO	3	2	13	---	---	43	38
	HOMO	68	20	10	---	---	2	0
	H -1	47	1	42	---	---	10	0

Table S.3 – Natural transition orbitals (NTO) associated with absorption bands **T1** to **T12**

(Isovalue = 0.02) of complex **2** obtained by TD-DFT (PCM = CH_2Cl_2)

	λ_{Calc}, nm (Osc. Strenght) / Eigenvalue	**NTO Hole**	**NTO Particle**		**λ_{Calc}, nm (Osc. Strenght) / Eigenvalue**	**NTO Hole**	**NTO Particle**
T1	647 (0.388) / >0.99	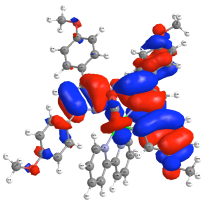	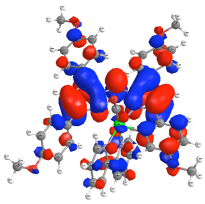	**T7**	484 (0.048) / 0.95	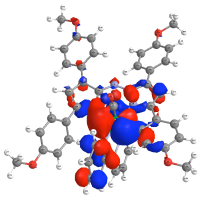	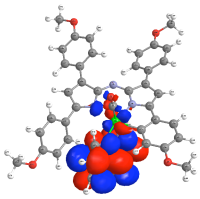
T2	637 (0.048) / 0.99	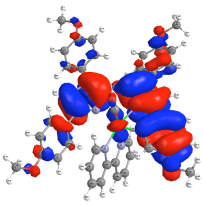	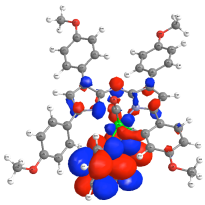	**T8**	463 (0.015) / 0.99	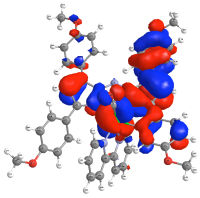	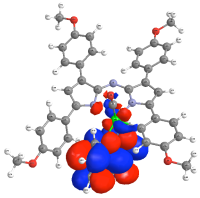
T3	560 (0.080) / >0.99	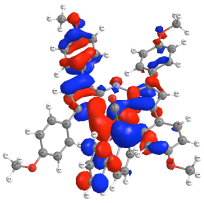	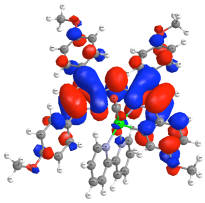	**T9**	438 (0.232) / 0.92	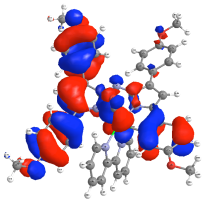	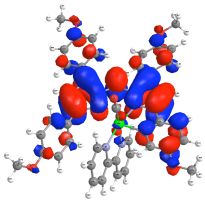
T4	538 (0.169) / 0.98	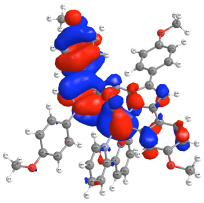	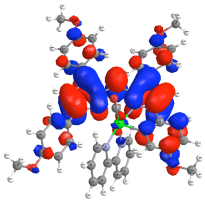	**T10**	434 (0.033) / 0.93	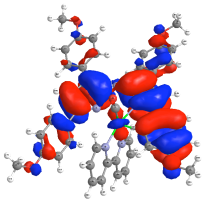	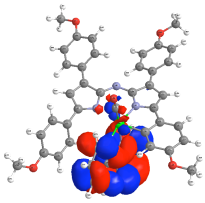
T5	524 (0.163) / 0.96	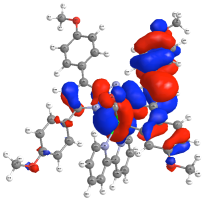	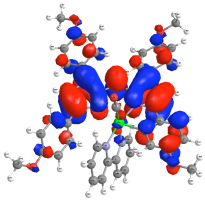	**T11**	411 (0.134) / 0.98	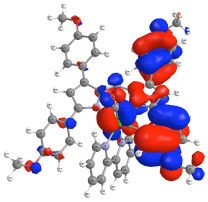	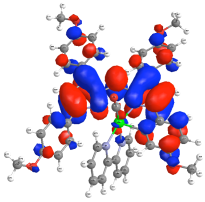
T6	487 (0.001) / >0.99	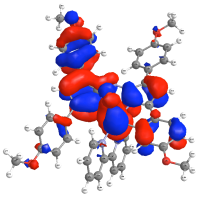	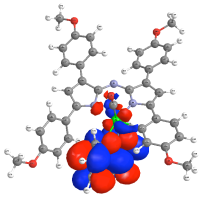	**T12**	406 (0.002) / 0.99	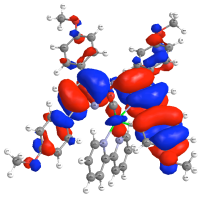	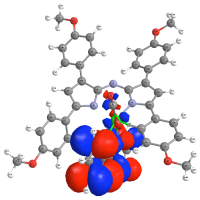

Table S.4 - Assignation of optical absorption bands of ADPM photosensitizer **2** based on

TD-DFT calculations (B3LYP/6-31G*; Ru = LANL2DZ; PCM = CH_2Cl_2)

λ, nm				
Observed (ε, x10^3 $M^{-1}cm^{-1}$)	**Calculated** (Osc. Strength)	**Trans. No.**	**Major contributions to excitation**	**Assignation**
712 (15)	647 (0.388)	T1	H -> L (81%)	Cyclo + Ru + CO --> N^N + ADPM
660 (17)	637 (0.048)	T2	H -> L+1 (90%)	ADPM + Cyclo --> N^N + CO + Ru
550 (15)	560 (0.080)	T3	H-3 (30%), H-2 (36%), H-1 (29%) -> L	Ru + N^N + CO --> ADPM + Cyclo
	538 (0.169)	T4	H-3 (39%), H-1 (53%) -> L	Ru + N^N + CO --> ADPM + Cyclo
	524 (0.163)	T5	H-3 (28%), H-2 (57%) -> L	Ru + N^N + CO --> ADPM + Cyclo
	487 (0.001)	T6	H-3 (19%), H-1 (63%) -> L+1	ADPM + Cyclo + Ru + CO --> N^N
	484 (0.048)	T7	H-3 (62%), H-1 (26%) -> L+1	Ru + ADPM + Cyclo + CO --> N^N
436 (13)	463 (0.015)	T8	H-2 -> L+1 (81%)	ADPM + Cyclo + Ru + CO --> N^N
	438 (0.232)	T9	H-4 -> L (86%)	Ru + Cyclo + CO --> ADPM + N^N
	434 (0.033)	T10	H -> L+2 (91%)	ADPM + Cyclo --> N^N + CO
	411 (0.134)	T11	H-5 -> L (90%)	Cyclo + Ru + CO + N^N --> ADPM
	406 (0.002)	T12	H -> L+3 (97%)	ADPM + Cyclo + Ru + CO --> N^N

Figure S.32 – Experimental absorption spectrum in CH_2Cl_2 vs calculated optical absorption bands of ADPM photosensitizer **3** based on TD-DFT calculations

(B3LYP/6-31G*; Ru = LANL2DZ; PCM = CH_2Cl_2)

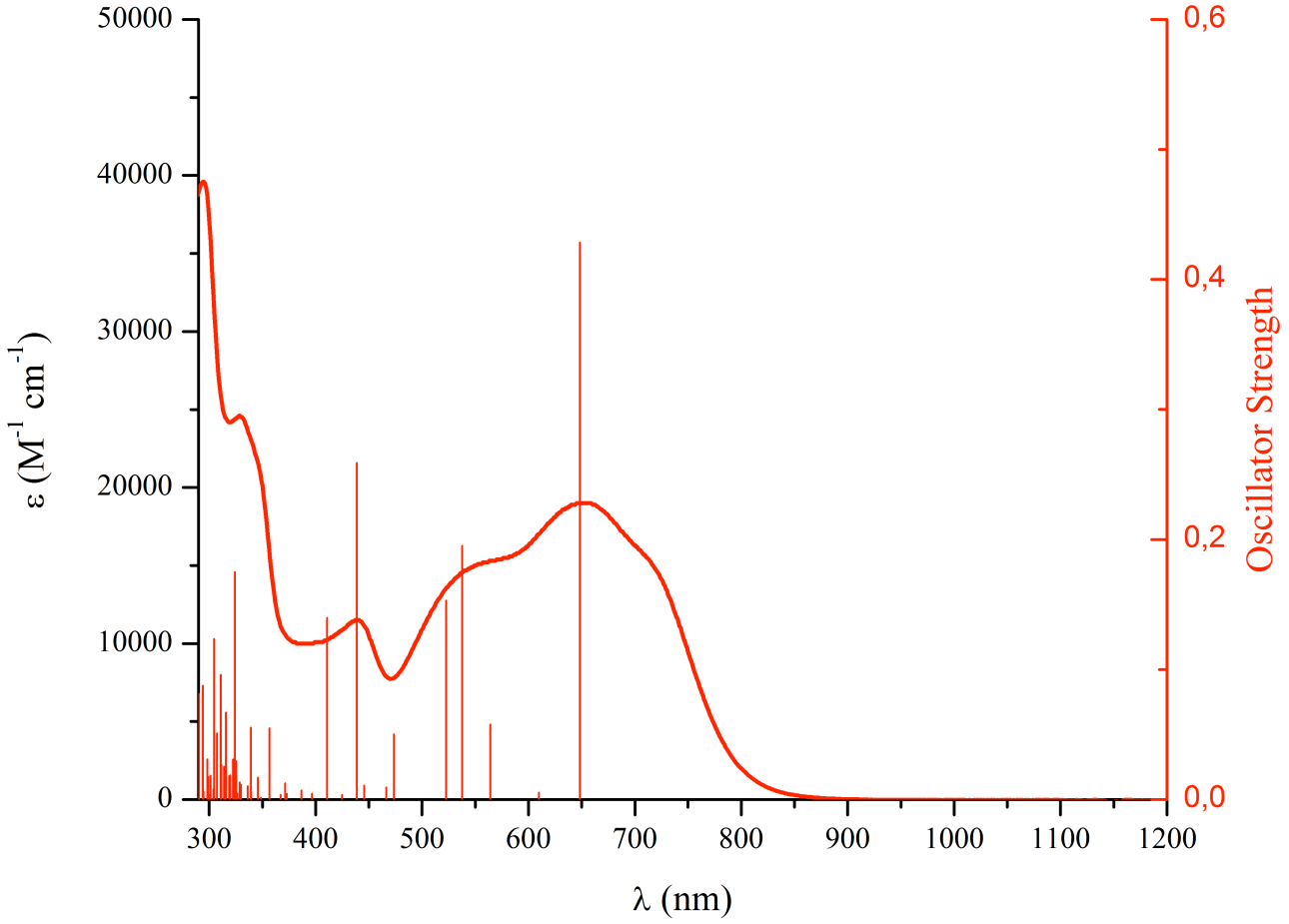

Table S.5 – Natural transition orbitals (NTO) associated with absorption bands **T1** to **T12** (Isovalue = 0.02) of complex **3** obtained by TD-DFT (PCM = CH_2Cl_2)

	λ_{Calc}, nm (Osc. Strenght) / Eigenvalue	NTO Hole	NTO Particle		λ_{Calc}, nm (Osc. Strenght) / Eigenvalue	NTO Hole	NTO Particle
T1	648 (0.429) / >0.99	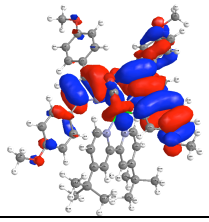	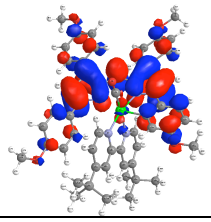	**T7**	467 (0.009) / 0.99	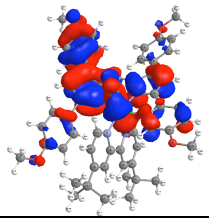	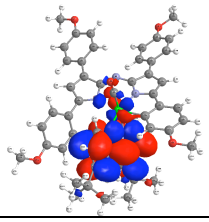
T2	610 (0.005) / >0.99	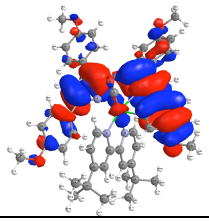	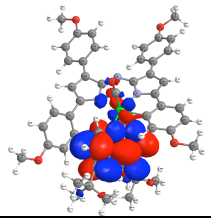	**T8**	446 (0.011) / 0.99	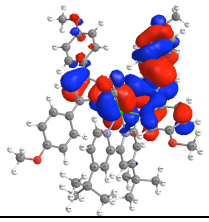	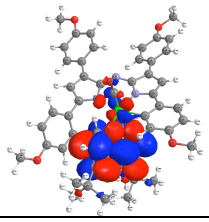
T3	564 (0.058) / >0.99	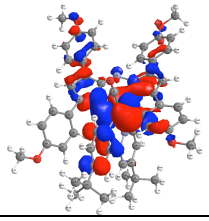	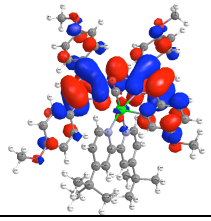	**T9**	439 (0.259) / 0.99	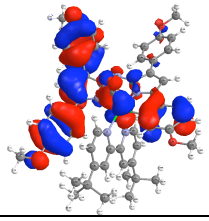	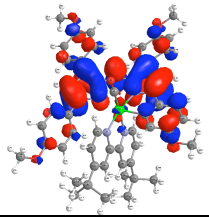
T4	538 (0.195) / 0.99	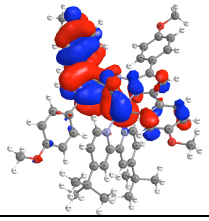	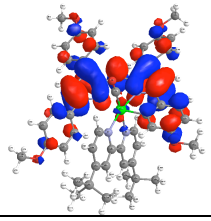	**T10**	425 (0.004) / 0.99	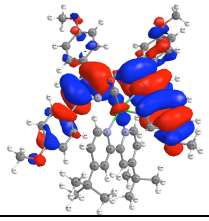	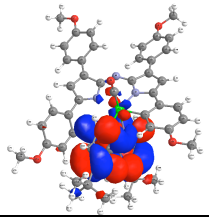
T5	523 (0.153) / 0.97	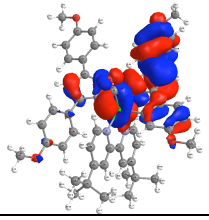	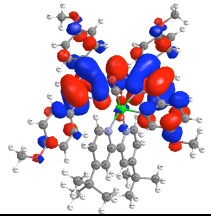	**T11**	411 (0.140) / 0.98	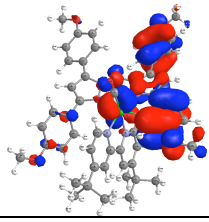	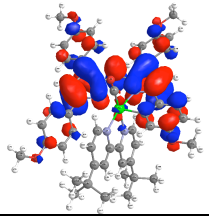
T6	474 (0.050) / 0.96	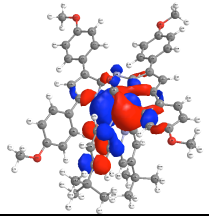	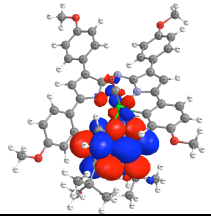	**T12**	397 (0.005) / 0.99	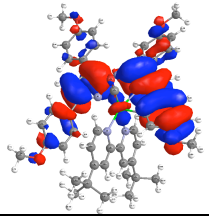	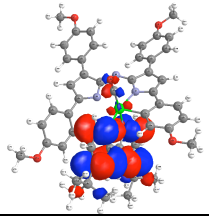

Table S.6 - Assignation of optical absorption bands of ADPM photosensitizer **3** based on

TD-DFT calculations (B3LYP/6-31G*; Ru = LANL2DZ; PCM = CH_2Cl_2)

λ, nm				
Observed (ε, x10^3 $M^{-1}cm^{-1}$)	**Calculated** (Osc. Strength)	**Trans. No.**	**Major contributions to excitation**	**Assignation**
712 (16)	648 (0.429)	T1	H -> L (89%)	Cyclo + Ru + CO --> N^N + ADPM
654 (19)	610 (0.005)	T2	H -> L+1 (99%)	ADPM + Cyclo --> N^N + CO + Ru
552 (15)	564 (0.058)	T3	H-3 (23%), H-2 (51%), H-1 (23%) -> L	Ru + N^N + CO --> ADPM + Cyclo
	538 (0.195)	T4	H-3 (28%), H-1 (61%) -> L	Ru + N^N + CO --> ADPM + Cyclo
	523 (0.153)	T5	H-3 (46%), H-2 (42%) -> L	Ru + N^N + CO --> ADPM + Cyclo
	474 (0.050)	T6	H-3 (56%), H-2 (32%) -> L+1	ADPM + Cyclo + Ru + CO --> N^N
439 (12)	467 (0.009)	T7	H-1 -> L+1 (84%)	ADPM + Cyclo + Ru + CO --> N^N
	446 (0.011)	T8	H-3 (35%), H-2 (54%) -> L+1	ADPM + Cyclo + Ru + CO --> N^N
	439 (0.259)	T9	H-4 -> L (92%)	Ru + Cyclo + CO --> ADPM
	425 (0.004)	T10	H -> L+2 (97%)	ADPM + Cyclo --> N^N + Ru
	411 (0.140)	T11	H-5 -> L (90%)	Cyclo + Ru + CO + N^N --> ADPM
	397 (0.005)	T12	H -> L+3 (97%)	ADPM + Cyclo + Ru --> N^N + CO

Figure S.33 – Experimental absorption spectrum in CH_2Cl_2 vs calculated optical absorption bands of ADPM photosensitizer **4** based on TD-DFT calculations

(B3LYP/6-31G*; Ru = LANL2DZ; PCM = CH_2Cl_2)

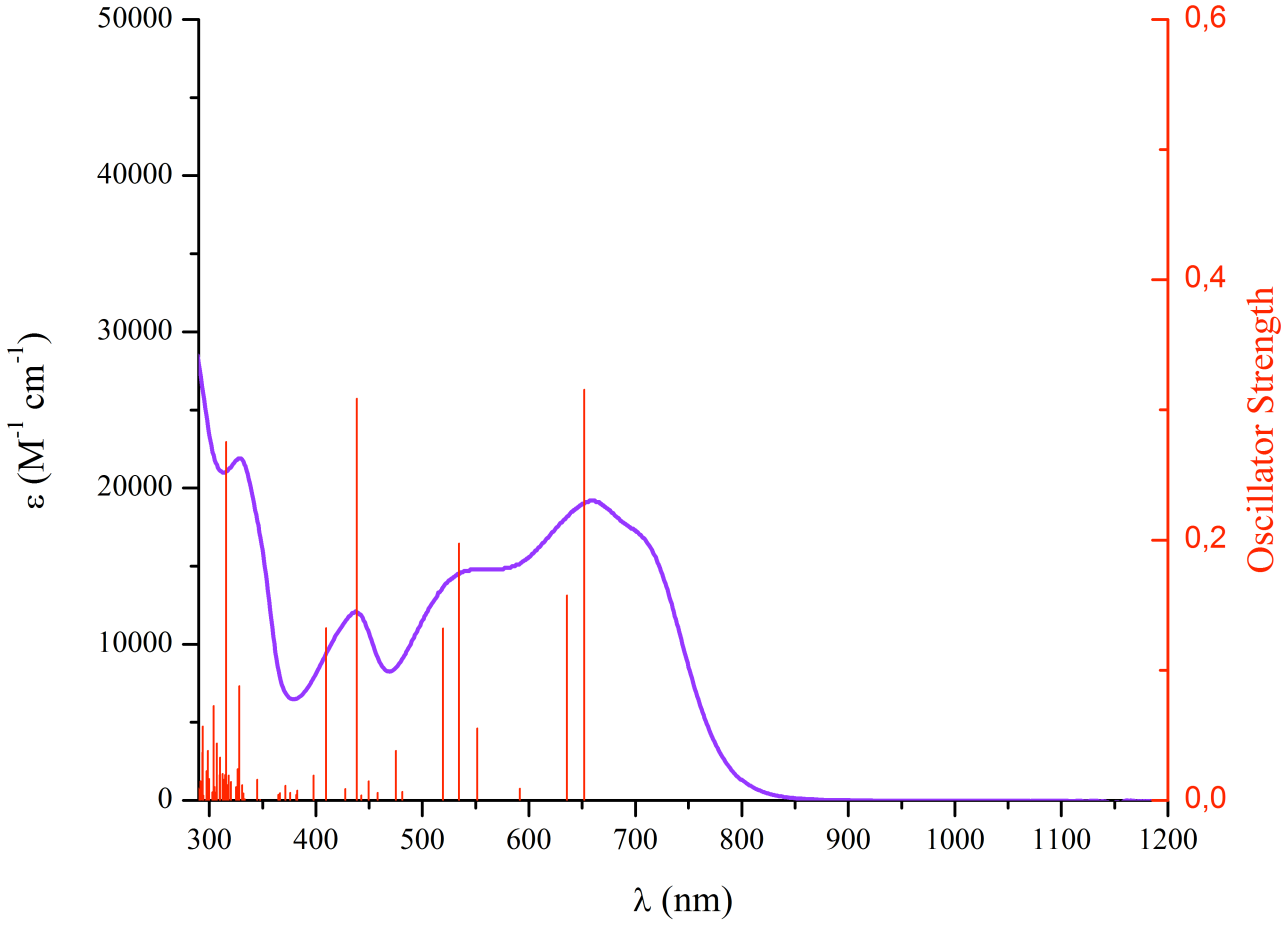

Table S.7 – Natural transition orbitals (NTO) associated with absorption bands **T1** to **T14** (Isovalue = 0.02) of complex **4** obtained by TD-DFT (PCM = CH_2Cl_2)

	λ_{Calc}, nm (Osc. Strenght) / Eigenvalue	**NTO Hole**	**NTO Particle**		**λ_{Calc}, nm (Osc. Strenght) / Eigenvalue**	**NTO Hole**	**NTO Particle**
T1	652 (0.316) / 0.99	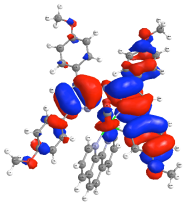	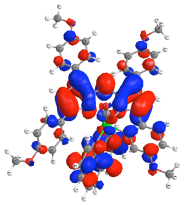	**T7**	481 (0.007) / 0.98	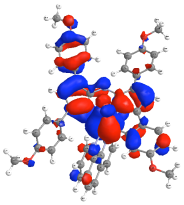	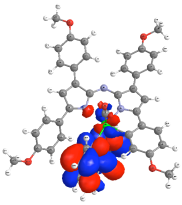
T2	636 (0.158) / 0.99	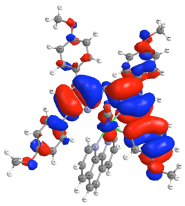	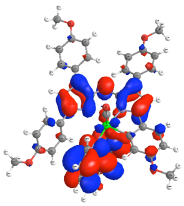	**T8**	475 (0.038) / 0.93	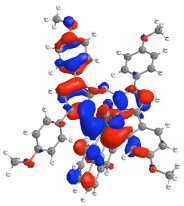	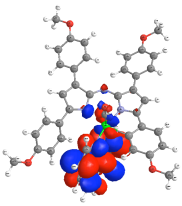
T3	591 (0.009) / >0.99	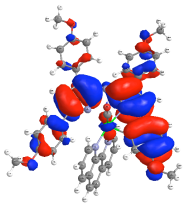	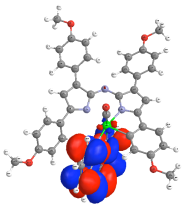	**T9**	458 (0.006) / 0.92	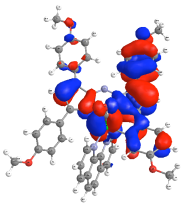	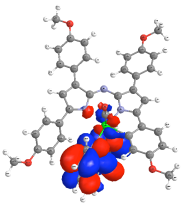
T4	552 (0.055) / >0.99	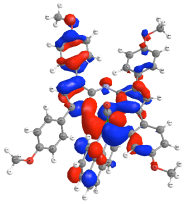	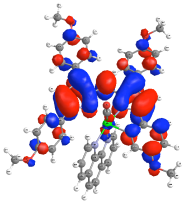	**T10**	450 (0.015) / 0.96	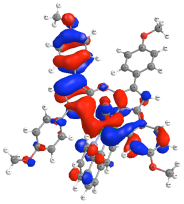	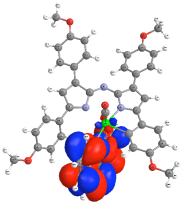
T5	534 (0.197) / 0.98	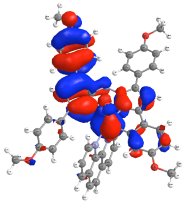	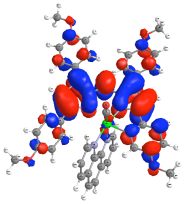	**T11**	443 (0.004) / 0.84	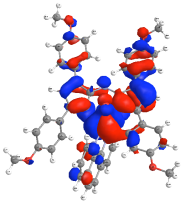	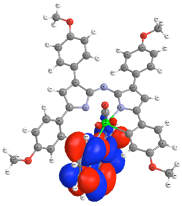
T6	520 (0.132) / 0.97	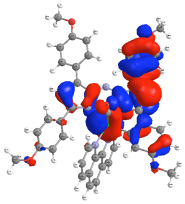	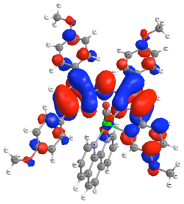	**T12**	439 (0.309) / 0.92	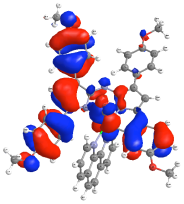	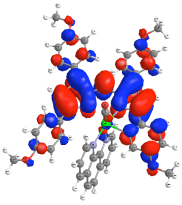

Table S.7 (Continued) – Natural transition orbitals (NTO) associated with absorption bands **T1** to **T14** (Isovalue = 0.02) of complex **4** obtained by TD-DFT (PCM = CH_2Cl_2)

	λ_{Calc}, nm (Osc. Strenght) / Eigenvalue	**NTO Hole**	**NTO Particle**		**λ_{Calc}, nm (Osc. Strenght) / Eigenvalue**	**NTO Hole**	**NTO Particle**
T13	428 (0.009) / 0.84	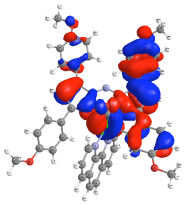	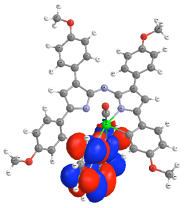	**T14**	410 (0.132) / 0.97	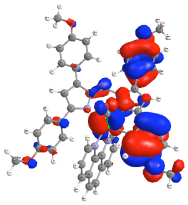	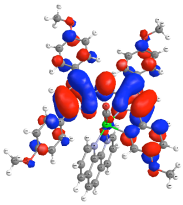

Table S.8 - Assignation of optical absorption bands of ADPM photosensitizer **4** based on

TD-DFT calculations (B3LYP/6-31G*; Ru = LANL2DZ; PCM = CH_2Cl_2)

λ, nm				
Observed (ε, x10^3 $M^{-1}cm^{-1}$)	**Calculated** (Osc. Strength)	**Trans. No.**	**Major contributions to excitation**	**Assignation**
702 (17)	652 (0.316)	T1	H -> L (68%), H -> L+1 (26%)	Cyclo + ADPM + Ru --> N^N
659 (19)	636 (0.158)	T2	H -> L (24%), H -> L+1 (73%)	ADPM + Cyclo --> N^N + CO + Ru
544 (15)	591 (0.009)	T3	H -> L+2 (99%)	ADPM + Cyclo + Ru --> N^N
	552 (0.055)	T4	H-3 (35%), H-2 (45%), H-1 (17%) -> L	Ru + N^N + CO --> ADPM + Cyclo
	534 (0.197)	T5	H-3 (25%), H-1 (68%)->L	Ru + N^N + CO --> ADPM + Cyclo
	520 (0.132)	T6	H-3 (37%), H-2 (51%) -> L	Ru + N^N + CO --> ADPM + Cyclo
437 (12)	481 (0.007)	T7	H-3 (37%), H-2 (13%), H-1 (41%) -> L+1	ADPM + Cyclo + Ru + CO --> N^N
	475 (0.038)	T8	H-3 (37%), H-1 (47%) -> L+1	ADPM + Cyclo + Ru + CO --> N^N
	458 (0.006)	T9	H-3 (17%), H-2 (66%) -> L+1	ADPM + Cyclo + Ru + CO --> N^N
	450 (0.015)	T10	H-3 (15%), H-1 (67%) -> L+2	ADPM + Cyclo + Ru + CO --> N^N
	443 (0.004)	T11	H-3 (27%), H-2 (29%), H-1 (25%) -> L+2	ADPM + Cyclo + Ru + CO --> N^N
	439 (0.309)	T12	H-4 -> L (84%)	Ru + Cyclo + CO --> ADPM + N^N
	428 (0.009)	T13	H-3 (40%), H-2 (53%) -> L+2	ADPM + Cyclo + Ru + CO --> N^N
	410 (0.132)	T14	H-5 -> L (88%)	Ru + Cyclo + CO --> ADPM + N^N

Figure S.34 – Experimental absorption spectrum in CH_2Cl_2 vs calculated optical absorption bands of ADPM photosensitizer **5** based on TD-DFT calculations

(B3LYP/6-31G*; Ru = LANL2DZ; PCM = CH_2Cl_2)

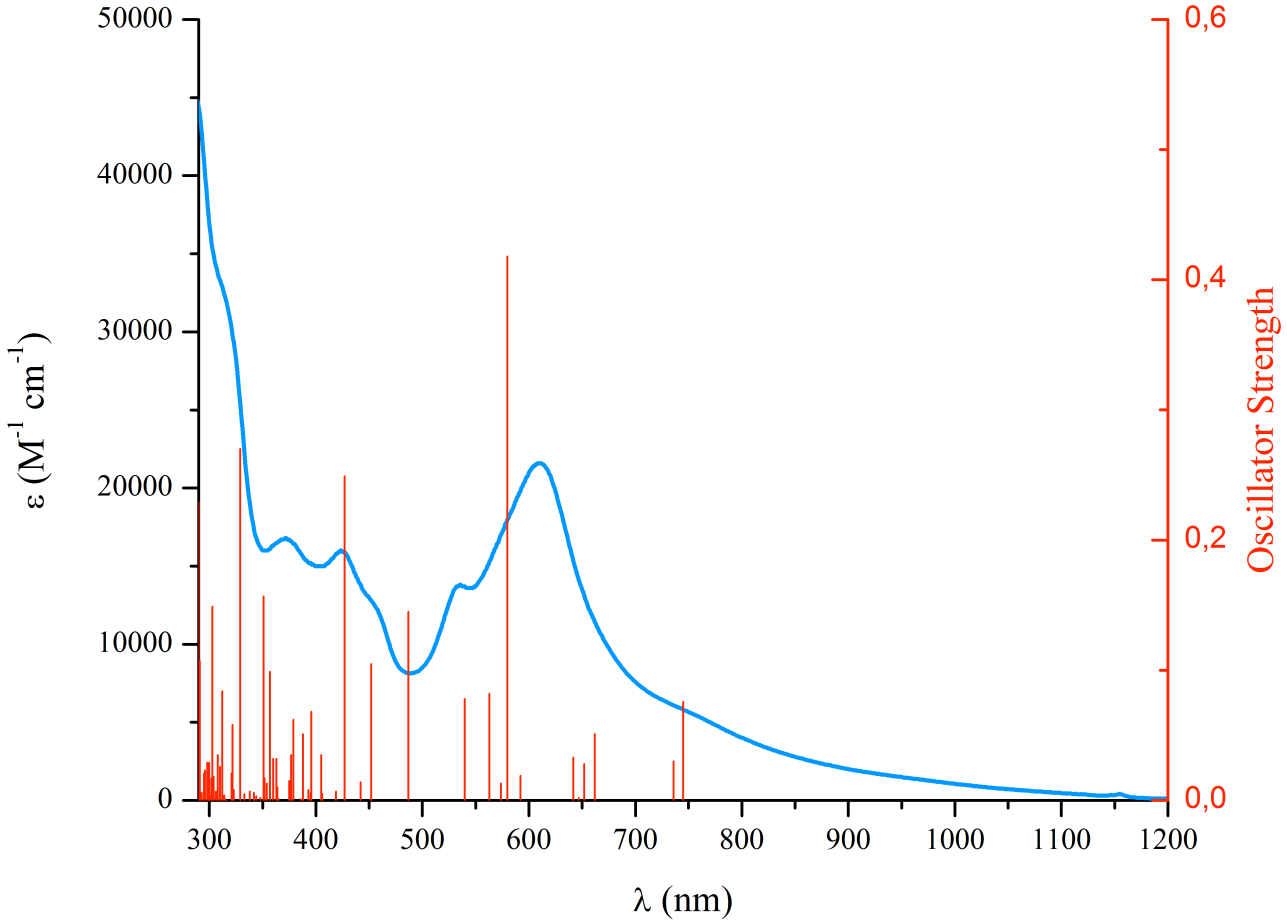

Table S.9 – Natural transition orbitals (NTO) associated with absorption bands **T1** to **T18** (Isovalue = 0.02) of complex **5** obtained by TD-DFT (PCM = CH_2Cl_2)

	λ_{Calc}, nm (Osc. Strenght) / Eigenvalue	NTO Hole	NTO Particle		λ_{Calc}, nm (Osc. Strenght) / Eigenvalue	NTO Hole	NTO Particle
T1	745 (0.076) / 0.99	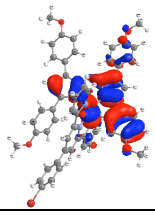	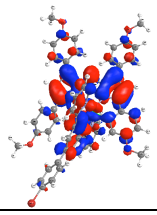	**T7**	592 (0.019) / 0.91	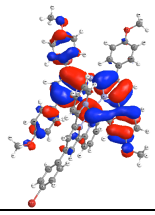	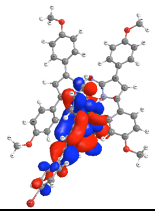
T2	736 (0.030) / 0.98	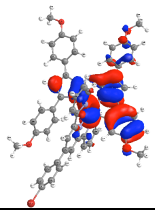	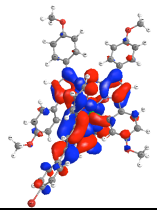	**T8**	580 (0.418) / 0.93	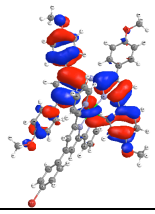	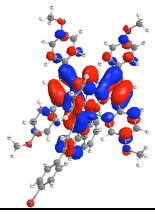
T3	662 (0.051) / 0.98	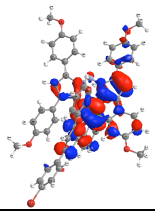	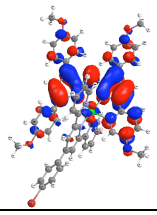	**T9**	574 (0.013) / 0.81	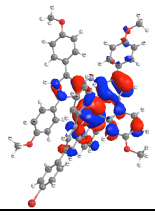	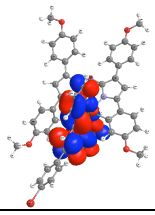
T4	652 (0.028) / 0.81	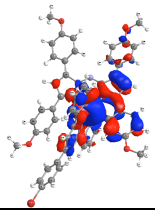	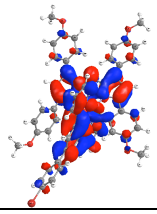	**T10**	563 (0.082) / 0.82	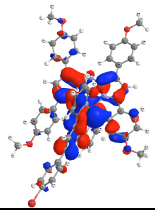	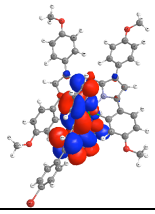
T5	647 (0.002) / 0.70	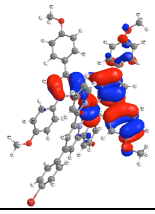	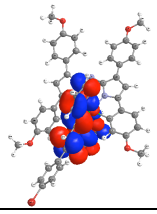	**T11**	540 (0.078) / 0.96	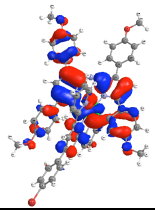	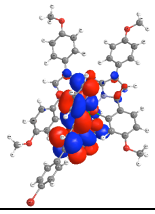
T6	642 (0.033) / 0.63	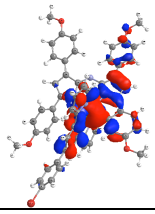	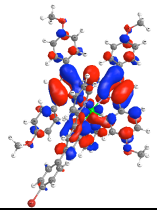	**T12**	487 (0.145) / 0.56	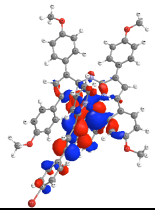	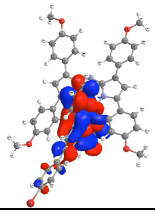

Table S.9 (Continued) – Natural transition orbitals (NTO) associated with absorption bands **T1** to **T18** (Isovalue = 0.02) of complex **5** obtained by TD-DFT (PCM = CH_2Cl_2)q

	λ_{Calc}, nm (Osc. Strenght) / Eigenvalue	**NTO Hole**	**NTO Particle**		**λ_{Calc}, nm (Osc. Strenght) / Eigenvalue**	**NTO Hole**	**NTO Particle**
T13	452 (0.105)	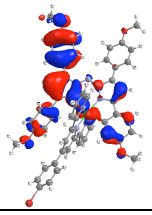	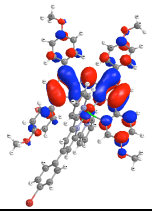	**T16**	419 (0.007)	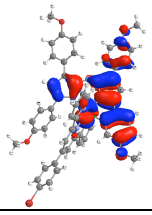	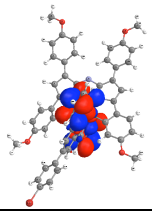
T14	442 (0.014)	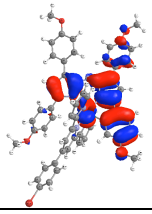	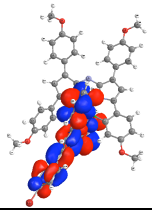	**T17**	406 (0.005)	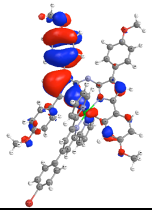	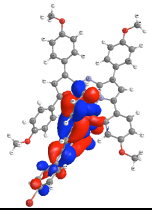
T15	427 (0.249)	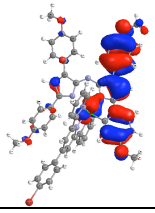	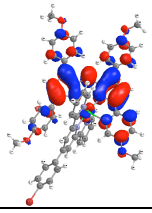	**T18**	405 (0.035)	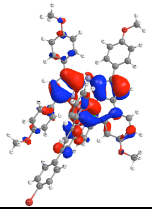	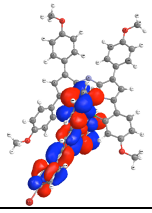

Table S.10 - Assignation of optical absorption bands of ADPM photosensitizer **5** based on TD-DFT calculations

(B3LYP/6-31G*; Ru = LANL2DZ; PCM = CH_2Cl_2)

λ, nm				
Observed (ε, x10^3 $M^{-1}cm^{-1}$)	**Calculated** (Osc. Strength)	**Trans. No.**	**Major contributions to excitation**	**Assignation**
752 (5.6)	745 (0.076)	T1	H-1 (10%), H (53%) -> L; H -> L+1 (18%)	Ru + Cyclo --> TPY + PhBr + ADPM
	736 (0.030)	T2	H-1 (18%), H (50%) -> L+1; H -> L (16%)	ADPM + Cyclo + Ru --> TPY + PhBr
610 (22)	662 (0.051)	T3	H-3 (16%), H-2 (34%), H-1 (45%) -> L	Ru + TPY + PhBr --> ADPM + Cyclo
	652 (0.028)	T4	H-3 (21%), H-2 (22%) -> L; H-2 -> L+1 (38%)	Ru + Cyclo --> TPY + PhBr + ADPM
	647 (0.002)	T5	H-2 -> L+1 (15%), H -> L+2 (62%)	ADPM + Cyclo + Ru --> TPY + PhBr
	642 (0.033)	T6	H-3 (32%), H-2 (15%) -> L; H-2 -> L+1 (20%); H -> L+2 (19%)	Ru + Cyclo --> TPY + PhBr + ADPM
	592 (0.019)	T7	H-2 (14%), H-1 (48%), H (25%) -> L+1	ADPM + Cyclo + Ru --> TPY + PhBr
	580 (0.418)	T8	H-3 (19%), H-2 (12%), H-1 (26%), H (22%) -> L; H-3 -> L+1 (10%)	Ru + Cyclo --> TPY + ADPM
	574 (0.013)	T9	H-3 -> L+1 (15%); H-2 (39%), H-1 (38%) -> L+2	ADPM + Cyclo + Ru --> TPY + PhBr
536 (14)	563 (0.082)	T10	H-3 (27%), H-2 (20%), H-1 (29%) -> L+2	ADPM + Cyclo + Ru --> TPY
	540 (0.078)	T11	H-3 (65%), H-1 (16%) -> L+2	ADPM + Cyclo + Ru + PhBr --> TPY
	487 (0.145)	T12	H-3 -> L+1 (48%); H-2 -> L+2 (27%)	ADPM + Cyclo + Ru --> TPY + PhBr
423 (16)	452 (0.105)	T13	H-4 -> L (96%)	Ru --> ADPM + Cyclo
	442 (0.014)	T14	H -> L+3 (86%)	ADPM + Cyclo + Ru --> TPY + PhBr
	427 (0.249)	T15	H-5 -> L (96%)	Cyclo + Ru --> ADPM + TPY
	419 (0.007)	T16	H-1 (11%), H (79%) -> L+4	ADPM + Cyclo + Ru --> TPY + PhBr
	406 (0.005)	T17	H-4 -> L+1 (87%)	ADPM + Cyclo --> TPY + PhBr + Ru
	405 (0.035)	T18	H-1 -> L+3 (71%)	ADPM + Ru + Cyclo --> TPY + PhBr

Figure S.35 – Experimental absorption spectrum in CH_2Cl_2 vs calculated optical absorption bands of ADPM photosensitizer **6** based on TD-DFT calculations

(B3LYP/6-31G*; Ru = LANL2DZ; PCM = CH_2Cl_2)

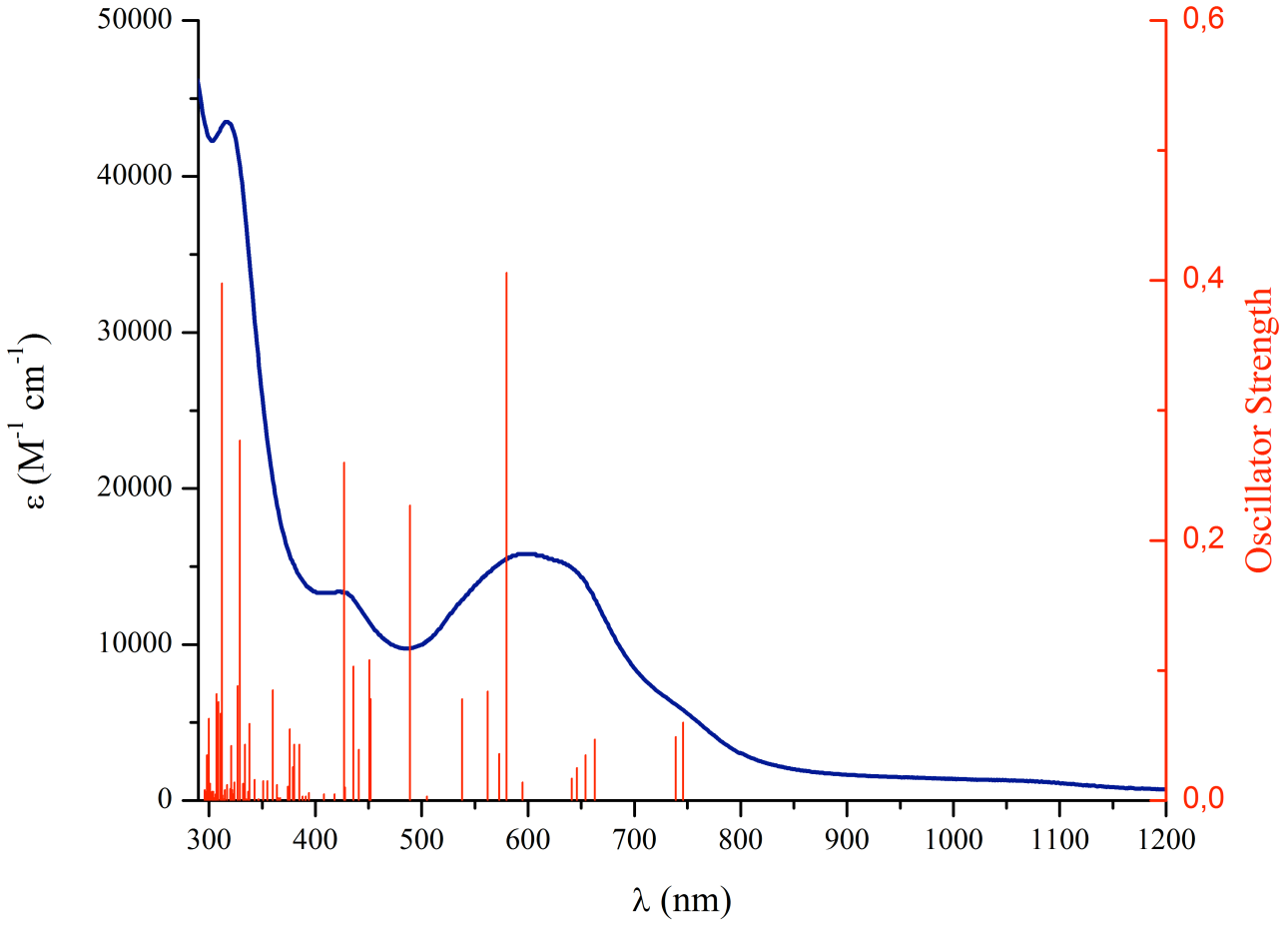

Table S.11 – Natural transition orbitals (NTO) associated with absorption bands **T1** to **T21** (Isovalue = 0.02) of complex **6** obtained by TD-DFT (PCM = CH_2Cl_2)

	λ_{Calc}, nm (Osc. Strenght) / Eigenvalue	**NTO Hole**	**NTO Particle**		**λ_{Calc}, nm (Osc. Strenght) / Eigenvalue**	**NTO Hole**	**NTO Particle**
T1	746 (0.060) / 0.98	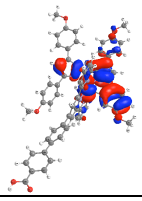	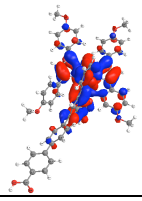	**T7**	595 (0.014) / 0.92	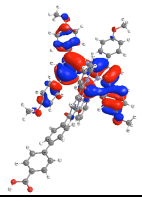	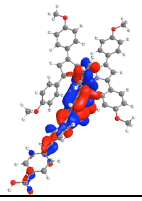
T2	739 (0.049) / 0.98	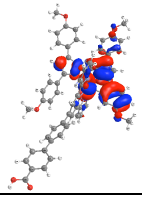	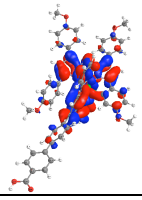	**T8**	580 (0.406) / 0.89	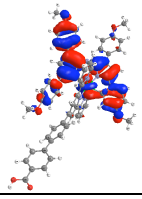	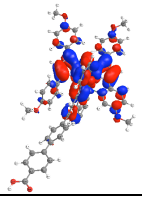
T3	663 (0.047) / 0.98	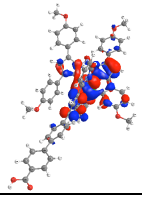	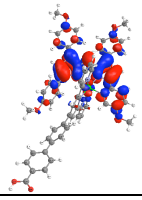	**T9**	573 (0.036) / 0.80	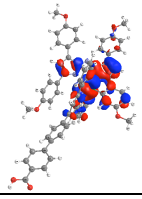	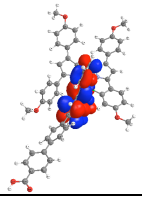
T4	654 (0.035) / 0.89	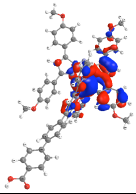	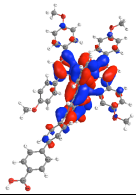	**T10**	562 (0.084) / 0.83	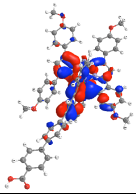	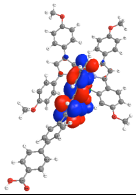
T5	646 (0.025) / 0.55	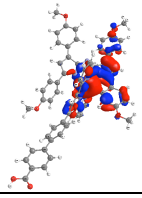	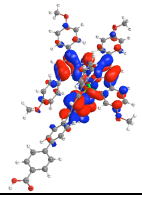	**T11**	538 (0.078) / 0.95	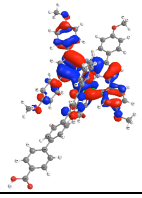	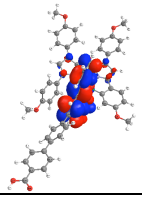
T6	641 (0.017) / 0.75	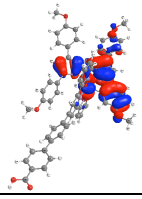	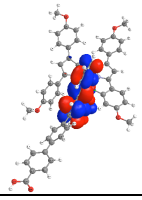	**T12**	505 (0.003) / 0.99	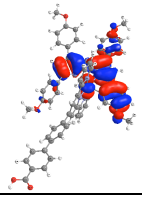	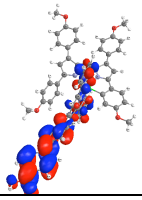

Table S.11 (Continued) – Natural transition orbitals (NTO) associated with absorption bands **T1** to **T21** (Isovalue = 0.02) of complex **6** obtained by TD-DFT (PCM = CH_2Cl_2)

	λ_{Calc}, nm (Osc. Strenght) / Eigenvalue	**NTO Hole**	**NTO Particle**		**λ_{Calc}, nm (Osc. Strenght) / Eigenvalue**	**NTO Hole**	**NTO Particle**
T13	489 (0.227) / 0.53	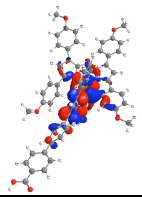	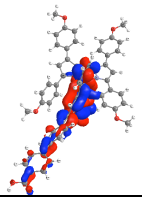	**T18**	428 (0.010) / 0.93	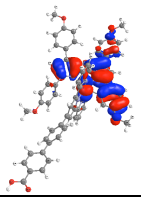	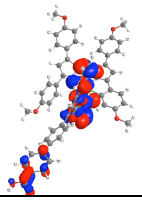
T14	452 (0.078) / 0.98	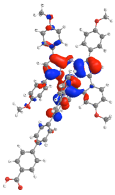	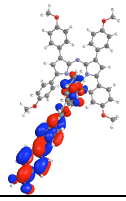	**T19**	427 (0.260) / 0.98	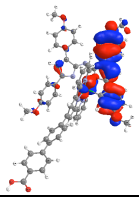	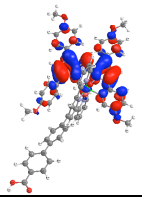
T15	451 (0.108) / 0.99	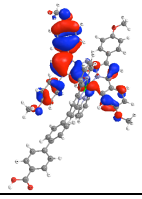	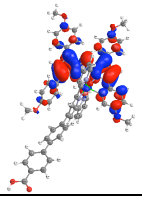	**T20**	418 (0.005) / 0.95	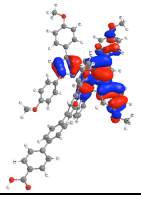	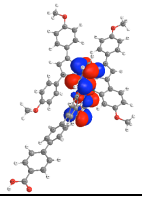
T16	441 (0.039) / 0.98	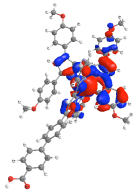	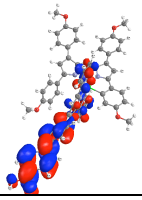	**T21**	408 (0.005) / 0.97	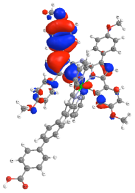	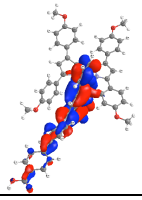
T17	436 (0.103) / 0.94	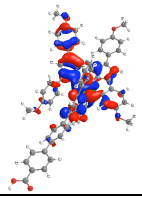	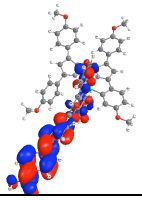				

Table S.12 - Assignation of optical absorption bands of ADPM photosensitizer **6** based on

TD-DFT calculations (B3LYP/6-31G*; Ru = LANL2DZ; PCM = CH_2Cl_2)

λ, nm				
Observed (ε, x10^3 $M^{-1}cm^{-1}$)	**Calculated** (Osc. Strength)	**Trans. No.**	**Major contributions to excitation**	**Assignation**
753 (5.4)	746 (0.060)	T1	H->L (42%), H->L+1 (26%)	Ru + Cyclo + ADPM --> TPY + Ph2COOH
	739 (0.049)	T2	H-1 (12%), H (36%) -> L+1; H -> L (27%)	Ru + Cyclo + ADPM --> TPY + Ph2COOH
600 (16)	663 (0.047)	T3	H-3 (22%), H-2 (25%), H-1 (47%) -> L	Ru + TPY --> ADPM + Cyclo + Ph2COOH
	654 (0.035)	T4	H-3 (14%), H-2 (28%) -> L; H-2 -> L+1 (37%)	Ru + Cyclo --> TPY + Ph2COOH + ADPM
	646 (0.025)	T5	H-3 (20%), H-2 (16%) ->L; H-2 (23%), H-1 (10%) -> L+1; H -> L+2 (19%)	Ru + Cyclo --> TPY + Ph2COOH + ADPM
	641 (0.017)	T6	H-3 -> L (12%), H -> L+2 (64%)	ADPM + Cyclo + Ru --> TPY + Ph2COOH
	595 (0.014)	T7	H-2 (13%), H-1 (44%), H (24%) -> L+1	ADPM + Cyclo + Ru --> TPY + Ph2COOH
538 (13)	580 (0.406)	T8	H-3 (20%), H-2 (11%), H-1 (23%), H (22%) -> L; H-3 -> L+1 (14%)	Ru + Cyclo --> ADPM + TPY + Ph2COOH
	573 (0.036)	T9	H-3 -> L+1 (12%); H-2 (37%), H-1 (40%) -> L+2	Ru + ADPM + Cyclo --> TPY + Ph2COOH
	562 (0.084)	T10	H-3 (27%), H-2 (19%), H-1 (31%) -> L+2	Ru + ADPM + Cyclo --> TPY + Ph2COOH
	538 (0.078)	T11	H-3 (64%), H-1 (16%) -> L+2	Ru + ADPM + Cyclo --> TPY
	505 (0.003)	T12	H -> L+3 (88%)	ADPM + Cyclo + Ru --> Ph2COOH + TPY
	489 (0.227)	T13	H-3 -> L+1 (42%), H-2 -> L+2 (30%)	Ru + ADPM + Cyclo --> TPY + Ph2COOH
422 (13)	452 (0.078)	T14	H-1 -> L+1 (10%), H-1 -> L+3 (78%)	Ru + ADPM + Cyclo --> Ph2COOH + TPY
	451 (0.108)	T15	H-4 -> L (97%)	Ru --> ADPM + Cyclo
	441 (0.039)	T16	H-2 -> L+1 (10%), H-2 -> L+3 (77%)	Ru + ADPM + Cyclo --> Ph2COOH + TPY
	436 (0.103)	T17	H-3 -> L+3 (70%)	Ru + ADPM + Cyclo --> Ph2COOH + TPY
	428 (0.010)	T18	H -> L+4 (82%)	ADPM + Cyclo + Ru --> TPY + Ph2COOH
	427 (0.260)	T19	H-5 -> L (96%)	Cyclo + Ru --> ADPM + TPY
	418 (0.005)	T20	H-1 (11%), H (79%) -> L+5	ADPM + Cyclo + Ru --> TPY + Ph2COOH
	408 (0.005)	T21	H-4 -> L+1 (88%)	ADPM + Cyclo --> TPY + PhBr + Ru

Table S.13 – Natural transition orbitals (NTO) associated with absorption bands **T1** to **T21** (Isovalue = 0.02) of complex **6** obtained by TD-DFT (PCM = MeOH)

	λ_{Calc}, nm (Osc. Strenght) / Eigenvalue	NTO Hole	NTO Particle		λ_{Calc}, nm (Osc. Strenght) / Eigenvalue	NTO Hole	NTO Particle
T1	752 (0.088) / 0.99	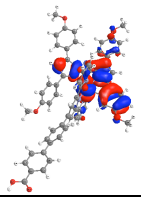	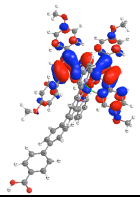	**T7**	583 (0.097) / 0.87	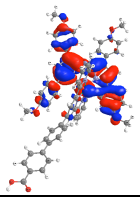	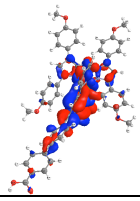
T2	727 (0.004) / 0.96	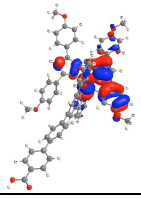	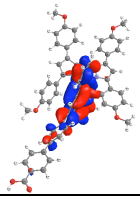	**T8**	577 (0.363) / 0.96	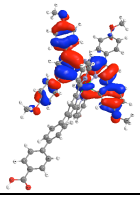	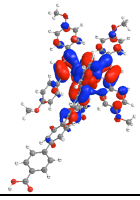
T3	674 (0.029) / 0.97	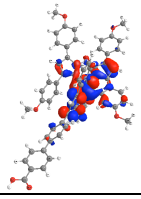	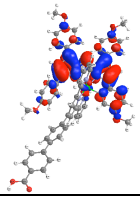	**T9**	565 (0.028) / 0.76	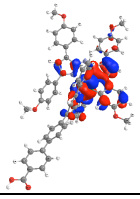	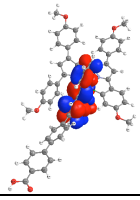
T4	660 (0.077) / 0.97	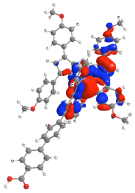	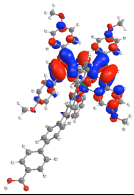	**T10**	555 (0.057) / 0.85	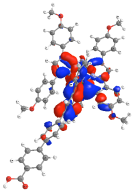	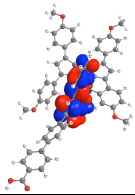
T5	641 (0.008) / 0.93	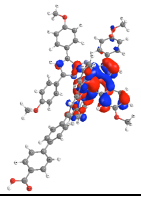	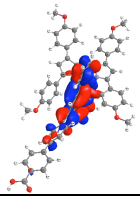	**T11**	529 (0.061) / 0.95	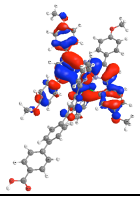	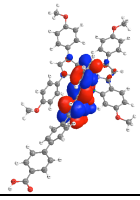
T6	628 (0.002) / 0.95	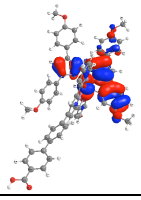	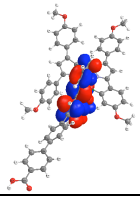	**T12**	491 (0.004) / 0.98	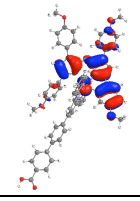	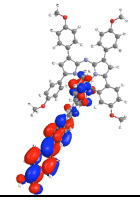

Table S.13 (Continued) – Natural transition orbitals (NTO) associated with absorption bands **T1** to **T21** (Isovalue = 0.02) of complex **6** obtained by TD-DFT (PCM = MeOH)

	λ_{Calc}, nm (Osc. Strenght) / Eigenvalue	**NTO Hole**	**NTO Particle**		**λ_{Calc}, nm (Osc. Strenght) / Eigenvalue**	**NTO Hole**	**NTO Particle**
T13	485 (0.209) / 0.52	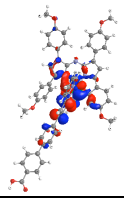	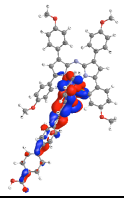	**T18**	428 (0.233) / 0.98	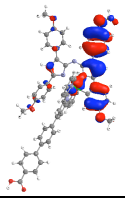	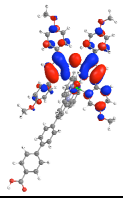
T14	452 (0.105) / 0.99	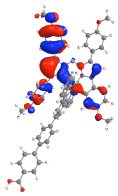	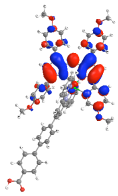	**T19**	422 (0.013) / 0.89	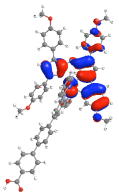	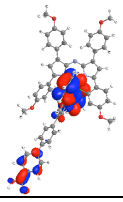
T15	444 (0.100) / 0.98	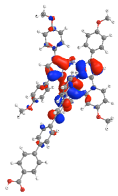	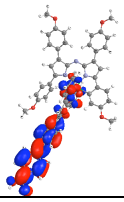	**T20**	413 (0.005) / 0.95	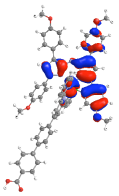	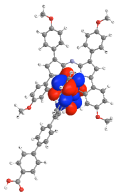
T16	434 (0.046) / 0.97	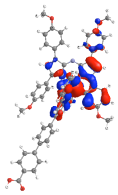	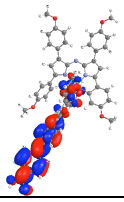	**T21**	401 (0.004) / 0.98	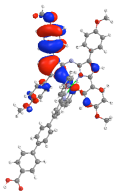	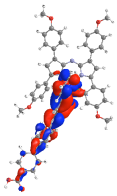
T17	429 (0.098) / 0.91	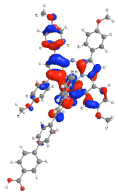	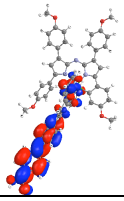				

Table S.14 - Assignation of optical absorption bands of ADPM photosensitizer **6** based on

TD-DFT calculations (B3LYP/6-31G*; Ru = LANL2DZ; PCM = MeOH)

λ, nm				
Observed (ε, x10^3 $M^{-1}cm^{-1}$)	**Calculated** (Osc. Strength)	**Trans. No.**	**Major contributions to excitation**	**Assignation**
753 (5.4)	752 (0.088)	T1	H-2 (12%), H-1 (12%), H (68%) -> L	Ru + Cyclo + TPY --> ADPM + Ph2COOH
	727 (0.004)	T2	H-1 (16%), H (61%) -> L+1	ADPM + Cyclo + Ru --> TPY +Ph2COOH
600 (16)	674 (0.029)	T3	H-3 (28%), H-2 (14%), H-1 (53%) -> L	Ru + TPY + Ph2COOH --> ADPM + Cyclo
	660 (0.077)	T4	H-3 (30%), H-2 (60%) -> L	Ru + TPY + Cyclo --> ADPM + Ph2COOH
	641 (0.008)	T5	H-2 (63%), H-1 (17%) -> L+1	Ru + ADPM + Cyclo --> TPY + Ph2COOH
	628 (0.002)	T6	H -> L+2 (82%)	ADPM + Cyclo + Ru --> TPY +Ph2COOH
	583 (0.097)	T7	H-2 (11%), H-1 (39%), H (18%) -> L+1	Ru + ADPM + Cyclo --> TPY +Ph2COOH
538 (13)	577 (0.363)	T8	H-3 (21%), H-1 (20%), H (19%) -> L; H-3 -> L+1 (13%)	Ru + Cyclo --> ADPM + Ph2COOH + TPY
	565 (0.028)	T9	H-3 -> L+1 (17%); H-2 (36%), H-1 (37%) -> L+2	Ru + ADPM + Cyclo --> TPY + Ph2COOH
	555 (0.057)	T10	H-3 (26%), H-2 (20%), H-1 (34%) -> L+2	Ru + ADPM + Cyclo --> TPY + Ph2COOH
	529 (0.061)	T11	H-3 (63%), H-1 (16%), H (10%) -> L+2	Ru + ADPM + Cyclo --> TPY
	491 (0.004)	T12	H -> L+3 (88%)	ADPM + Cyclo + Ru --> Ph2COOH + TPY
	485 (0.209)	T13	H-3 -> L+1 (38%), H-2 -> L+2 (31%)	Ru + ADPM + Cyclo --> TPY + Ph2COOH
422 (13)	452 (0.105)	T14	H-4 -> L (97%)	Ru --> ADPM + Cyclo
	444 (0.100)	T15	H-1 -> L+3 (79%)	Ru + ADPM + Cyclo --> Ph2COOH + TPY
	434 (0.046)	T16	H-3 (10%), H-2 (74%) -> L+3	Ru + ADPM + Cyclo --> Ph2COOH + TPY
	429 (0.098)	T17	H-3 (64%), H-2 (12%) -> L+3	Ru + ADPM + Cyclo --> Ph2COOH + TPY
	428 (0.233)	T18	H-5 -> L (96%)	Cyclo + Ru --> ADPM + TPY
	422 (0.013)	T19	H -> L+4 (79%)	ADPM + Ru + Cyclo --> TPY + Ph2COOH
	413 (0.005)	T20	H-1 (12%), H (78%) -> L+5	ADPM + Ru + Cyclo --> TPY + Ph2COOH
	401 (0.004)	T21	H-4 -> L+1 (89%)	ADPM + Cyclo --> TPY + Ph2COOH + Ru

X-ray diffraction measurements and structure determination

Crystallographic data for **2** were collected at 150 K, from single crystal samples, which were mounted on a loop fiber. Data were collected using a Bruker Microstar diffractometer equipped with a Platinum 135 CCD Detector, a Helios optics and a Kappa goniometer. The crystal-to-detector distance was 3.8 cm, and the data collection was carried out in 512 x 512 pixel mode. The initial unit cell parameters were determined by a least-squares fit of the angular setting of strong reflections, collected by a 110.0 degree scan in 110 frames over three different parts of the reciprocal space. Crystallographic data for **4** and **5** were collected at 100 K, using a Bruker D8 Venture diffractometer configured with a Metal Jet liquid-metal source, and a Photon 100 CMOS-based area detector. For data collection, determination of cell parameters, cell refinement, and data reduction *APEX2* and *SAINT* (Bruker, 2007) were used.[10] Absorption corrections were applied using *SADABS* and *TWINABS* (Bruker 2001).[11] Structure solution was performed using direct methods with *SHELXS* or *SHELXT* (Sheldrick, 2008 and 2015)[12] and refined on F^2 by full-matrix least squares using *SHELXL2014* (Sheldrick, 2008 and 2015).[12] *OLEX2* (Dolomanov *et al.*, 2009),[13] *ORTEP-3 for Windows* (Farrugia, 2012),[14] and POV-ray (2013)[15] were used for molecular graphics. The material was prepared for publication using *PLATON* (Spek, 2009),[16] Mercury,[17] and *publCIF* (Westrip, 2010).[18]

Crystal data, data collection and structure refinement details are summarized in Table S15. For **2**, **4** and **5**, all non-H atoms were refined by full-matrix least-squares with anisotropic displacement parameters. The H-atoms were included in calculated positions and treated as riding atoms: aromatic C—H 0.95 Å, methyl C—H 0.98 Å, with $U_{iso}(H) = k \times U_{eq}$ (parent C-atom), where k = 1.2 for the aromatic H-atoms and 1.5 for the methyl H-atoms.

Compound **2** contains a co-crystallized 4-chlorobenzene molecule. In addition, solvent accessible voids of 41 $Å^3$ were found, with an electron count of 2. The void is too small to accommodate molecules bigger than water; water didn't fit. The structures of the compounds **4** and **5** were obtained from the best available crystals, which unfortunately were very poor quality, resulting in overall poor data quality. In addition, both structures present high degree of disorder. The structure of **4** contains two molecules in the asymmetric unit. One molecule displays disorder at the level of one proximal 4-methoxy-phenyl group. The disorder was modelled as two

components using PART instructions. The disordered benzene groups were constrained to an ideal hexagon, with C—C distances equal to 1.39 Å. The occupation factors were first freely refined, and then fixed at the values obtained after refinement (50:50). Bond distance and mild displacement parameter (U^{ij}) restraints were also applied.). In order to improve the model, the reflections (hkl: 7 3 1; -6 7 2; 9 3 4) with $|F_o - F_c| > 5\sigma(F_o)$ were omitted from the refinement. The weight second parameter is unusually large for **4** (22.96), which can indicate twinning. No twin law was detected with TwinRotMat routine from *PLATON* (Spek, 2009);[16] treatment for non-merohedrally twinned crystal data was also performed using *CELL_NOW* (2 and 3 domains)/ *TWINABS*/ *BASF* / *HKLF5* (Bruker 2001),[11] but the models obtained were worse than the present model. Therefore the twinning treatment was not retained. The structure of compound **5** is highly disordered at the level of the ADPM moiety and of three of the four *p*-methoxy-phenyl groups. The disorder was modeled as described above, using in addition hard displacement parameter (U^{ij}) restraints. The occupation factors were first freely refined, and then fixed at the values obtained after refinement (60:40 and 55:45 for the distal 4-methoxy-phenyl groups, and 70:30 for the proximal one). The structure of **5** contains a co-crystallized disordered toluene molecule on a symmetry position, which was modelled using PART -1 instruction, together with bond distance and angle constraints. A calculated residual density of 1.52 e/Å^3 is present in **5**, at 0.95 Å from the Ru atom. As the presence of a Ru-H bond is chemically not possible, this remaining electron density is most likely a Fourier truncation error.

Crystallographic data for **2**, **4**, and **5** were deposited in CCDC[19] under the deposit numbers: CCDC 1419506 – 1419508. The alerts given by the checkCIF/ PLATON routine are commented in the crystallographic information files (cifs) of the corresponding compounds.

Selected bond lengths and angles for **2**, **4**, and **5** are presented in Table S.16, whereas Table S.17 shows selected parameters reported in relevant ruthenium(II) complexes. The hydrogen bonding geometry for **2**, **4**, and **5** is highlighted in Table S.18.

Table S.15 – Solid-state structure and refinement data for compounds **2**, **4** and **5**.

	2	**4**	**5**
Formula	$C_{47}H_{37}N_5O_5Ru \bullet C_6H_5Cl$	$C_{49}H_{37}N_5O_5Ru$	$C_{57}H_{43}BrN_6O_4Ru \bullet 0.5(C_7H_8)$
M_w(g/mol)	965.43	876.90	1103.02
T (K)	150	100	100
Wavelength (Å)	1.54178	1.3418	1.3418
Crystal System	Tetragonal	Monoclinic	Triclinic
Space Group	I-4	$P2_1/c$	P-1
Unit Cell: a (Å)	22.3944(5)	15.6633(7)	12.207(2)
b (Å)	22.3944(5)	24.0100(10)	13.408(3)
c (Å)	17.6264(4)	21.6141(10)	16.302(3)
α (°)	90	90	73.36(3)
β (°)	90	104.679(2)	70.90(3)
γ (°)	90	90	73.29(3)
V (Å^3)	8839.8(4)	7863.2(6)	2359.8(10)
Z	8	8	2
$d_{calcd.}$ (g/cm^3)	1.451	1.481	1.552
μ (mm^{-1})	3.884	2.453	2.789
F(000)	3968	3600	1126
θ range (°)	3.19 to 70.50	2.43 to 54.30	2.55 to 61.29
Reflections collected	93738	83129	42720
Independent reflections	8397	14471	10177
GoF	1.051	1.058	1.020
R1(F) [I > 2σ(I)]	0.0270	0.0745	0.0768
wR(F^2) [I > 2σ(I)]	0.0689	0.1959	0.1666
R1(F) (all data)	0.0275	0.1045	0.1233
wR(F^2) (all data)	0.0694	0.2150	0.1911
Largest diff. peak and hole (e/Å^3)	0.57 and -0.41	1.33 and -1.02	1.61 and -1.02

Table S.16 – Selected bond lengths (Å) and angles (°) for compounds **2**, **4** and **5**

	2	**4**	**5**
Bond length (Å)/ Angle (°)			
Ru1-N1	2.032(3)	2.022(8)[a]	2.055(5)
Ru1-N3	2.222(3)	2.197(8)[a]	2.192(6)
Ru1-N4	2.138(3)	2.141(8)[a]	2.043(4)
Ru1-N5	2.087(3)	2.082(8)[a]	1.938(5)
Ru1-X	X=C47(carbonyl) 1.831(4)	X=C49(carbonyl) 1.814(11)[a]	X=N6(N”-tpy) 2.035(4)
Ru1-C12	2.071(3)	2.069(10)[a]	2.102(3)
C-O(carbonyl)	1.157(4)	1.159(12)[a]	-
N1-C1	1.372(4)	1.375(13)[a]	1.389(9)
C1-N2	1.320(4)	1.322(13)[a]	1.312(10)
N2-C17	1.341(4)	1.345(13)[a]	1.339(9)
C17-N3	1.400(4)	1.391(13)[a]	1.408(8)
N1-Ru1-N5	164.9(1)	163.8(4)[a]	168.7(2)
N3-Ru1-C12	161.6(1)	164.1(4)[a]	160.2(2)
N4-Ru1-X	X=C47(carbonyl) 171.8(1)	X=C49(carbonyl) 175.7(4)[a]	X=N6(N”-tpy) 158.2(2)
N1-Ru1-N3	82.1(1)	85.1(3)[a]	82.3(2)
N1-Ru1-C12	79.6(1)	79.5(4)[a]	78.0(2)
N1-Ru1-X	X=C47(carbonyl) 94.8(1)	X=C49(carbonyl) 94.9(4)[a]	X=N6(N”-tpy) 96.8(1)
N1-Ru1-N4	92.6(1)	89.0(3)[a]	105.0(1)
N3-Ru1-N4	90.0(1)	84.5(3)[a]	89.9(2)
N3-Ru1-N5	108.4(1)	104.3(3)[a]	108.5(1)
N3-Ru1-X	X=C47(carbonyl) 94.5(1)	X=C49(carbonyl) 96.0(4)[a]	X=N6(N”-tpy) 93.9(1)
N4-Ru1-N5	76.9(1)	79.1(3)[a]	79.0(1)
N4-Ru1-C12	88.7(1)	91.8(4)[a]	94.5(1)
N5-Ru1-C12	89.2(1)	90.1(4)[a]	91.2(1)
N5-Ru1-X	X=C47(carbonyl) 95.1(1)	X=C49(carbonyl) 97.2(4)[a]	X=N6(N”-tpy) 79.5(1)
C12-Ru1-X	X=C47(carbonyl) 89.2(1)	X=C49(carbonyl) 88.8(4)[a]	X=N6(N”-tpy) 89.2(1)
N1-C1-N2	125.6(3)	129.0(9)[a]	125.1(7)
C1-N2-C17	124.2(3)	124.9(8)[a]	124.4(6)
N2-C17-N3	127.8(3)	129.5(9)[a]	128.5(6)
Tilt angles (°) between the planes of the two central pyrrolic rings			
	13.5(1)	16.4(1); 18.0(1)[b]	8.9(1)
Tilt angles (°) between ADPM moiety and the aryl rings[c]			
Ar_1 (proximal)	23.5(1)	7.1(1); 10.3(1)[b]	3.4(1)
Ar_2 (distal)	19.7(1)	44.8(1); 41.0(1)[b]	3.4(1)
Ar_3 (distal)	35.1(1)	53.4(1); 45.5(1)[b]	32.0(1)
Ar_4 (proximal)	67.8(1)	52.2(1); 61.1(1)[b]	79.0(1)

[a] average values on the two molecules in the asymmetric unit; the error was calculated using the formula for propagation of error in calculations.

[b] values are shown for the two molecules in the asymmetric unit.

[c] Ar_1 is associated with the cyclometallated aryl moiety in proximal position, whereas the following aryls are numbered in a counter-clockwise fashion.

Table S.17 – Selected parameters for relevant reported ruthenium(II) complexes.

CSD Code	QUBZAO[20]	acetyl-carbonyl-bis(2,2'-bipyridyl)-ruthenium(II) hexafluorophosphate
Bond length (Å)		
Ru-N_{bpy} (*trans* to carbonyl)		2.137(5)
Ru- N_{bpy} (*trans* to N)		2.070(5)
Ru-$C_{carbonyl}$		1.837(6)
C-O		1.152(7)
Ru-C_{acetyl}		2.038(6)
CSD Code	EJOHUG[21]	$Ru(phen)_2(CN)_2$
Bond length (Å)		
Ru-N_{phen} (*trans* to C)		2.124(8) and 2.107(9)
Ru-N_{phen}		2.073(7) and 2.081(8)

Table S.18 – H-bonding geometry for compounds **2**, **4** and **5**. Distances are in (Å) and angles in (°); 3-center bifurcated H-bonds are displayed in italic.

***D*—H···*A* (type*)**	***D*—H**	**H···*A***	***D*···*A***	***D*—H···*A***
		2		
C10—H10···N2 (intra)	0.95(1)	2.51(1)	3.13(1)	123(1)
C10—H10···O4^{i} (inter)	0.95(1)	2.50(1)	3.18(1)	129(1)
C22—H22···N2 (intra)	0.95(1)	2.57(1)	3.09(1)	115(1)
C7—H7···O2^{ii} (inter)	0.95(1)	2.67(1)	3.29(1)	123(1)
		4		
		(for each of the 2 molecules in the asymmetric unit)		
C10—H10···N2 (intra)	0.95(1)	2.70(1)	3.13 (1)	108(1)
C22—H22···N2 (intra)	0.95(1)	2.72(1)	3.09(1)	104(1)
C37—H37···N1 (intra)	0.95(1)	2.64(1)	3.13(1)	113(1)
C9—H9···O10^{iii} (inter)	0.95(1)	2.60(1)	3.41(1)	144(1)
C23—H23···O10^{iii} (inter)	0.95(1)	2.38(1)	3.18(1)	142(1)
C42—H42···O3^{iv} (inter)	0.95(1)	2.38(1)	3.32(1)	171(1)
C86—H86···N6 (intra)	0.95(1)	2.61(1)	3.12(1)	114(1)
C71A—H71A···N7 (intra)	0.95(1)	2.55(1)	3.00(2)	109(1)
C59—H59···N7 (intra)	0.95(1)	2.64(1)	3.13(1)	113(1)
C59—H59···O5^{v} (inter)	0.95(1)	2.71(1)	3.26(1)	118(1)
C58—H58···O5^{v} (inter)	0.95(1)	2.66(1)	3.25(1)	121(1)
C72A—H72A···O5^{v} (inter)	0.95(1)	2.53(1)	3.28(1)	135(1)
C93—H93···O5^{v} (inter)	0.95(1)	2.51(1)	3.31(1)	141(1)
C75A—H75A···O4^{vi} (inter)	0.95(1)	2.57(1)	3.30(2)	134(1)
		5		
C10A—H10A···N2 (intra)	0.95(1)	2.56(1)	3.29(1)	134(1)
C22A—H22A···N2 (intra)	0.95(1)	2.46(1)	2.96(1)	113(1)
C32A—H32A···Br1^{vii} (inter)	0.95(1)	2.94(1)	3.84(1)	159(1)
C48—H48···O2^{viii} (inter)	0.95(1)	2.44(1)	3.19(1)	135(1)

*intra = intramolecular; inter = intermolecular

Symmetry codes: (i) ½-x, ½-y, -½+z; (ii) x, 1-y; 1-z (iii) x, ½+y, ½-z; (iiv) 1+x, y, z; (v) -x, -½+y, ½-z; (vi) 1-x, 1-y; 1-z; (vii) -1+x, y, z; (viii) 2-x, 2-y, 1-z.

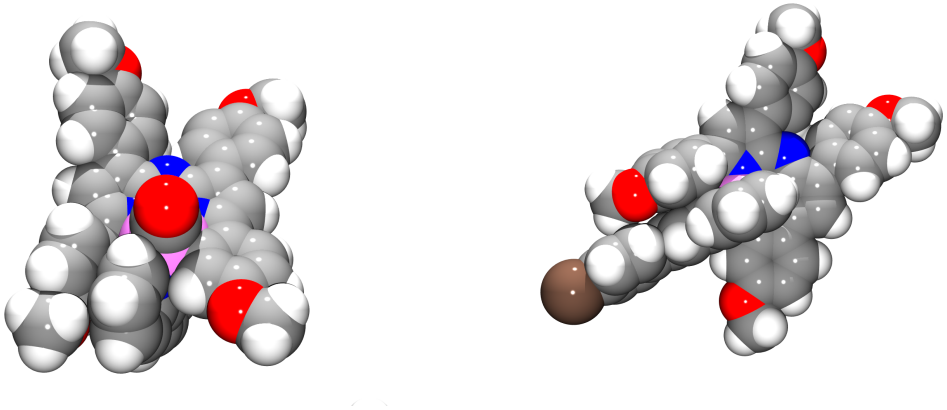

Figure S.36 – The solid-state structure of **2** (left) and **5** (right) – space-fill models showing the π – π and π – H-C(sp^2) intramolecular interactions. Co-crystallized solvent and the minor-disorder components have been omitted for clarity.

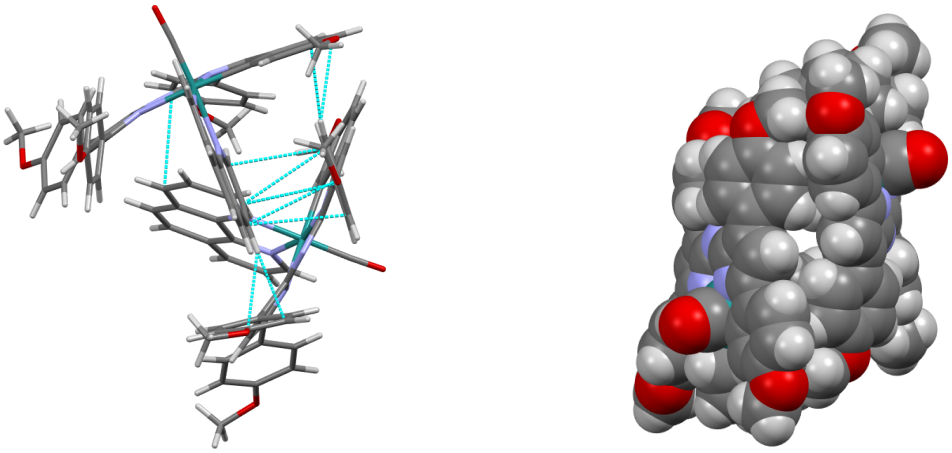

Figure S.37 – The solid-state structure of **4** (asymmetric unit) – capped stick model (left) and space-fill model (right) showing the π – π and π – H-C(sp^2) intermolecular interactions. The minor-disorder components have been omitted for clarity.

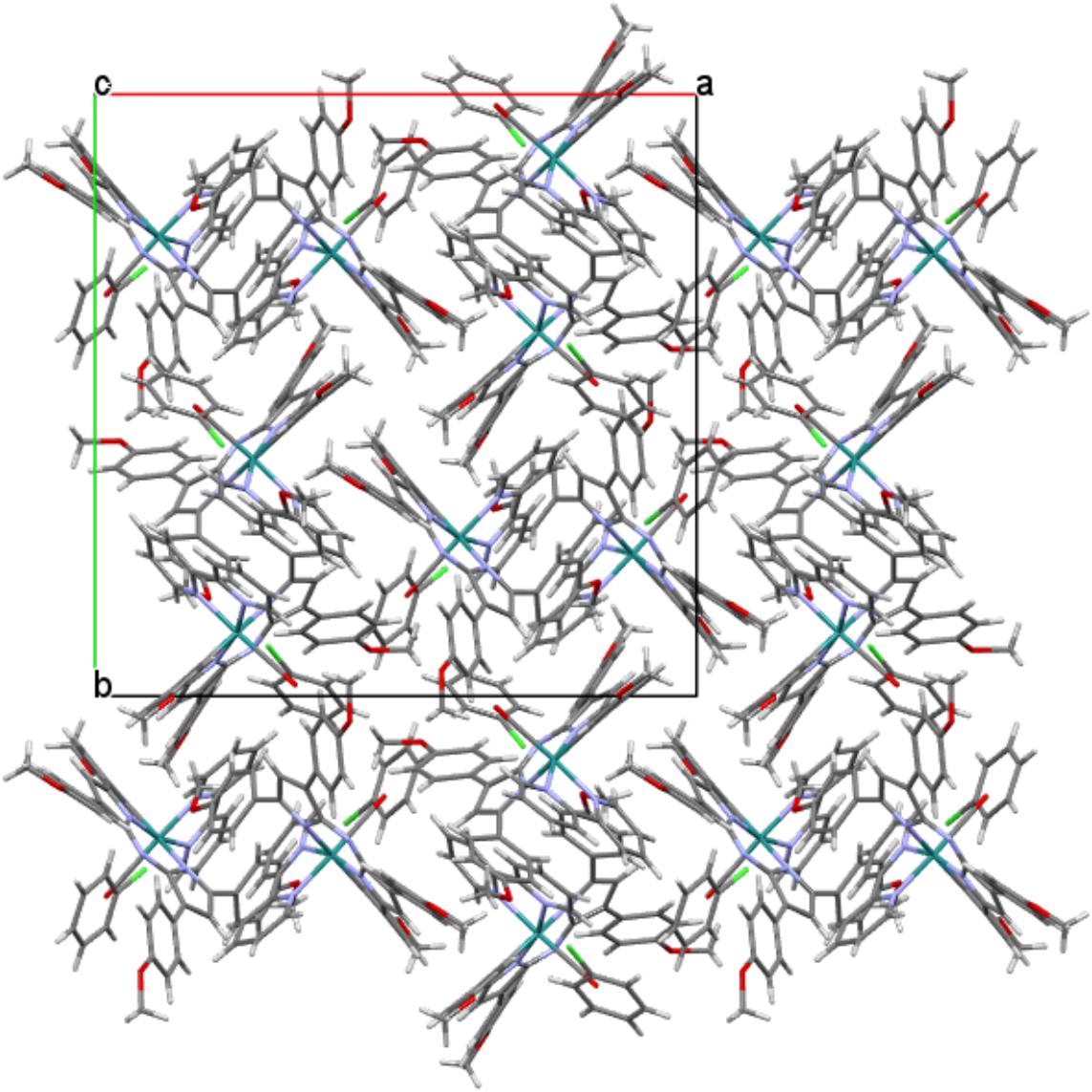

Figure S.38 – A packing diagram for compound **2** – view along *c* axis.

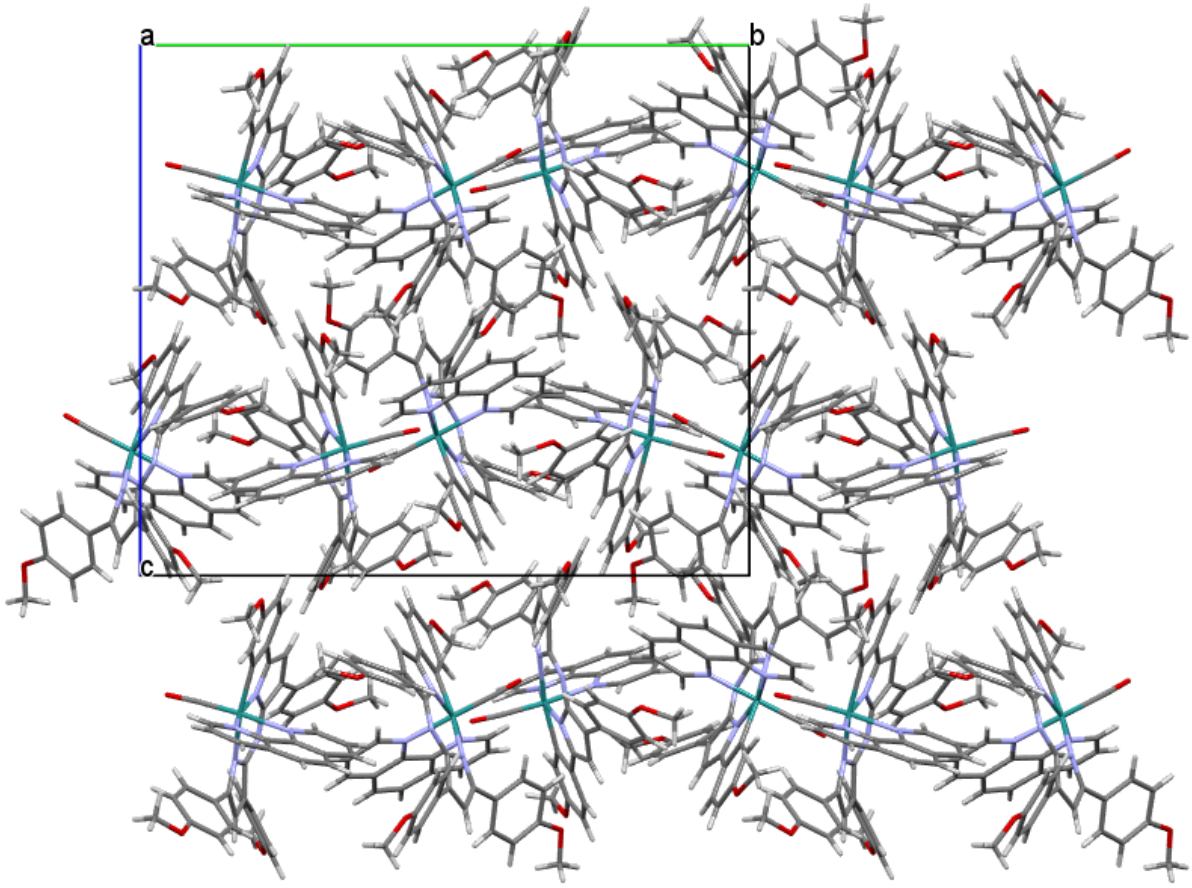

Figure S.39 – A packing diagram for compound **4** – view along *a* axis. The minor-disorder components have been omitted for clarity.

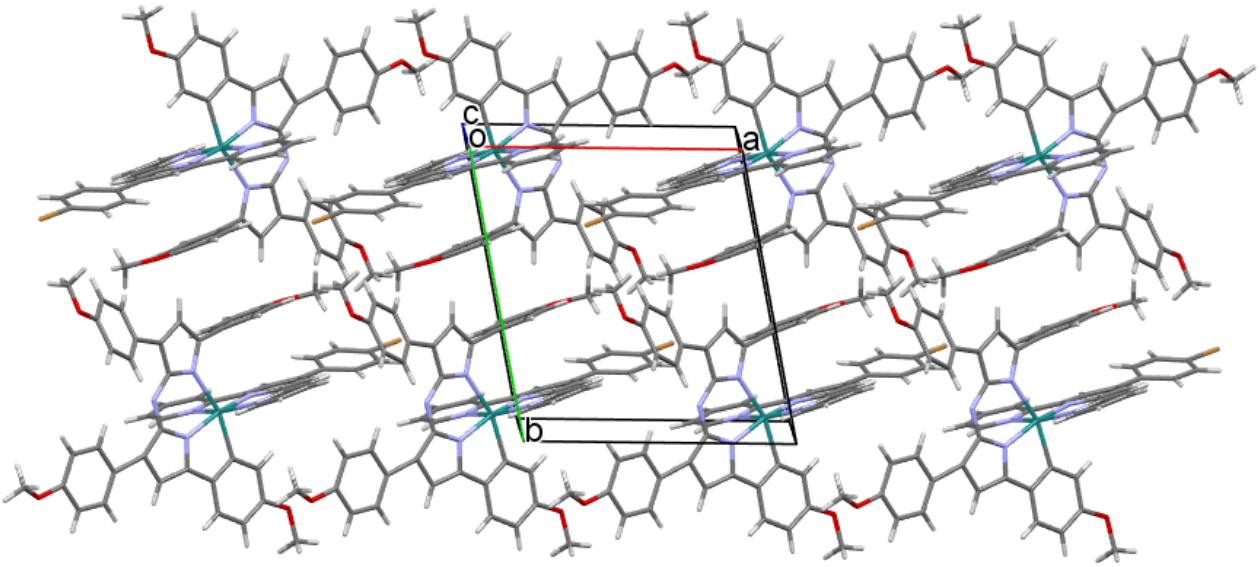

Figure S.40 – A packing diagram for compound **5** – view along *c* axis showing the intramolecular and intermolecular π – π interactions. Co-crystallized solvent and the minor-disorder components have been omitted for clarity.

References

1. (a) Eskelinen, E.; Da Costa, P.; Haukka, M. *J. Electroanal. Chem.* **2005,** *579*, 257-265; (b) Santoni, M.-P.; Pal, A. K.; Hanan, G. S.; Proust, A.; Hasenknopf, B. *Inorg. Chem. Commun.* **2011,** *14*, 399-402.
2. Connelly, N. G.; Geiger, W. E. *Chem. Rev.* **1996,** *96*, 877-910.
3. Frisch, M. J.; Trucks, G. W.; Schlegel, H. B.; Scuseria, G. E.; Robb, M. A.; Cheeseman, J. R.; Scalmani, G.; Barone, V.; Mennucci, B.; Petersson, G. A.; Nakatsuji, H.; Caricato, M.; Li, X.; Hratchian, H. P.; Izmaylov, A. F.; Bloino, J.; Zheng, G.; Sonnenberg, J. L.; Hada, M.; Ehara, M.; Toyota, K.; Fukuda, R.; Hasegawa, J.; Ishida, M.; Nakajima, T.; Honda, Y.; Kitao, O.; Nakai, H.; Vreven, T.; J. A. Montgomery, J.; Peralta, J. E.; Ogliaro, F.; Bearpark, M.; Heyd, J. J.; Brothers, E.; Kudin, K. N.; Staroverov, V. N.; Kobayashi, R.; Normand, J.; Raghavachari, K.; Rendell, A.; Burant, J. C.; Iyengar, S. S.; Tomasi, J.; Cossi, M.; Rega, N.; Millam, J. M.; Klene, M.; Knox, J. E.; Cross, J. B.; Bakken, V.; Adamo, C.; Jaramillo, J.; Gomperts, R.; Stratmann, R. E.; Yazyev, O.; Austin, A. J.; Cammi, R.; Pomelli, C.; Ochterski, J. W.; Martin, R. L.; Morokuma, K.; Zakrzewski, V. G.; Voth, G. A.; Salvador, P.; Dannenberg, J. J.; Dapprich, S.; Daniels, A. D.; Farkas, Ö.; Foresman, J. B.; Ortiz, J. V.; Cioslowski, J.; Fox, D. J. *Gaussian 09 Revision D.01*, Gaussian Inc.: Wallingford CT **2009**.
4. (a) Becke, A. D. *J. Chem. Phys.* **1993,** *98*, 5648-5652; (b) Lee, C.; Yang, W.; Parr, R. *Phys. Rev. B* **1988,** *37*, 785-789; (c) Vosko, S. H.; Wilk, L.; Nusair, M. *Can. J. Phys.* **1980,** *58*, 1200-1211; (d) Stephens, P. J.; Devlin, F. J.; Chabalowski, C. F.; Frisch, M. J. *J. Phys. Chem.* **1994,** *98*, 11623-11627.
5. Tomasi, J.; Mennucci, B.; Cammi, R. *Chem. Rev.* **2005,** *105*, 2999-3093.
6. Dennington, R.; Keith, T.; Millam, J.; Eppinnett, K.; Hovell, W. L.; Gilliland, R. *GaussView Version 3.09*, Semichem Inc.: Shawnee Mission KS, **2003**.
7. O'Boyle, N. M.; Tenderholt, A. L.; Langner, K. M. *J. Comp. Chem.* **2008,** *29*, 839-845.
8. Chemissian, a computer program to analyze and visualize quantum-chemical calculations, by L. Skripnikov. For the current version, see http://www.chemissian.com
9. Bessette, A.; Ferreira, J. G.; Giguère, M.; Bélanger, F.; Désilets, D.; Hanan, G. S. *Inorg. Chem.* **2012,** *51*, 12132-12141.
10. Bruker *APEX2 and SAINT*, Bruker AXS Inc.: Madison, Wisconsin, USA., **2007**.
11. Bruker *SADABS and TWINABS*, Bruker AXS Inc.: Madison, Wisconsin, USA., **2001**.
12. (a) Sheldrick, G. M. *Acta Crystallogr., Sect. A: Found. Crystallogr.* **2008,** *64*, 112-122; (b) Sheldrick, G. M. *Acta Crystallogr., Sect. A* **2015,** *71*, 3-8.
13. Dolomanov, O. V., Bourhis, L. J., Gildea, R. J., Howard, J. A. K., Puschmann, H. *J. Appl. Cryst.* **2009,** *42*, 339-341.
14. Farrugia, L. J. *J. Appl. Crystallogr.* **1997,** *30*, 565.
15. POV-Ray *POV-Ray 3.7.0*, Persistence of Vision Pty. Ltd., Persistence of Vision Raytracer, retrieved from http://www.povray.org/download/: **2013**.
16. Spek, A. L. *Acta Crystallogr., Sect. D: Biol. Crystallogr.* **2009,** *65*, 148-155.
17. CCDC *Mercury 3.1 - 3.3*, **2001-2013**.
18. Westrip, S. P. *J. Appl. Crystallogr.* **2010,** *43*, 920-925.
19. Allen, F. *Acta Crystallogr., Sect. B: Struct. Sci.* **2002,** *58*, 380-388.
20. Ooyama, D.; Tomon, T.; Tsuge, K.; Tanaka, K. *J. Organomet. Chem.* **2001,** *619*, 299-304.
21. Chow, C.-F.; Chiu, B. K. W.; Lam, M. H. W.; Wong, W.-Y. *J. Am. Chem. Soc.* **2003,** *125*, 7802-7803.